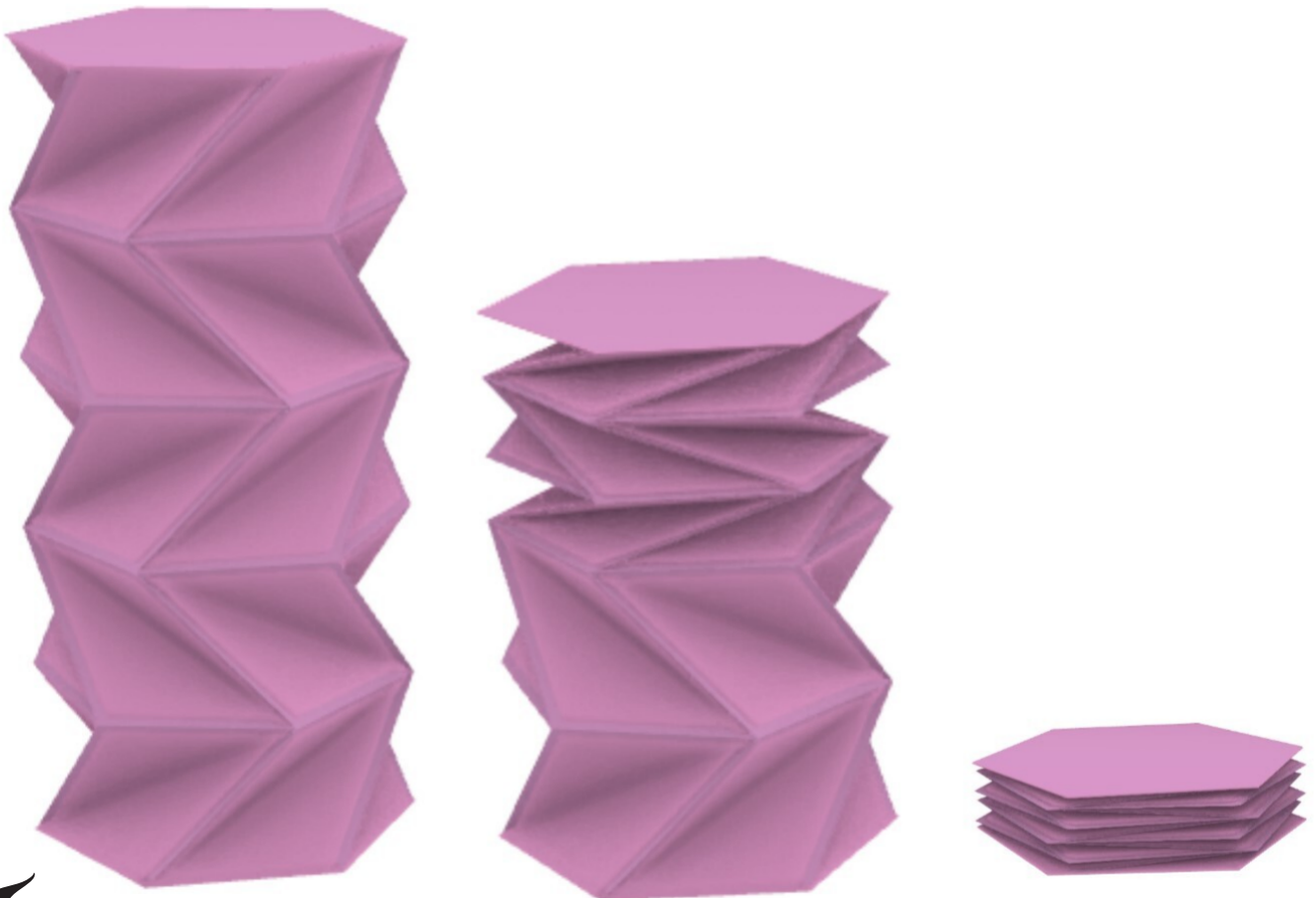


Preliminary Design of Origami-inspired Deployable Structure

Thesis - Aerospace Structures and Materials
AE-5722

Joshika Sachithanandan



Preliminary Design of Origami-inspired Deployable Structure

Thesis - Aerospace Structures and Materials
AE-5722

by

Joshika Sachithanandan

Student Name	Student Number
Joshika Sachithanandan	5452147

Primary Supervisor: Ines Uriol Balbin
Secondary Supervisor: Pablo Solano Lopez
Project Duration: November, 2022 - August, 2023
Faculty: Faculty of Aerospace Engineering, TU Delft

Cover: Origami Deployable Structure generated on Grasshopper

Acknowledgements

This thesis marks the culmination of my transformative journey at the TU Delft Faculty of Aerospace Engineering. The past two years have been nothing short of life-changing thanks to my dear friends, teachers, and mentors who have supported me every step of the way.

Firstly, I would like to extend my deepest appreciation to my supervisor, Ines Uriol Balbin, for being the most supportive mentor anyone could ask for. This work could not have been half as enriching and enjoyable as it was without her guidance and constant encouragement to explore every idea I had. I would also like to thank my external supervisor, Pablo Solano Lopez, for his valuable inputs on the direction of my thesis, feedback on my work, and support with the inflation tests at the DASML lab.

Next, I would like to express my gratitude to Pietro Marchese for his assistance in the additive manufacturing lab and the Shaping Matter Lab students for their help with operating the laser cutter and 3D printers.

To the numerous students, academics, and technicians who have generously shared their knowledge and time with me, I am deeply grateful for your invaluable contributions.

Finally, I would like to thank – my friends, Evelien, Shreyasi, Danny, Davide, and Oscar, for making this place feel like a home away from home; Palak, Devi, Zayed, Kanu, my parents, and my extended family for their unwavering belief in my capabilities—none of this would have been possible without all of you cheering me on; thank you!

*Joshika Sachithanandan
Delft, August 2023*

Summary

In recent times, there has been a growing interest in spending extended amounts of time in outer space. To enable these endeavors, living and storage spaces will have to be much larger than current technologies can transport and set up in space. An interesting solution to this problem is the usage of a deployable structure that occupies a small volume in a launch vehicle but can be deployed to larger volumes in space.

This thesis explores the concept of origami—known for its compactness, ease of deployment, scalability, and structural integrity—to create a deployable structure by developing a technology demonstrator that fits in a 12U CubeSat. Engineering origami has been used across many fields, such as medicine, architecture, and, most recently, space. For applications like instrument booms and antennas, it is used to save space in the satellite housing them. The current work aims to translate this space-saving strategy to a larger application by creating an origami-inspired small-scale deployable structure that, if successful, can be scaled up for different purposes.

To that end, the research question that is explored in this thesis is,

"How can an origami-based deployable structure be designed for integration with a 12U CubeSat while ensuring structural integrity during and after folding and deployment?"

To answer this question, a demonstrator is designed to validate the proposed origami design and deployment concept. Based off requirements set by the mission, research objectives, and constraints, four design concepts are proposed. A qualitative tradeoff is conducted from which the concept chosen is a Kresling patterned cylinder deployed via inflation. The structure is then modelled on Rhino, and an optimum configuration is found, which provides maximum compactness and inner volume—two criteria that are critical for sizeable modules to be transported in rockets with limited space.

Before proceeding with more resource-heavy manufacturing options, laser-cut paper models were used to initially validate the pattern and deployment choices. Next, a tradeoff is conducted to find suitable materials and a compatible manufacturing technique. Taking into consideration the resource availability, manufacturing time, and novelty of the approach, the prototyping option chosen is 3D printing with thermoplastic filaments (PLA and TPU). Dual extrusion 3D printing is used for prototyping the structure with PLA and TPU, iteratively fine-tuning printing parameters to achieve desired function and optimum print quality.

Next, the structural performance of the deployable unit during folding and deployment is studied using ABAQUS simulations. It was found that the structure mostly performs well under the expected loads and also shows indications of multiple stable states. Lastly, a set of design guidelines are presented based on observations made during modelling, optimisation, and prototyping. These guidelines define limits within which different parameters can be tuned to design Kresling origami structures.

This thesis work lays the foundation for developing Kresling origami-based deployable structures with insights into optimal configurations, material and manufacturing options, and the development of a parametric model to rapidly check the geometric feasibility of a proposed structure.

Contents

Acknowledgements	i
Summary	ii
Nomenclature	ix
1 Introduction	1
2 Research Framework	4
2.1 Literature Study	5
2.1.1 Origami Patterns	5
2.1.2 Deployment Mechanisms	10
2.1.3 Materials and Manufacturing	11
2.2 Research Questions	16
2.3 Research Objectives and Methodology	16
3 Requirements and Concept Generation	19
3.1 Requirements Table	19
3.2 Design Concepts	21
3.2.1 Design Concepts	21
3.2.2 Design Option Trade-Off	24
4 Modeling	27
4.1 Kresling Cylinder Geometry	27
4.2 Deployable Structure	29
4.3 3D Modelling	30
5 Validation	38
6 Parametric Study and Optimisation	50
7 Prototyping	59
7.1 Prototypes for Model Validation	59
7.1.1 Cutting - Outer Silhouette	61
7.1.2 Engraving - Mountains and Valleys	61
7.1.3 Forming the 3D structure	63
7.1.4 Inflation of paper model	66
7.2 Materials and Manufacturing	69
7.3 3D Printing	70
7.4 Packaging Ratio and Deployment Ratio	76
8 Structural Performance	77
8.1 Origami Model Generation	77

8.2	Analysis Procedure	78
8.3	Simulation Results	79
8.3.1	Folding Force	79
8.3.2	Packaging Ratio	80
8.3.3	Strain Energy	81
8.3.4	Contour Plots	83
9	Design Guidelines	87
10	Requirements Verification	90
11	Conclusions and Recommendations	92
11.1	Research Questions	92
11.2	Recommendations	94
	Bibliography	96

List of Figures

2.1	Yoshimura Pattern and Parameters[22]	7
2.2	Yoshimura Reconfiguration Method[24]	7
2.3	Kresling Pattern and Parameters[25]	8
2.4	Miura Ori Unit Cell[28]	9
2.5	TMP Pattern[29]	9
2.6	Research Objectives and Workflow	17
3.1	Telescopically deployed Yoshimura	21
3.2	Kresling deployment via lanyard	22
3.3	Kresling deployment via inflation	22
3.4	Yoshimura structure with boom deployment	23
4.1	Kresling geometric parameters	28
4.2	Grasshopper algorithm inputs	30
4.3	Polygonal planes	31
4.4	Expression Designer	32
4.5	Crease generation	33
4.6	Kresling origami structure	33
4.7	Kangaroo Constraints and Solver	34
4.8	Folding Controls	34
4.9	Folding Process	36
4.10	Outputs	36
5.1	Three cases with varying number of sides and fixed radius, $r = 5$ cm	39
5.2	Three cases with varying radius and fixed number of sides, $n = 5$	39
5.3	Measurement of inner radius	40
5.4	Measurements and Uncertainties - 5-sided polygon with fixed radius	45
5.5	Measurements and Uncertainties - 6-sided polygon with fixed radius	46
5.6	Measurements and Uncertainties - 7-sided polygon with fixed radius	47
5.7	Measurements and Uncertainties - Polygon with fixed sides and radius = 4.5 cm	48
5.8	Measurements and Uncertainties - Polygon with fixed sides and radius = 5.5 cm	49
6.1	Effect of origami structure parameters on usable inner volume	52
6.2	Effect of origami structure parameters on packaging ratio	53
6.3	Galapagos Solver settings	55
6.4	Reduced Rhino-Grasshopper model	56
6.5	Galapagos Solver - Optimisation	57
7.1	Snapmaker laser bed	60
7.2	Lightburn Interface	60

7.3	Lightburn - Flat Pattern	61
7.4	Kresling double units	61
7.5	Lightburn final settings	62
7.6	Lightburn sketch	63
7.7	Laser cut Kresling flat pattern	63
7.8	Original tab design - half an origami unit	64
7.9	Tabs created for attachment	64
7.10	Closed origami structure	65
7.11	Attached covering	66
7.12	Inflation setup	66
7.13	3D printed gripper	67
7.14	Inflation of paper prototype	68
7.15	Feasibility check of proposed material choice and manufacturing technique	71
7.16	Dual hot end extrusion technique	71
7.17	Solidworks Assembly	72
7.18	Cura preview	73
7.19	Mesh overlap at creases	74
7.20	Printed flat pattern	74
7.21	Welded tabs - flat pattern	75
7.22	Closed 3D printed origami structure	75
7.23	Printed top covering	76
8.1	ABAQUS origami model generation	78
8.2	Force-Displacement Plot	79
8.3	Contact definition error	80
8.4	Total Energy-Displacement Plot for Folding	80
8.5	Strain Energy-Displacement Plot for Folding	81
8.6	Strain Energy during folding and release	82
8.7	Displacement during folding and release	82
8.8	Strain Energy-Displacement Plot for Inflation	83
8.9	Stress Distribution	84
8.10	Strains after folding	85
8.11	Strains after folding force is released	85
8.12	Strains after inflation	86
9.1	Prototypes with radius 5 cm - increasing number of sides(left to right)	88
9.2	Prototypes with radius 4 cm - increasing number of sides(left to right)	88

List of Tables

3.1	Requirements Table	20
3.2	Design Options Generation	24
3.3	Design Options Trade-off	24
3.4	Telescopic Deployment - Weight Estimation	25
3.5	Inflation Deployment - Weight Estimation	25
4.1	Example - Input Parameters	37
4.2	Example - Output Parameters	37
5.1	Measurements and Uncertainties - Varying Number of Sides, Fixed Radius = 5 cm	43
5.2	Measurements and Uncertainties - Varying Radius, Fixed Number of Sides = 5	43
6.1	Optimised Parameters	57
6.2	Optimal Outputs	57
7.1	Laser engraving iterations	62
7.2	Prototyping Options Trade-off	69
7.3	PLA and TPU Material Properties[64]	71
10.1	Requirements compliance check	91

Nomenclature

Abbreviations

Abbreviation	Definition
AM	Additive Manufacturing
CAD	Computer-Aided Design
CFRP	Carbon Fiber Reinforced Polymer
CGG	Cool Gas Generator
DOF	Degree Of Freedom
DMC	Dual Matrix Composite
FDM	Fused Deposition Modeling
LEO	Low Earth Orbit
MM3DP	Multi-Material 3D Printing
PLA	Polylactic Acid
RSS	Root Sum of Squares
SMP	Shape Memory Polymer
STL	Standard Tessellation Language
TPU	Thermoplastic Polyurethane

Symbols

Symbol	Definition	Unit
V_F	Folded/Stowed volume	[cm ³]
V_D	Deployed volume	[cm ³]
H_F	Folded/Stowed height	[cm]
H_D	Deployed height	[cm]
n	Number of polygon sides	[-]
a	Polygon edge length	[cm]
r_1	Radius of inscribed polygon	[cm]
r_2	Apothem(Radius of inner polygon)	[cm]
d	⊥ distance from base vertex to valley crease	[cm]
l_b	Length of vertical mountain crease	[cm]
h_f	Flat pattern height of one Kresling origami layer	[cm]
h_{3d}	3D height of one Kresling origami layer	[cm]
η	Packaging ratio	[-]
θ	Twist angle	[radians]
ϕ	Angle between valley fold and vertical mountain fold	[radians]
γ	Angle between valley fold and horizontal mountain fold	[radians]
σ	Uncertainty	[cm]

1

Introduction

Due to the rising commercialisation and privatisation of the space industry[1], access to space is getting more and more affordable. Now more than ever, the interest in not just going up to space, but also living there, has increased manifold. To cater to this demand, over the past two decades, the space industry has been studying the best way to sustain humans in space for the long run. This has resulted in a few fruitful attempts like BEAM, the Bigelow Expandable Activity Module, an inflatable habitat module that is attachable to the ISS [2]. Axiom Space is currently building something similar, a commercial habitat module, though not inflatable[3]. However, there is still a long way to go with regard to optimising the way we take and operate large living and storage modules to space in an economically feasible manner.

As the demand to go to space rises, launch vehicle space is still at a premium. The limited volume available in payload fairings and the massive costs involved call for a solution that takes up as little space as possible[1]. Reducing the size of the habitats is not really a great option because a minimum living space is a must for human life. A potential solution would be to create a deployable module that is compressible down to a small volume for stowage in a launch vehicle, but that has a deployed volume of many times that of its stowage volume. The BEAM and the Axiom Space module, as mentioned before, have already explored this concept. The technologies used on BEAM were first developed for the TransHab module, a 36 ft long, 27 ft. diameter inflatable structure that was never flown[4].

Deployable structures have widely been used in the past for a multitude of space applications, most commonly, antennas, but also solar arrays, booms, and telescopes. There are several criteria that a deployable module must follow in order to be suitable for long-term use in space and these include deployability, rigidity, structural strength, low mass, high volume, low stowage volume[5][6], among others.

A concept that has recently begun to be considered for such an application is origami, the Japanese art of paper folding[5]. The traditional art form was historically used as a form of recreation or for religious purposes and has only recently, over the past few decades, been of interest for scientific applications. In origami, the structure is folded at pre-defined locations

(creases) and variations in origami are defined by unique crease patterns. Due to the ability of origami to dynamically change its structure and structural integrity to suit multiple objectives through geometric transformation, it is of interest in the scientific community, most recently, in the design of space structures.

Origami has several advantages and disadvantages, the advantages being its deployability, re-configurability, ability to self-actuate, tunability, and scalability[5]. These have proved to be very valuable for applications such as minimally invasive surgical equipment[7], adaptive and climate responsive architecture[8], artificial limbs[9], and many others.

These properties of origami have already proven to be an asset to designing for space; they have been used in the past for deployable booms[10][11], Starshade[12], antennas[13] and other applications, primarily as a space-saving mechanism. Researchers have now begun to try to translate the origami concept to much larger space structures. However, designing and testing on such a large scale on ground and in-orbit is not feasible due to large costs, facility size limitations, gravity effects, and so on[14]. From this project, we see that entire test facilities and new testing approaches had to be developed to test the structure and there were still many unavoidable constraints and implications. The TransHab inflatable module[4] also had a majority of tests conducted on sub-scale models due to size and cost limitations.

Over the past few decades, Cubesats have become a convenient testbed for such cases. CubeSats were first developed by the California State Polytechnic University and Stanford University's Space Systems Development Laboratory in 1999 by Prof. Jordi Puig-Suari and Prof. Bob Twiggs with the intent to open up access to space for educational purposes, reduce costs and development time, and allow for frequent launches[15]. Though initially used to give students hands-on experience with building spacecraft, CubeSats soon began to be sought for their commercial benefits as well, such as the easy availability of off-the-shelf components and less complex verification and validation procedures. The adoption of the standard CubeSat form factor by the commercial sector has also opened up a myriad of launch options and ridesharing opportunities, further bringing the cost down for users. CubeSats now provide a cost-effective platform for science investigations, new technology demonstrations and advanced mission concepts, allowing for testing in desired operating environments as opposed to ground testing.

Designing and prototyping a demonstrator that would fit in a CubeSat is an ideal way not just to test the deployment concept and origami pattern suitability on ground at a feasible cost but also to deploy it in orbit and monitor its performance. If successful, the proposed design can also be used as a test bench for future deployable structure applications. Since origami is largely scalable[5], this would allow us to translate the lessons learnt to a larger scale model with confidence in its capabilities.

In this thesis project, the aim is to design and prototype a deployable origami demonstrator that fits in a 12U CubeSat. This involves identifying suitable origami patterns, dimensions, materials, and manufacturing techniques and assessing structural performance.

The report starts with a brief look into the state-of-the-art in the field of origami deployable structures, followed by a description of the research methodology and the research questions being explored. In Chapter 3, a requirement analysis is done to identify key requirements to prioritise during the design process. This is followed by a discussion of the initial conceptual designs, which are traded off qualitatively. With the chosen design, Chapter 4 delves into the 3D modelling process, followed by the validation of the model with physical prototypes, as described in Chapter 5. Chapter 6 dives into the parametric study to observe the behaviour of the structure with variations in different parameters. Then, an optimisation process is conducted to identify an ideal configuration. Once an optimal design is chosen, a suitable manufacturing method must be identified. This process is described in Chapter 7. Next, Chapter 8 discusses the structural performance of the origami structure during and after folding and deployment. Based on observations during the design and prototyping process, a set of design guidelines are developed and laid out in Chapter 9. Chapter ?? looks into how the proposed design satisfies the requirements generated in Chapter 3. The final chapter discusses the answers to the research questions posed in Chapter 2 and provides some recommendations based on lessons learnt during the course of the project.

2

Research Framework

Over the past few decades, engineering origami has proved to be an intriguing concept for a variety of applications across fields like architecture and bio-medical engineering[5] to space structures and mechanisms like booms, antennas, and solar arrays[16][17]. This project aims to create a foundation for the design of large space structures. With the growing privatisation of space and access to space becoming increasingly affordable, more and more people want to go up to space and experience life there which will require much larger structures in space than currently feasible for living, working, and storage purposes. In order to create a pleasant experience, safety is of the utmost priority as well as making it as affordable as possible. To this end, the structures designed must be structurally sound and cost-efficient i.e., save space in the launcher, and hence, lower the costs. One of the most promising ways to do this is using origami patterns that are capable of being folded down to a much smaller volume than its operational configuration while also maintaining sufficient rigidity when in use.

This project will focus on developing a small-scale demonstrator that can be deployed from a 12U CubeSat into LEO in order to test the proposed deployment concept and origami design. A small-scale demonstrator design is proposed as testing a large-scale prototype in space can quickly become very expensive. Alternatively, relying only on ground testing will result in negligence of space effects that cannot fully be simulated on the ground. The outcome of this thesis will allow for a low-cost technology demonstration of deployable origami structures, thereby informing future work and contributing to a better understanding of the use of origami in large-scale deployable space structures.

This chapter provides a brief overview of the existing state-of-the-art in the field of origami deployable structures, followed by a discussion of the research questions, objectives and methodology.

2.1. Literature Study

To begin the engineering design process, it is first necessary to peruse the state-of-the-art in the associated field to obtain a clear understanding of the available options that could suit the research goals. To do so, a review of current literature is done. This section dives into existing work on the usage of various origami patterns for deployable structures, deployment mechanisms currently used for space applications, suitable materials for space structures, and conventional and new manufacturing techniques.

2.1.1. Origami Patterns

Origami structures have been used in the past for a multitude of applications in fields ranging from medicine to space exploration. Each of these applications has different requirements to adhere to, so no one origami pattern is considered superior to the rest. For deployable structures, certain origami patterns have been used for ground and space applications. There are several considerations to be made while choosing an origami pattern, and extensive studies have been carried out to identify appropriate patterns for different applications. Common criteria include bistability[18], flat-foldability[10], rigid foldability[5], high packaging ratio[10], controlled deployability[10], straight line deployment[10], and structural integrity before, during, and after deployment. The definitions of each of these criteria are as follows.

- **Bistability:** Refers to the structure's ability to maintain stability in two configurations, which in the case of deployables, are the deployed and folded configurations. This is a desirable property as the origami would then be able to self-lock itself in the deployed configuration requiring minimum actuation energy[19].
- **Flat-foldability:** Some origami patterns are considered to be flat-foldable. This means that the fold angles of the mountain and valley folds have a maximum value of $-\pi$ to π [5], [6], [20].
- **Rigid foldability:** This is an assumption that the facets do not deform during folding and unfolding, and the only deformation is at the crease lines. This assumption can be made for a high-level analysis, but facet deformation does occur as it stretches and compresses, and to understand its effect on deployment accurately, it is necessary to model these as well.
- **Packaging ratio:** This is defined as the ratio of stowed volume to deployed volume, which is to be minimised as far as possible.

$$\eta = \frac{V_F}{V_D} \quad (2.1)$$

where,

V_F = *Folded volume*,

V_D = *Deployed volume*

Considering a constant radius and cylindrical shape, the packaging ratio can be simplified as follows.

$$\eta = \frac{H_F}{H_D} \quad (2.2)$$

where,

$H_F =$ *Folded height*,

$H_D =$ *Deployed height*

Increasing the number of creases is a tried-and-tested method to reduce the packaged height of origami structures, but also negatively affects the stresses experienced [21]. This ratio is an especially important criterion for any deployable in space because saving volume in the launch vehicle (and hence, costs) is one of the primary objectives and would allow for larger deployables to be sent to and deployed in space.

- **Straight-line deployment:** This is important if the structure is to serve a scientific objective like antennas. Not doing could result in structural issues and derail the mission. In [10], it was proven that certain patterns are more inclined to straight-line deployment than others, and these are usually ones with only 1-DOF. Multiple patterns were studied to find out which one has the best performance in terms of straight-line deployment, and it was found to be Miura Ori. Further, can also be tuned by varying certain geometric parameters like the fold angle.

Yoshimura Pattern

The Yoshimura pattern is a triangular mesh buckling pattern that was first observed when a thin cylinder was subjected to axial compression[22]. It is made of repeating diamonds i.e., triangles sharing a single edge. A half unit of the Yoshimura pattern is depicted in Figure 2.1a, which when repeated in the axial and circumferential directions, generates the whole pattern as shown in Figure 2.1b.

A cylinder with this pattern is extremely stiff in the axial direction, which is ideal for deployable structures like antennas and booms. However, the pattern is not rigid-foldable, so, on compression, it experiences increasingly larger strains on its facets and creases, thus being unable to maintain its internal envelope and axis. Senda et al.[23] studied the deployment characteristics of a Yoshimura-based boom, and it was found to have much worse straight-line deployment than a Miura-ori boom.

However, some studies have been conducted to identify a folding method other than compression for better packaging of the cylinder. The cylinder is transitioned from its operational configuration to a bellows-like folding configuration, obtained by strategically pushing certain vertices inwards. In this configuration, the cylinder was found to be less resistant to axial compression and exhibited lesser deformation[24]. While this is a possible way to utilise the Yoshimura pattern for a deployable structure, the extra actuation required to bring the cylinder to its intermediate configuration may require more power, more mechanisms, and, generally, more overhead.

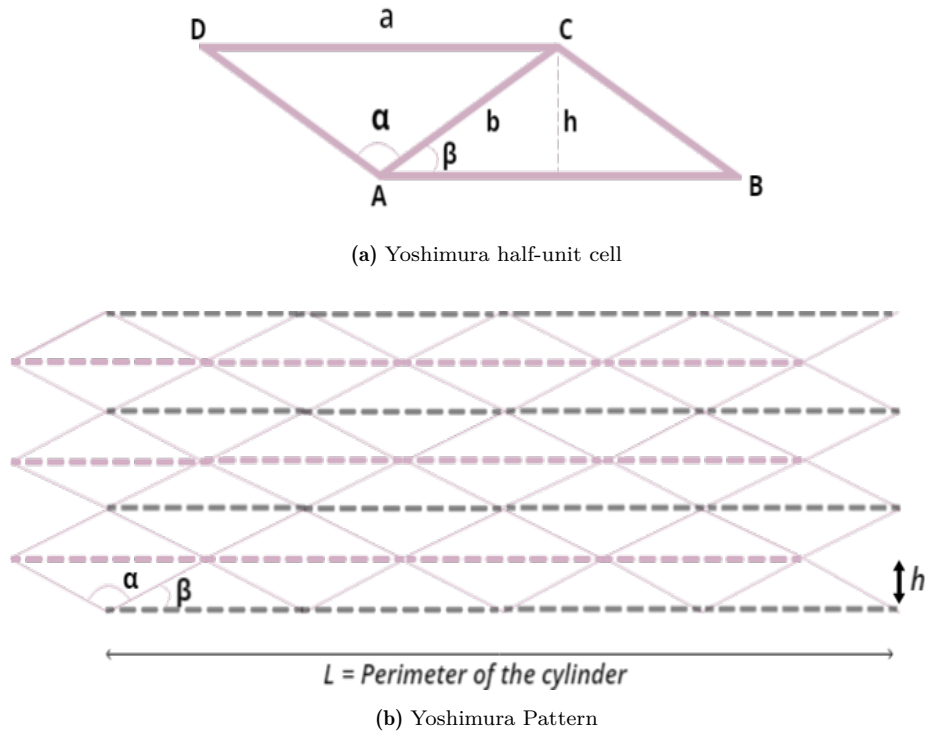


Figure 2.1: Yoshimura Pattern and Parameters[22]

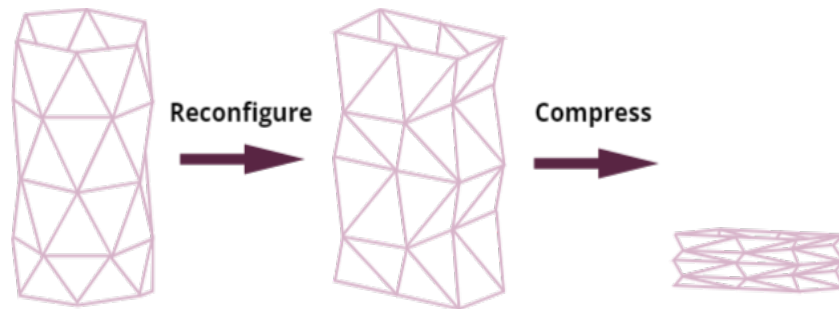


Figure 2.2: Yoshimura Reconfiguration Method[24]

Kresling Pattern

When a thin-walled cylinder is subjected to axial twisting, it gives rise to the Kresling buckling pattern, characterised by alternating mountain and valley folds angled in the direction of the applied twist[25]. It is not rigidly foldable, however, it may be bistable in some configurations. This means it will not require extensive facet deformation to fold down to its fully stowed state. The Kresling unit cell is depicted in Figure 2.3a.

Studies have shown that the Kresling pattern exhibits tuneable stiffness and bistability and can bear large loads by exploiting a mechanical diode-like effect to lock into a deployed state[26]. Kidambi et al.[27] found that the Kresling pattern is not always bistable but can have its geometrical parameters tuned to fluctuate between mono-, bi-, and multistability, also confirmed in a compression test by Lee et al.[18]. Each of these conditions can be suitable for different deployment strategies depending on the deployment accuracy needed and the forces available to compress the cylinder to a compact state. It is to be noted that changing between mono-,

bi-, and multistability does not depend on the material of the structure, which is an advantage as any material can be used for its construction.

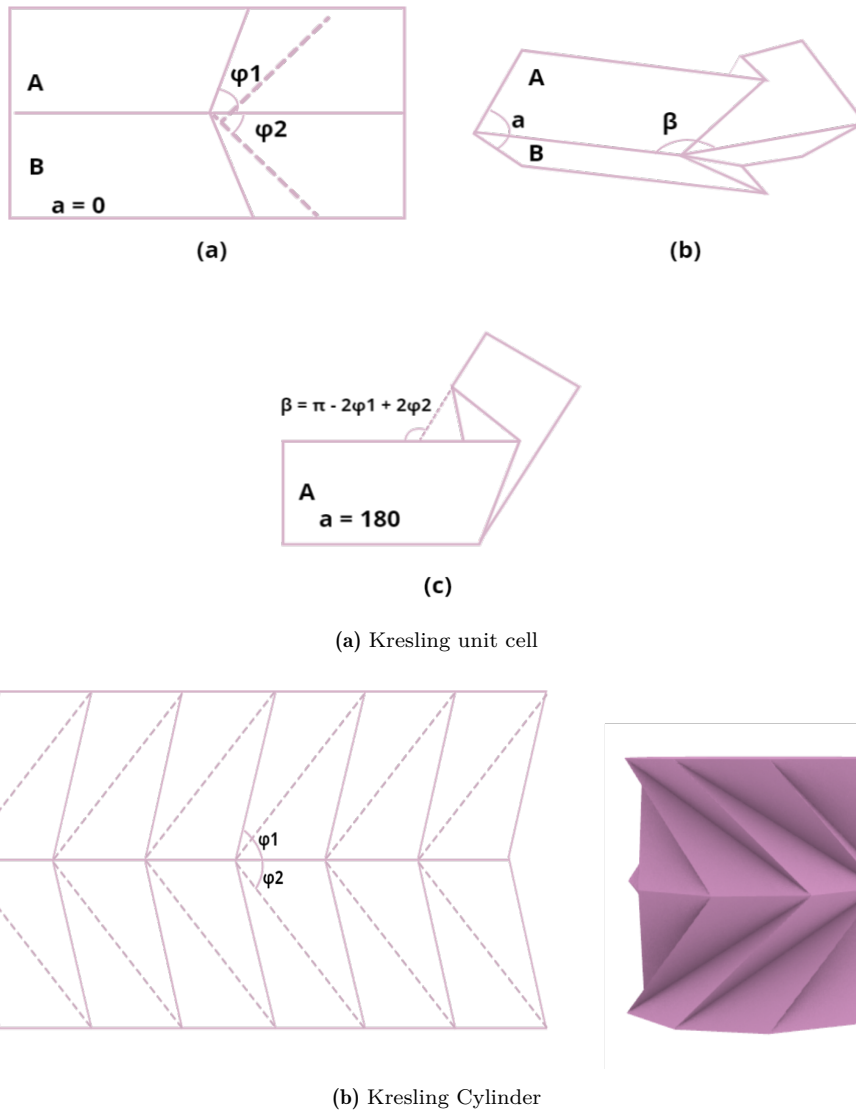


Figure 2.3: Kresling Pattern and Parameters[25]

Miura-Ori Pattern

The Miura-Ori origami pattern is by far the most sought-after for deployable structures. It is characterised by parallelograms as shown in Figure 2.4. In one direction, the creases are formed by zigzag lines alternating between mountain and valley folds and in the other direction, the creases are formed by straight lines alternating between mountain and valley folds. Sheets of the pattern can be combined to form a cylindrical structure. The pattern has particularly desirable characteristics for a deployable structure, like its rigid-foldability, 1-DOF mechanism, negative Poissons ratio, and a large packaging ratio[28].

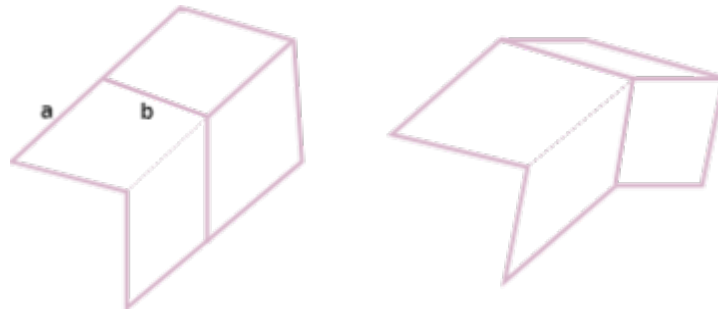
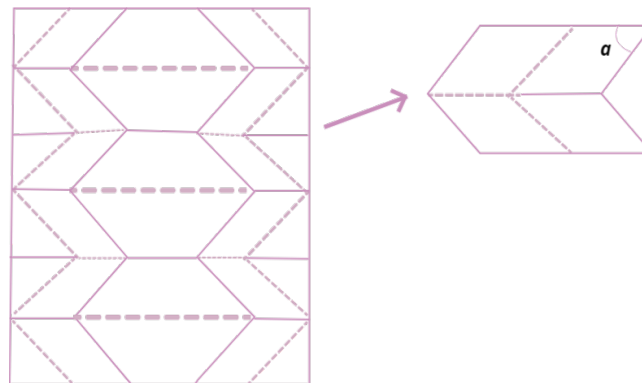


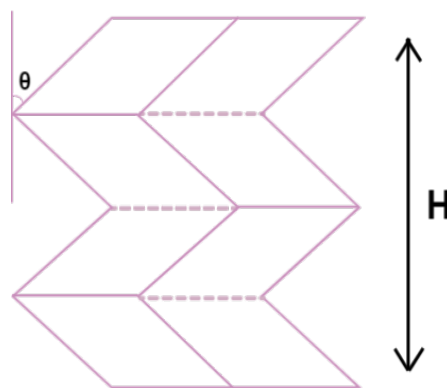
Figure 2.4: Miura Ori Unit Cell[28]

Tachi-Miura Polyhedron(TMP)

The Tachi-Miura polyhedron is formed by joining the classic Miura-Ori pattern with its mirror image[29]. The TMP folding pattern includes horizontal main folds as well as sub-folds that are creased at an angle to the main fold. While folding, the main folds remain parallel to the base of the polyhedron; however, its cross section keeps changing, rendering it hard to form a sealed structure which, depending on the application, may be considered an unsuitable feature. The TMP unit cell is shown in Figure 2.5.



(a) TMP - Miura cell highlighted



(b) TMP Closed Structure

Figure 2.5: TMP Pattern[29]

The TMP polyhedron has the advantage of being rigidly foldable while filling a three-dimensional space[29] i.e., deforms only at the creases and not at the facets during compression. The crease pattern can also be modified to have a range of Poisson's ratios, from positive to negative[30].

2.1.2. Deployment Mechanisms

The deployment mechanisms are split into two broad categories: Strut structures and surface structures[31][32].

- **Strut Structures:** These structures resist loads by elements being in tension, compression, or bending. This includes scissor hinge mechanisms(or pantographs), sliding mechanisms, and hinged collapsible strut mechanisms.
- **Surface Structures:** These structures resist loads by continuous elements, which mostly carry tension forces. This includes inflatable or pneumatic structures, folded structures, and telescopic structures.

This work focuses only on surface structures as the aim is to develop a simple, lightweight system, whereas strut structures involve many mechanical parts, adding to the weight and complexity of the system.

In this review, telescopic deployment, deployment via inflation, and lanyard deployment are discussed.

Telescopic Deployment

Telescopic structures consist of cylindrical or rectangular sections that fit inside one another. They have been used in telescopic masts that are deployed either sequentially using a spindle and nut mechanism or simultaneously using cables and pulleys. Some applications also use pneumatic deployment of telescopic sections, like in [33], which reduces the mechanical complexity and the number of moving parts in the system.

While telescopic deployment might be an option to consider for the origami structure inside a CubeSat, the length and volume limitations could be a problem when scaled up to a larger structure such as a habitat or storage unit.

Inflation

Inflatable structures are those that are either air-inflated or air-supported, but for the purpose of classifying deployable mechanisms, they shall be considered as an air-inflated structure. In Merchan's description[32], it is evident that the inflation is not necessarily achieved by air but by any two elements inducing a pressure differential to inflate the structure.

This deployment method has low stowed volume and few mechanical parts, reducing complexity. However, it does require gas to be carried on board for inflation and supplementary gas to hold it in its deployed configuration, thereby adding to the mass of the spacecraft. This extra mass can be avoided to some extent if a rigidisation mechanism can be used, such as strain hardening, UV curing, and thermal curing. Inflation is a particularly attractive option due to the above advantages and because it has already been studied alongside origami structures which may be a viable method of folding for inflatable structures[11].

Inflatable structures have considerable spaceflight heritage—they have typically been used for antennas, booms for solar arrays and sails, and, less commonly, for bases and research modules such as the Bigelow Expandable Activity Module(BEAM). Other examples are the ECHO

balloons launched by NASA in the 1960s[34] and the Inflatable Antenna Experiment[35].

Conventionally, a pressurised gas system is used to inflate a structure in space, but this is very heavy and complex, with a possibility of leakage. It is also not easy to miniaturise. The ECHO I and II communication satellites[34] used a different inflation system involving sublimation compounds. This method could be unreliable as uniform heating is not guaranteed. The rate of inflation is also unpredictable.

In the recent past, a Dutch research institute, TNO, developed Cool Gas Generators(CGGs) as an alternative to other forms of inflation and propulsion[36]. A cool gas generator uses a solid propellant charge in which the gas is chemically stored. On initiation, the gas is released at an ambient temperature and the rest of the propellant stays in the generator as slack. These generators are compact, have a long storage time, and since cool gases are used, no thermal problems will arise.

Lanyard Deployment

In the past, lanyard deployment has been used as a means of deploying coilable masts. The lanyard is attached to a top plate that rotates to deploy the coiled mast. The coiled longerons of the mast straighten on complete deployment, and the tensioning diagonals preload the trusses to provide rigidity to the structure. The lanyard in the middle controls the rate of deployment. The Astromast uses this mechanism to deploy antennas, instruments, and cameras[37].

While it may not be possible to use this method exactly as is, the idea of a rotating central guide to deploy the origami pattern could be useful. The structure can derive its stiffness from the rigidised origami pattern instead of the truss cables.

2.1.3. Materials and Manufacturing

An important consideration to be made for the design of the origami structure is the choice of material. There are several materials that have great space heritage and are suitable for the Low Earth Orbit environment. There are several other materials that have promising properties but have not been used widely in space so far. Five types of materials will be discussed together with the associated manufacturing techniques, namely fabrics, metallic materials, composites, shape memory polymers, and thermoplastics.

Fabrics

Fabrics are considered a viable option for deployable structures due to attractive properties such as their flexibility. Commonly used materials in space are Mylar, Kapton, and Nylon, amongst others.

Mylar is a thin sheet of flexible, transparent plastic, often PET film, that is coated with a metallic reflecting agent, giving it its metallic sheen and attractive thermal insulation properties[38]. It provides mechanical support and flexibility, while the thin layer of metal provides reflectivity. The fabric is highly homogeneous and exhibits isotropic elastic behaviour. However, its susceptibility to rips and punctures, which is partly dependent on its thickness, is a concern. While thin sheets are desirable for maximum compactness, thicker sheets will be more resistant to punctures which is also a desired quality for any structure exposed to the

space environment.

Kapton is a thin polyimide thermoplastic material, considered to be space-grade due to its ability to function across a wide range of temperatures (cryogenic upto 400 ° C), high resistance to UV radiation(>100 MRad) and atomic oxygen, and low outgassing.

Aluminised Kapton foil was first used in space aboard the Apollo Lunar Module descent for thermal protection during re-entry, giving it its golden colour[39]. In addition to thermal insulation for spacecraft, Kapton is widely used in flexible printed circuits. These are its primary uses, but it has also been considered for use potentially in solar sails as plastic support.

For fabrics, the hand fabrication method is used. The mountain and valley folds of the origami pattern are embossed onto the fabric using a pen while tracing the fold lines from a separate sheet of paper. The creases are then folded by hand to create the pattern. It is then formed into a cylinder by welding or using an adhesive[40]. Wilson et al.[12] also used hand folding to create a Kresling fold pattern, and small holes were punched at the vertices for stress relief. This method may be suitable for a small prototype, but larger ones will require a more standardised, precise method.

Metallic Materials

Metals have long-standing flight heritage and have been the most trusted and used materials in spaceflight since its inception. This can be attributed to their well-documented and tested properties like high strength, low weight, fracture resistance, and high resistance to atomic oxygen. A drawback to note is, all metals have the tendency to cold weld in the vacuum of space i.e., fuse together. Some of the most commonly used metals for load-bearing space structures are aluminium and titanium.

Aluminium is the most commonly used metal in spacecraft structures due to its low density, low cost, high strength-to-weight ratio, easy availability, and machinability. Aluminium has a binding energy of 28.36 eV, making it resistant to degradation due to atomic oxygen and can therefore be used as a protective coating.

Aluminium laminates sandwiching a thin polymer film have extensive spaceflight heritage, especially in inflatable structures. The ECHO-I communication satellite used a 12.7 micrometre Mylar film with a thin layer of aluminium vapor deposited on it[34]. For its successor, the ECHO-II satellite, Aluminium-Mylar laminates were used. A 9-mm Mylar film was sandwiched between two layers of 4.5mm thick aluminium foil. While ECHO-I required a make-up gas system to keep the balloon inflated, ECHO-II had the possibility of being strain rigidised[41]. The balloon could be inflated to a pressure where the aluminium layers were stretched beyond their yield point while the Mylar remained elastic. This resulted in a smooth, rigid structure.

Manufacturing origami structures is challenging. The process must be highly controlled since deployment properties depend on the fold parameters. There is the possibility of stress concentrations at the vertices resulting in pinhole fractures and cracking due to reversal of fold direction. Schenk et al.[11] explored two approaches.

In one approach, the Al-Mylar laminate was sandwiched between pre-folded cardstock paper. It is then folded into the cylindrical configuration upon which the fold lines are transferred to the laminate. The cardstock is then removed and the laminate is sealed in position. This method involves placing the seam in the structure at the end of the process.

In another approach, the structure is manufactured as a straight cylinder and then compressed in a controlled manner to form the required origami geometry with the help of a master sheet. This process ensures that there is no misalignment of the seam and is, therefore, preferred to the previous approach.

Titanium is another extremely lightweight metal widely desired for aerospace applications due to its low coefficient of thermal expansion, high strength, high melting point, corrosion resistance, and good damping properties. The most commonly used titanium alloy is Ti-6Al-4V, in propulsion systems for its thermal resistance and in optical bench flexures for the low CTE to maintain instrument accuracy[42]. They are also used in fuel tanks due to their long-term chemical compatibility with fuels[43]. However, it is expensive and difficult to manufacture.

Dual Matrix Composites(DMCs)

Dual matrix composites are a subset of High Strain Composites(HSCs). High strain composites act as a lighter, monolithic alternative to structures with mechanical, non-integral hinges[44]. These composites are capable of large deformations but also possess high stiffness, allowing them to carry structural loads. Stiff fibres in a softer matrix allow HSCs to attain large deformations without undergoing phase transformations(like superelastic metallic alloys) which means they can be strained and released repeatedly.

Dual Matrix Composites(DMCs) utilise the high flexibility of a soft matrix alongside a stiffer polymer matrix to create localised flexible hinge regions within the composite resulting in a stiff composite in the load-bearing sections and a softer composite at the folding regions. These composites have garnered considerable interest in the field of deployable space structures but are yet to be flown.

Sakovsky et al.[45] developed and hand-fabricated a wide band antenna for CubeSats using a dual matrix composite. The materials used were Astroquartz fiberglass, UV cured silicone for the creases, and epoxy for the stiff regions. L'Garde[44] has developed a carbon fiber composite material which is embedded in a stiff polymer matrix in load carrying regions, and soft silicone matrix in the flexible hinge regions. This allows for deformation of the composite structure at the hinges without much damage as the elastic microbuckling in the brittle fibers prevents them from breaking.

One caveat with these composites is that a reliable manufacturing method has not yet been established. Hand fabrication can be done but is a painstaking task, requires extreme precision and is not a viable option if a product is being developed for mass production[46].

Shape Memory Polymers(SMPs)

Shape memory polymers are a type of smart material that possess dual shape capability, transitioning from one shape to another on the application of some external stimuli like heat or light. For heat-activated SMPs, for example, while the temperature is below its glass transition temperature T_g , the structure can be folded or deformed to reduce its volume. On application of the requisite heat, the structure is deployed and rigidised in its final configuration. It is also reconfigurable as the temperature can be changed as required. Thermoset SMPs, in particular, are desired for their high material stiffness, transition temperature, and environmental durability. These materials are advantageous due to their low cost, low density, and high strain capacity. However, pure shape memory polymers have low strength and recovery stress, and therefore, several applications resort to the use of fibre reinforced shape memory polymer composites(SMPCs)[47].

SMPC hinges provide better deployment characteristics than conventional tape spring hinges, but there are some issues. The usage of discrete hinges by itself adds a layer of complexity to the origami structure, which will have a large number of elements that need to be deployed individually. Moreover, having a heat-activated deployment mechanism is considered somewhat unreliable if depending entirely on solar radiation and may take a significant amount of time to deploy fully. On-board heating is cumbersome as it requires extra power and volume for the heating mechanisms, which may be feasible for a larger satellite but not so much for a space-restricted CubeSat.

Suh et al.[24] used a laser cutter to create a perforated pattern along the crease lines of the shape memory polymer to act as a compliant hinge. The SMP was then hand folded at the creases. Another study used a vacuum-forming process to mold polymer into a Miura-ori cylinder[48]. However, it cannot be manufactured in one step, it requires two sheets to be bonded together to form the required cylinder.

Thermoplastics - Additive Manufacturing

Thermoplastics are materials that are pliable above a certain transition temperature and rigidise upon cooling. This phase transition is reversible due to which they can be easily molded, extruded, or formed into various shapes using methods like injection molding, blow molding, and extrusion. Thermoplastics like polylactic acid(PLA), acrylonitrile butadiene styrene(ABS), and thermoplastic polyurethane(TPU) are used extensively in many industries, like automotive[49], aerospace[50][51], and medicine[50][52], for rapid prototyping as well as for end-use components.

PLA in particular, is easily manufacturable and non-toxic, making it useful for medical applications[53]. It is stiff with a glass transition temperature of 60-70 ° C and a melting point of 170-180 ° C. So, it does not lose plasticity or toughness with use[54]. It has been used in space applications such as to build CubeSat buses[55] and satellite antenna prototypes[56]. However, PLA is brittle which limits the scope of its applications.

While PLA is used to create rigid structures, another material in this category, thermoplastic polyurethane(TPU), is used to build more flexible parts. TPU is made of two segments-its

flexibility comes from its soft segment, which is polyester or polyether, while the toughness is provided by the carbamate segments. It is characterised by a low elastic modulus and high toughness. TPU is often used in applications that require mechanical strength while also being flexible, such as automobile interiors and industrial tools, providing high resistance to impact, fatigue, and stress.

Given the rigidity of PLA and the flexibility of TPU, a combination of these two materials to form origami structures is considered. Thermoplastic materials like these are most commonly manufactured by 3D printing.

Additive manufacturing (AM) or 3D printing is the manufacturing of a 3D object layer by layer from a digital design. Fused deposition modeling (FDM) is the most widely used additive manufacturing technology due to its accessibility and easy-to-moderate learning curve[3]. Thermoplastic filament is softened, extruded from a nozzle, and deposited in layers. FDM is especially ideal for applications that do not require high resolution and surface finish, such as for early-stage prototypes and proof-of-concept models. Conventionally, FDM only allows for printing with a single filament which greatly limits the mechanical properties and functionalities of the products that can be built.

In the case of origami, if the entire structure is printed with rigid material, it can withstand loads but will not be foldable, whereas if it is printed entirely with flexible material, it is foldable but foregoes its load-bearing capacity.

However, in the past decade, multi-material 3D printing (MM3DP) has become increasingly popular. Printing with more than one material allows for a range of mechanical properties within a single part which also reduces the need to manufacture separate components and assemble them, thereby reducing production cost and time. It does also pose some problems, like the possibility of weakened interfaces between the two or more materials due to usage or environmental changes.

Faber et al.[57] developed a spring origami which uses rigid ABS for the origami facets printed onto rubbery TPU. The spring exhibits origami like folding but the interfacial bonding between the two materials was expected to weaken along the folding lines, causing delamination and hence, structural failure. Ye et al.[58] developed a method to design and print thick-panel origami that can support large cyclic loads under compressive strain. In this method, the rigid panels made of PLA are wrapped and joined by stretchable TPU, effectively avoiding delamination at the material interfaces. However, it is not clear if the origami structure thus formed will be able to maintain its folded configuration as required for the current project or spring back to its unfolded state.

As a whole, additive manufacturing presents some difficulties as well, that are yet to be overcome. A key disadvantage is that the dimensions of the 3D printed parts are limited to the print bed size, which, for most commercially available low cost printers is about 25 x 25 x 30 cm³ i.e., not very large[59][60]. This limitation is not a dealbreaker for a small-scale technology demonstrator like the current project but, for larger structures, multiple print cycles have to

be run, and individual parts will require assembly.

With this literature review, the usage of PLA for the rigid origami panels and TPU for the flexible creases, manufactured by multi-material 3D printing seems to be a promising option. The exact 3D printing setup and parameters are to be determined with further study.

2.2. Research Questions

This section defines the research questions and goals the thesis work aims to achieve. These will serve as a foundation upon which the research is carried out and helps develop a plan of action for the course of the project. The formulation of these research questions is a result of careful consideration of available resources and a thorough review of existing literature. By systematically addressing these questions, meaningful insights and evidence-based conclusions are offered to contribute to the field of origami-inspired deployable space structures.

Main Research Question

How can an origami-based deployable structure be designed for integration with a 12U CubeSat while ensuring structural integrity during and after folding and deployment?

To answer this question, a series of sub-questions have been formulated, as listed below.

1. What origami pattern and deployment mechanism combination is suitable for simple, predictable, and repeatable deployment?
2. What pattern configuration is ideal for maximising inner volume and minimising packaging ratio?
3. How can the proposed origami structure be manufactured?
4. How do the folding and deployment loads affect the structural integrity of the proposed structure?

2.3. Research Objectives and Methodology

For any engineering design process, a set of requirements is of primary importance to constrain the design space and provide goals to optimise. First, the requirements for the design of the CubeSat origami demonstrator are defined, taking into account the loads and space environment conditions it must withstand and CubeSat specifications and restrictions, among other aspects. Additionally, mission requirements are defined that must be satisfied to attain the research goals defined. Defining a set of requirements will help conduct trade-offs based on the extent to which different options satisfy them. Based on these, the workflow outlined in Flowchart 2.6 is executed to achieve the research objectives detailed below.

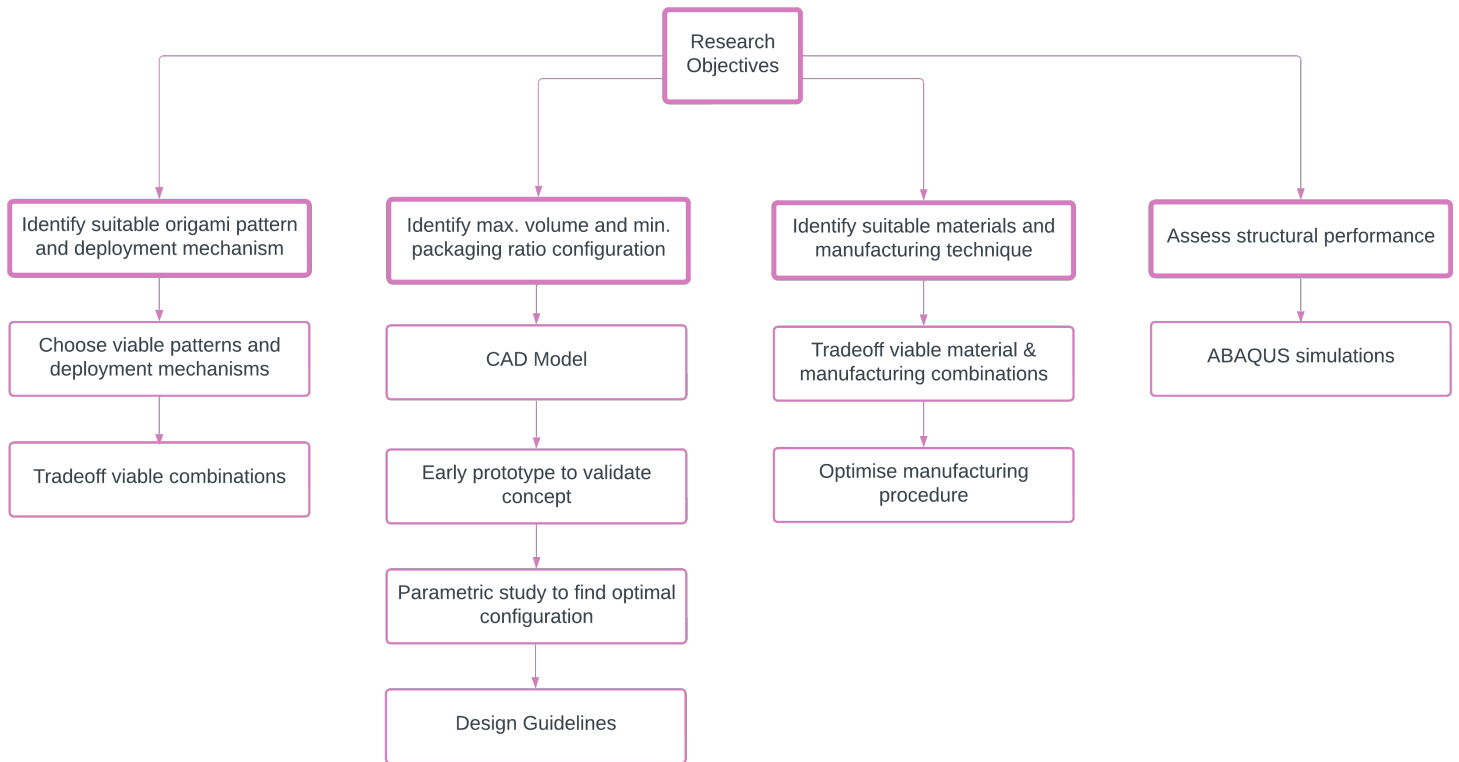


Figure 2.6: Research Objectives and Workflow

Objective 1: Identify suitable origami pattern and deployment mechanism

The next step is selection of the origami pattern to be used for the demonstrator. 2-3 suitable patterns are picked based on the literature study conducted. Similarly, feasible deployment concepts are chosen. However, all patterns are not compatible with all deployment techniques; therefore, a brief compatibility assessment is done. From here, pattern and deployment combinations are finalised, then traded off based on mission-critical criteria derived from the requirements.

Objective 2: Identify optimal configuration for maximum volume and minimum packaging ratio

Once a concept is chosen, the origami structure is modelled in CAD software, Rhino, using existing origami theory to define geometric parameters. The model is then validated using prototypes made of paper. The validated model is used to conduct parametric studies and identify an optimal configuration for maximum inner volume and minimum packaging ratio. At this stage, a set of design guidelines are defined that can be used to design origami structures for the aforementioned optimisation criteria.

Objective 3: Identify suitable manufacturing technique

To validate the chosen configuration, the origami structure is to be manufactured. The materials and manufacturing options presented in the literature study are traded off. Then, the chosen manufacturing procedure is optimised for enhanced prototype quality and function. Following this, a suitable joining method is chosen to create a closed 3D origami structure. The feasibility of the inflation concept should also be checked for which laser-cut paper prototypes are initially used early in the project timeline.

Objective 4: Assess the structural performance of the proposed structure

Once the structure is manufactured, it is replicated in ABAQUS to observe its behaviour during folding and deployment.

Finally, with the manufactured model and the observed structural performance, the defined requirements are verified, and recommendations are made for future work.

3

Requirements and Concept Generation

This chapter first discusses the requirements generated as a result of mission objectives, requisite system functions, and constraints. In the first section, the requirements are listed along with the rationale, verification criteria and acceptance criteria. With these requirements in mind, four design concepts are generated as discussed in the consequent section. The two most viable options are traded off, resulting in one concept chosen for further design.

3.1. Requirements Table

The requirements are sorted into three categories: driving and killer requirements, and constraints. The three types are defined as follows.

- **Driving Requirements:** These are requirements set by the stakeholders that strongly define how the system is designed and built. They guide design choices and details. These requirements use the identifier **ORI-DRI**.
- **Killer Requirements:** These are requirements which, if not satisfied, make the system completely nonfunctional i.e., they are tied to the success or failure of the project. These requirements use the identifier **ORI-KIL**.
- **Constraints:** These can be defined as non-negotiable specifications that certain parameters have to adhere to such as dimensions, costs, regulations etc. These use the identifier **ORI-CON**.

Table 3.1: Requirements Table

ID	REQUIREMENT	RATIONALE	ACCEPTANCE CRITERIA	VERIFICATION METHOD
ORI-KIL-1	The origami structure must be able to withstand deployment(unfolding) loads	The structure will be deployed from its folded to unfolded functional configuration in space. To be considered functional, it must maintain structural integrity throughout and after deployment.	The structure does not break or deform during deployment	Deployment test and simulation
ORI-KIL-2	The origami structure must be able to withstand compression(folding) loads	The structure will be transported to space in its folded configuration. In order to later deploy to its functional deployed state, it must remain structurally sound under the forces holding it in compression, without breaking or deforming.	The structure does not break or deform during folding	Folding test and simulation
ORI-DRI-1	The origami structure shall be deployable multiple times	The structure is intended to be scaled up for use in applications like habitats, research bases, and fuel tanks, which will require folding and unfolding in multiple locations, multiple times. The structure has to be deployable without significant damage over multiple cycles.	The structure does not break or deform during multiple folding and unfolding cycles	Deployment and folding tests, simulations
ORI-CON-1	The origami structure in its stowed configuration shall have a volume no larger than 100 mm x 100 mm x 150 mm	It is estimated that other subsystems in the 12U CubeSat besides the payload will occupy a maximum volume of 6U, leaving a volume of 6U for the origami structure. Taking tolerances into account, the dimensions 100 x 100 x 150 mm ³ are specified ¹ .	The folded configuration has a volume of no larger than half a 12U CubeSat, in accordance with tolerances, i.e., 100 x 100 x 150 mm ³	Measurement of model and prototype
ORI-CON-2	The origami structure shall not weigh more than ~10 kg (~41% of 24 kg)	According to SE guidelines ² , the payload occupies approximately 41% of the satellite weight, which for the case of a 12U CubeSat is ~10 kg.	The prototype has a weight of <=10 kg	Weight measurement of the prototype
ORI-DRI-2	The origami structure shall exhibit a predictable deployment	It is necessary to ensure that the structure deploys in the desired direction, at a constant rate, without any deviations. Undesirable behavior such as getting stuck in an intermediate state, deploying at an unpredictable rate or in the wrong direction makes the design concept unreliable.	The prototype deploys in the correct direction at a consistent rate and does not get stuck during deployment.	Observation
ORI-DRI-3	The origami structure shall be rigid once deployed.	For the intended applications of the deployable structure, it is necessary that it remains in its deployed configuration once deployed.	The prototype shall not revert to its folded configuration after deployment is complete.	Observation
ORI-DRI-4	The origami structure shall be deployable from a stowed to unfolded configuration of atleast twice the height.	The intent behind using origami folding techniques is to get large structures to space. To do so, the origami folding mechanism has to provide a sufficiently large deployed-to-stowed height ratio to choose it over a conventional deployable structure.	The deployed height of the prototype is atleast twice the height of the folded structure	Height Measurement
ORI-DRI-5	The material of the origami structure shall be easily available	Since the purpose of the current structure is to act as a technology demonstrator, the materials used to manufacture it must be easily attainable at a low cost.	The material is affordable and easily accessible for purchase online or in store	Observation
ORI-DRI-6	The chosen manufacturing technique must be accessible	Since the purpose of the current structure is to act as a technology demonstrator, the manufacturing facilities and equipment must be easily accessible without requiring excessive bureaucracy, training, or financial resources.	The manufacturing technique should be an existing one, accessible by institutional staff, and inexpensive to use.	Observation

¹I. Uriol Balbin and P. Solano Lopez, *Preliminary study of an origami-inspired deployable structure for a small-scale demonstrator*, 73rd International Astronautical Congress (IAC), Paris, France, September 2022.

²W. J. Larson and J. R. Wertz, *Space Mission Analysis and Design*. Dordrecht: Kluwer Academic Publishers, 2005.

3.2. Design Concepts

This section deals with the selection of a suitable origami pattern and deployment mechanism for the proposed deployable structure. Four design concepts are proposed from which the two most viable candidates are further studied and traded off based on the defined requirements. A winning candidate is chosen as the final design concept from the trade-off.

3.2.1. Design Concepts

Solution 1: Telescopically deployed Yoshimura structure

The proposed solution is a telescopically deployable structure based on the Yoshimura origami pattern.

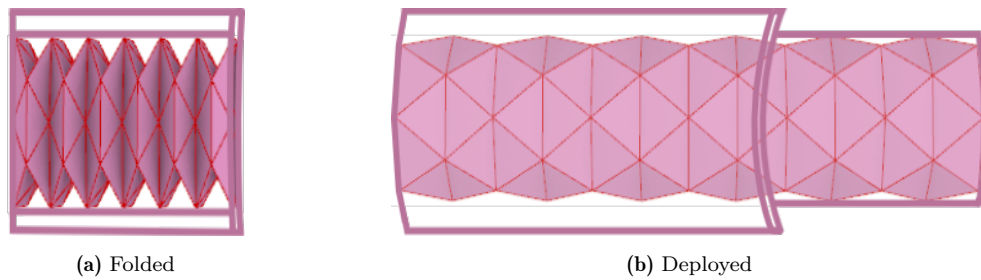


Figure 3.1: Telescopically deployed Yoshimura

Pattern Choice: Yoshimura. The Yoshimura pattern only compresses axially and does not rotate. Therefore, it is considered suitable for telescopic deployment as it can be deployed linearly.

Deployment Mechanism: Telescopic. This method is chosen as the pattern only deploys linearly, and telescopic deployment facilitates that. Telescopic deployment also allows room for some rotation, but this is considered insufficient for the amount of rotation certain origami patterns need to deploy.

Additional systems: Motor to drive extension.

Description: The mechanism consists of a tube contained within another tube of larger circumference. The origami structure is mechanically attached to the rim of the inner tube such that it can be unfolded while the tube is deployed. Guide rails along the inside of the larger tube allow for smooth deployment and add stiffness to the structure. To lock the structure in place, ball pins or latches on the smaller tube latch onto tapered holes or latches on the rim of the large tube.

Brief Analysis: It is a simple, retractable mechanism with considerable flight heritage. However, it poses a length and volume limitation due to the tubes being nested within each other.

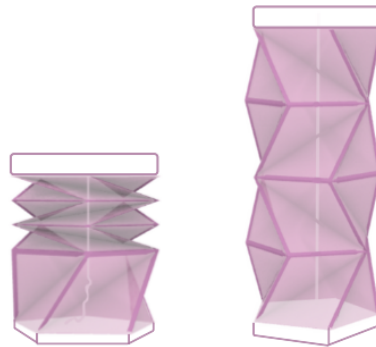
Solution 2: Kresling pattern deployment via lanyard

Figure 3.2: Kresling deployment via lanyard

Pattern Choice: Kresling pattern. This pattern has a slight rotation to it in its cylindrical form, which makes it a viable match for the proposed lanyard deployment.

Deployment Mechanism: Lanyard. A central motor-controlled lanyard attached to a plate is used to unfold the origami structure similar to antennas and space instruments deployed in the past[37].

Description: A motor-controlled lanyard attached to a top and bottom plate is allowed to unfold, with some rotation as the Kresling pattern calls for, until the rope/wire is taut and the structure is fully deployed, which is detected by in-built microswitches.

Brief Analysis: The proposed method is a retractable, controlled form of deployment. However, there is a risk of deformation due to uncontrolled twisting. This method is also completely new, has no flight heritage, and will require an in-depth study of its mechanics to understand its behaviour.

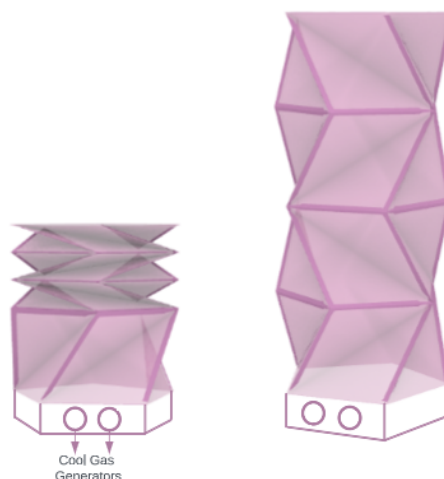
Solution 3: Kresling deployment via inflation

Figure 3.3: Kresling deployment via inflation

Pattern Choice: Kresling pattern. Several origami patterns are compatible with inflation deployment, but the Kresling is chosen due to its tunable bistability[26], and relative ease of folding in comparison to the Yoshimura pattern, which is stiff in the axial direction. Additionally, each layer of the Kresling structure can be made bistable, so they can be deployed and collapsed independently of one another.

Deployment Mechanism: Inflation. Cool gas generators(CGGs) placed beneath the structure can be used to deploy it as well as pressurise it to maintain the deployed configuration if required.

Description: CGGs are placed beneath the folded Kresling structure and used to deploy it to its full length. CGGs are chosen as they are compact, lightweight, and store gas at an ambient temperature.

Brief Analysis: Since there are no additional mechanical parts, the stowed volume is much lower than other solutions. The gas is maintained at an ambient temperature, so there is no risk of thermal problems. However, once deployed, depending on the material used, it may not be possible to revert to the folded configuration. This could be a problem, depending on the application of this concept.

Solution 4: Yoshimura structure with boom deployment

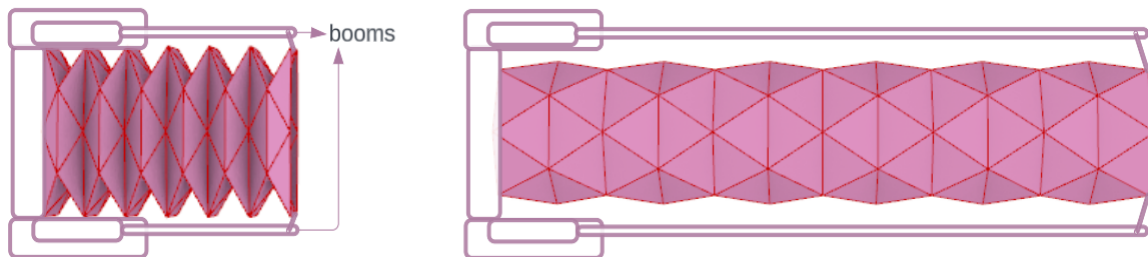


Figure 3.4: Yoshimura structure with boom deployment

Pattern Choice: The Yoshimura pattern is proposed to deploy via booms as they deploy linearly.

Deployment Mechanism: Via Triangular Rollable and Collapsible(TRAC) booms. These booms have a flat surface that can be attached to the origami structure to deploy it.

Description: Two TRAC booms along the length of the Yoshimura structure are used to unfold it to its fully deployed configuration. The edges of the origami structure are attached to the tips of the booms with grommets, split rings, or hooks.

Brief Analysis: The proposed system is quite heavy and runs the risk of asynchronous deployment as the two booms have to deploy at exactly the same time and rate, which is a precision level that is hard to achieve. It does, however, offer guided deployment.

Table 3.2: Design Options Generation

Concepts	Solution 1	Solution 2	Solution 3	Solution 4
Specifications				
Pattern	Yoshimura	Kresling	Kresling	Yoshimura
Deployment	Telescopic	Lanyard	Inflation	Booms
Advantages	Simple, retractable, has flight heritage	Retractable, controllable	Lower stowed volume, no temperature problems	Guided deployment
Disadvantages	Length and volume limitation	Risk of deformation due to excessive twisting, no flight heritage	Depending on material, may not be retractable	Heavy, risk of asynchronous deployment

The four proposed options are summarised in Table 3.2, from which Solutions 2 and 4 are discarded for the following reasons.

- **Solution 2:** Complex analysis is required, whereas the current thesis work is more focused on developing a complete system which may not be possible if just this analysis of its behaviour is time-consuming.
- **Solution 4:** The system is too heavy to be miniaturised to fit within 6U, per the requirements.

Now that the design space has been narrowed down to two concepts, they can be traded off based on certain criteria defined according to the requisite functionalities and constraints.

3.2.2. Design Option Trade-Off

Next, the two design concepts, telescopic deployment of a Yoshimura structure and inflation of a Kresling structure, are traded off on a qualitative basis. The reasons for choosing the trade-off criteria are detailed below, followed by justifications for the choices made.

Table 3.3: Design Options Trade-off

Tradeoff Criteria	Weight	Usable Inner Volume	Scalability	Deployment Predictability
Design Concepts				
Yoshimura via Telescopic Deployment	Excellent	Meets requirements	Average	Excellent
Kresling Deployment via Inflation	Meets requirements	Meets requirements	Average	Excellent



- **Weight:** The weight of the structure is a crucial constraint as the present demonstrator must fit within a 12U CubeSat(**ORI-CON-2**) and even if scaled up, lightweight systems are desired to reduce launch costs. Below are the weight estimations for each option. For the telescopic deployment, a three-stage setup with CFRP tubes is assumed.

Table 3.4: Telescopic Deployment - Weight Estimation

Telescopic Deployment			
Component	No. of items	Weight per item (g)	Total weight (g)
Telescopic Tubes	3	60	180
Motor, nuts, spindles	-	~100	~100
TOTAL WEIGHT			~280

Table 3.5: Inflation Deployment - Weight Estimation

Inflation Deployment			
Component	No. of items	Weight per item (g)	Total weight (g)
Cool Gas Generators	2	8	16
Feed lines, ignition device	-	~100	~100
TOTAL WEIGHT			~116

The telescopic deployment setup is heavier than the inflation. The majority of its weight comes from the multiple tubes, whereas the additional systems add up to approximately the same weight as the inflation system. The weight of the origami structure itself is not considered here, assuming it is the same pattern with the same dimensions for both cases.

- **Usable Inner Volume:** The demonstrator, if successful, is intended to be scaled up for use in applications like fuel tanks and habitats where maximum space is desired inside the deployable structure(**ORI-DRI-4**).

The telescopic system consists of multiple tubes nested in each other, occupying considerable space, thereby not leaving much volume available for the actual intended application of the structure. For instance, consider a two-stage telescopic deployment system with a deployed height of 30 cm and a diameter of 10 cm for the largest telescopic section and 8.8 cm for the secondary tube, considering a wall thickness of 3 mm.

$$Available\ Volume(cylindrical) = \pi r^2 h = \pi \cdot (4.4)^2 \cdot 30 = 1824.64\ cm^3 \quad (3.1)$$

For an inflatable structure, a straight cylinder with the same diameter of 10 cm is considered.

$$Available\ Volume = \pi r^2 h = \pi \cdot (4.7)^2 \cdot 30 = 2081.93\ cm^3 \quad (3.2)$$

The difference in available volume is,

$$Volume\ Difference = \frac{2081.93 - 1824.64}{2081.93} * 100 = 12.35\% \quad (3.3)$$

As shown in Equation 3.3, with just one additional tube within the structure, the available volume reduces by 12.35%. The inflation system does not have any obstructive elements within the volume of the structure; the CGGs are only placed below it. Therefore, the inflation deployment system performs better in terms of available volume for a structure of the same radius.

- **Scalability:** As the current project is a small-scale technology demonstrator to validate the deployment concept, it must also be scalable to the sizes the concept is meant to be used at.

The telescopic system can only be scaled up to a certain extent until the available volume is so low due to the nested tubes that the design concept is not feasible anymore. The inflation system performs better in this regard, having had flight heritage with much larger structures, but could potentially have weight issues with the amount of inflation gas required onboard for a much larger system.

- **Deployment Predictability:** For the intended applications, the deployable structure may be deployed and folded multiple times during testing, transportation, and operation. Exhibiting predictable behaviour across multiple deployment cycles is crucial to building a reliable system(**ORI-DRI-2**).

Both forms of deployment, the telescope and inflation, perform similarly in terms of predictability. The telescopic option provides guided deployment, whereas the predictability of an inflation system depends on the origami pattern used. In this trade-off, the Kresling pattern is chosen, which can exhibit predictable straight-line deployment, given a controlled source of air[23].

From the trade-off table, it is evident that **the most favourable design concept is the Kresling structure deployed via inflation**. It performs similar to or better than the telescopic deployment in every criterion and is, therefore, the concept that is chosen for further detailed design in the following chapter.

4

Modeling

This chapter goes into detail about the modelling of the Kresling origami structure. First, the Kresling geometric parameters are discussed. The deployable structure is then discussed as a whole - important parameters, equations, and definitions. Following the theoretical background, a detailed description of the modelling of the structure on the algorithmic 3D modelling software, Rhino3D is presented. At the end of this chapter, the aim is to have a clear understanding of the parameters at play in the deployable structure and how these are modelled.

4.1. Kresling Cylinder Geometry

This section serves to provide a deeper insight into the geometric parameters of the Kresling pattern. As discussed previously, the pattern is formed as a result of a thin-walled cylinder subjected to axial twisting.

For the current project, the flat pattern parameters are first generated, which can be used for manufacturing. Values extracted from these parameters are used to define the 3D structure for modelling. The flat pattern is as shown in Figure 4.1a. The mountain folds, defined as the folds protruding towards the viewer, are the horizontal and vertical folds in black. The valley folds, protruding inwards, are the diagonals in pink.

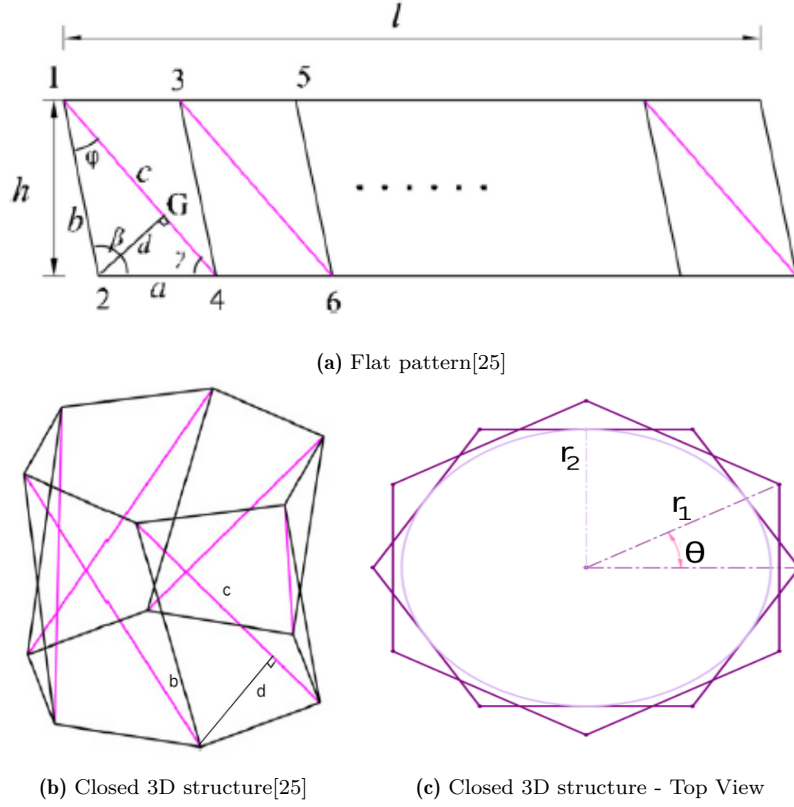


Figure 4.1: Kresling geometric parameters

The edge length, a , of the base polygon is calculated as:

$$\text{edge length, } a = 2r_1 \sin \frac{\pi}{n} \quad (4.1)$$

where r_1 is the radius of the inscribed polygon.

The angle between the vertical mountain fold and the horizontal mountain fold, β , is defined as:

$$\beta = \pi - \phi - \gamma = \frac{n-1}{n} \pi - \arcsin \frac{nd}{l} \quad (4.2)$$

where

ϕ = angle between the valley fold and the vertical mountain fold,
 γ = angle between the valley fold and the horizontal mountain fold,
 n = number of polygon sides

The twist angle θ (see Figure 4.1c) is the angle through which each consequent polygon rotates with respect to the base polygon in order to generate the Kresling cylinder. This is given by the equation:

$$l_b = \sqrt{h_{3d}^2 - 2r^2 \cos \theta + 2r^2} \quad (4.3)$$

where,

h_{3d} = height of one layer of the Kresling cylinder

l_b = length of vertical mountain crease

On the flat pattern, the perpendicular distance from a base vertex to the valley crease, d , is given by:

$$ah_f = d(d \cot \phi + \sqrt{a^2 - d^2}) \quad (4.4)$$

where,

h_f = height of one layer of the flat Kresling pattern, as shown in Figure 4.1a

With these geometric parameters defined, the 3D structure can be modelled, and the flat pattern parameters can be derived for use in manufacturing.

It is to be noted that with the current design process starting from 3D geometric inputs, no specific consideration has been made to design for bistability. Previous work done in this field only focuses on designing for bistability when starting from a flat pattern, not a 3D structure. Though when manufactured, in some configurations, the structure exhibits bistable behaviour, the current work does not predict this.

4.2. Deployable Structure

As per the requirements and tolerances determined in previous work by Uriol Balbin and Solano Lopez[61], the origami deployable structure is designed to have a fixed radius of 5 cm and a maximum stowed height of 15 cm. Throughout this report, various terms are used to define different important parameters. These are defined below to avoid confusion.

- **Stowed(Folded) Height(H_F):** The height of the origami structure when it is folded down completely. This height should be lower than the corresponding length of the CubeSat.
- **Deployed Height(H_D):** The height of the origami structure when it is fully deployed. At this point, tension cannot unfold the structure any further.
- **Packaging Ratio:** The ratio of the folded volume(or folded height) to the deployed volume(or deployed height) of the structure, as defined in Section 2.1.1. This is one of the parameters to minimise so as to get as compact a structure as possible.

$$\eta = \frac{H_F}{H_D} \quad (4.5)$$

- **Outer Volume:** This value is the volume occupied by the origami structure as a whole. When deployed, it is the deployed outer volume; when stowed, it is the stowed outer volume i.e., the volume it occupies within the CubeSat, which has to fit within 6U. This is calculated as volume of a cylinder, with the radius of the inscribed polygon, r_1 .

$$Outer\ Volume = \pi r_1^2 H \quad (4.6)$$

where,

H = deployed or folded height

- **Total Inner Volume:** This is the total volume on the inside of the structure, calculated by taking into account the wall thickness, t . The inside of the origami structure has valley folds protruding into it, creating some crevices. The volume added by these crevices is also accounted for.

- **Usable Inner Volume:** This is the inner polygonal volume that is actually available for use once deployed, calculated with the radius of the inner cylinder, r_2 . This value does not take into account the crevices, as these are considered to be obstructions, and the space cannot be used. This is another parameter that has to be maximised, considering the potential applications of the proposed design concept.

$$Usable\ Inner\ Volume = Inner\ Polygon\ Volume = \frac{1}{2}nar_2H_D$$

where,

n = number of polygon sides,

a = edge length,

r_2 = inner radius of the polygon

4.3. 3D Modelling

Next, to model the origami structure, the Rhinoceros 3D CAD modelling software is used in conjunction with the Grasshopper plug-in. Initially, the modelling was attempted with Solidworks, but Grasshopper was chosen instead as it allows for simple block-based visual programming, parametric modelling, and intuitive control of parameters. Additional plug-ins like Kangaroo and Galapagos are used for further functionality, to be discussed later.

Using this software, the cylinder-like deployable origami structure is created and parameterised. Each segment of the algorithm is explained below.

The first step is to generate the origami pattern in a 3D polygonal form.

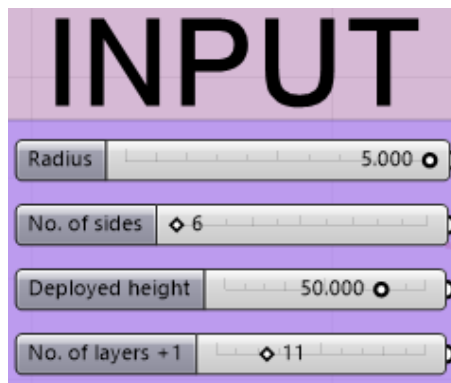


Figure 4.2: Grasshopper algorithm inputs

The given inputs, as shown in Figure 4.2, are:

- **Radius of the polygon** - Has an upper limit of 5 cm, adhering to pre-defined limits for the CubeSat demonstrator as discussed in the requirements(**ORI-CON-1**).
- **Number of sides** - Number of polygon sides. This parameter ranges from 5 to 15 sides i.e., limited to 3x the radius of the base polygon. The upper limit is such that the structure will pose manufacturing and folding difficulties beyond this value, as discussed in Chapter 9.

- **Deployed height** - This parameter refers to the total deployed(unfolded) height of the origami structure. The lower limit has been set to 30 cm since it is preferred to have the deployed height be at least twice the maximum folded height, as stated in the requirements(**ORI-DRI-4**). The upper limit has been set to 60 cm.
- **Number of layers** - This parameter allows the definition of the total number of origami layers in the structure. The lower limit has been set to 2, the minimum required to observe folding. The upper limit correlates to the number of sides and is set to 31 i.e., $(2*\text{number of sides}) + 1$, as explained in Chapter 9.

Using these four inputs, it is possible to calculate all other parameters needed to generate the origami cylinder and the flat pattern for manufacturing, as previously discussed in section 4.1. These parameters include:

For the 3D cylinder

- θ - **Twist angle**

For the flat pattern,

- ϕ - **Polygon angle**
- **a** - **Edge length**
- β - **Angle between valley fold and vertical mountain fold**
- **d** - **Perpendicular to the valley crease**

The aforementioned parameters for the 3D figure are used to generate the origami structure with the Kresling pattern as shown in Figure 4.6. The steps taken to do so are as follows.

1. The calculated twist angle(θ) is fed into a Series module which generates multiple instances of the twist value. This will later be used to define rotation.
2. Multiple instances of the base polygon are also created using the Series module, depending on the number of layers given as input, as shown in Figure 4.3.

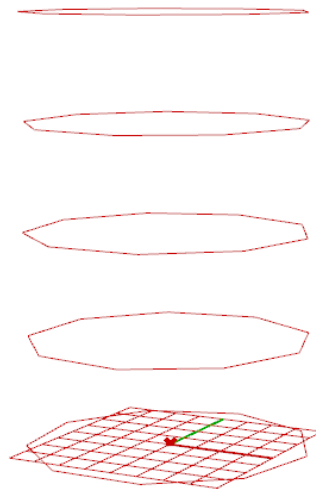


Figure 4.3: Polygonal planes

3. To define the rotation of each layer, a condition has to be imposed based on the twist angle. This is done using the Expression Designer module, as shown in Figure 4.4, where x is the θ value. Here, the assumption is made that for a twist angle below 0.55 radians, the model rotates each polygonal plane in alternating directions, and for angles greater than 0.55 radians, rotates only alternate planes in a single direction. The output of the Expression Designer is fed into Rotate modules that rotate the polygons accordingly.

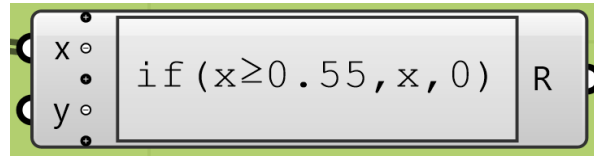


Figure 4.4: Expression Designer

4. At this point, only the rotated polygons exist. These have to be connected with line segments to generate the Kresling cylinder. To do so, first, the positions of each vertex of each polygon are stored in lists. To understand how the line segments are defined, consider three consequent polygons A, B, and C. Polygons A and B form the first origami layer. To create the vertical mountain creases, the list of vertices of polygon B is shifted by +1. So, each vertex of polygon A is connected diagonally to the corresponding vertex of polygon B, as shown in Figure 4.5a. Next, to create the valley creases, the vertices list of polygon B is shifted by +1 again. This creates a diagonal line segment from A to B as shown in Figure 4.5b. This process is repeated between polygons B and C, by shifting the vertices list of C in the opposite direction. The resultant mountain and valley creases are shown in Figures 4.5c and 4.5d. All these individual line segments are combined to form a single geometry using the Curve feature.

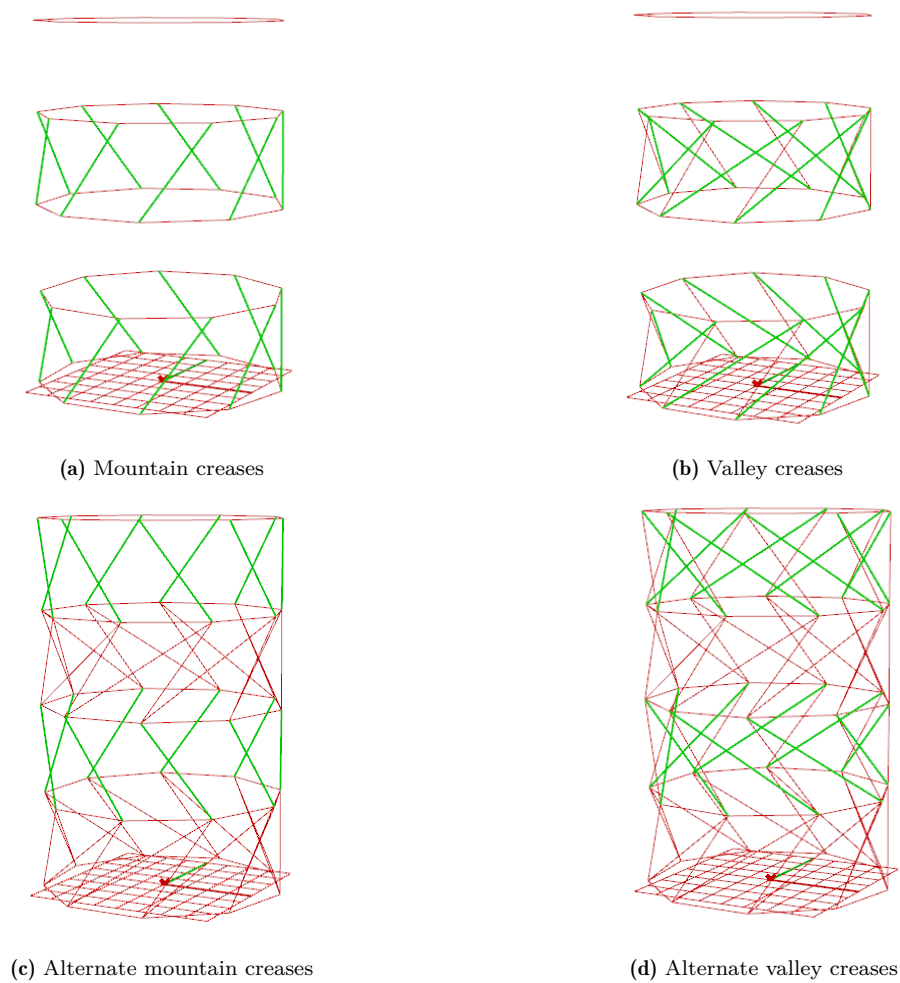


Figure 4.5: Crease generation

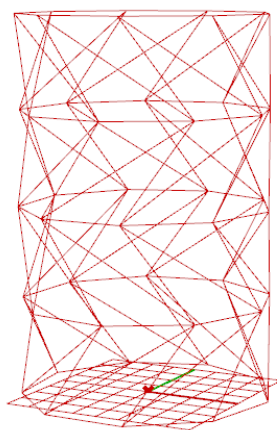


Figure 4.6: Kresling origami structure

The next step is to depict the physical behaviour of the origami structure and generate a meshed model. To do this, the Kangaroo plug-in for Grasshopper is used. The Kangaroo physics engine allows for interactive simulation, form-finding, optimization and constraint-solving[62]. It consists of a solver library and a set of Grasshopper components.

First, the constraints are defined. The objective is to simulate folding of the structure such that each layer collides with the layer below it, pushing it downwards to form a fully folded structure.

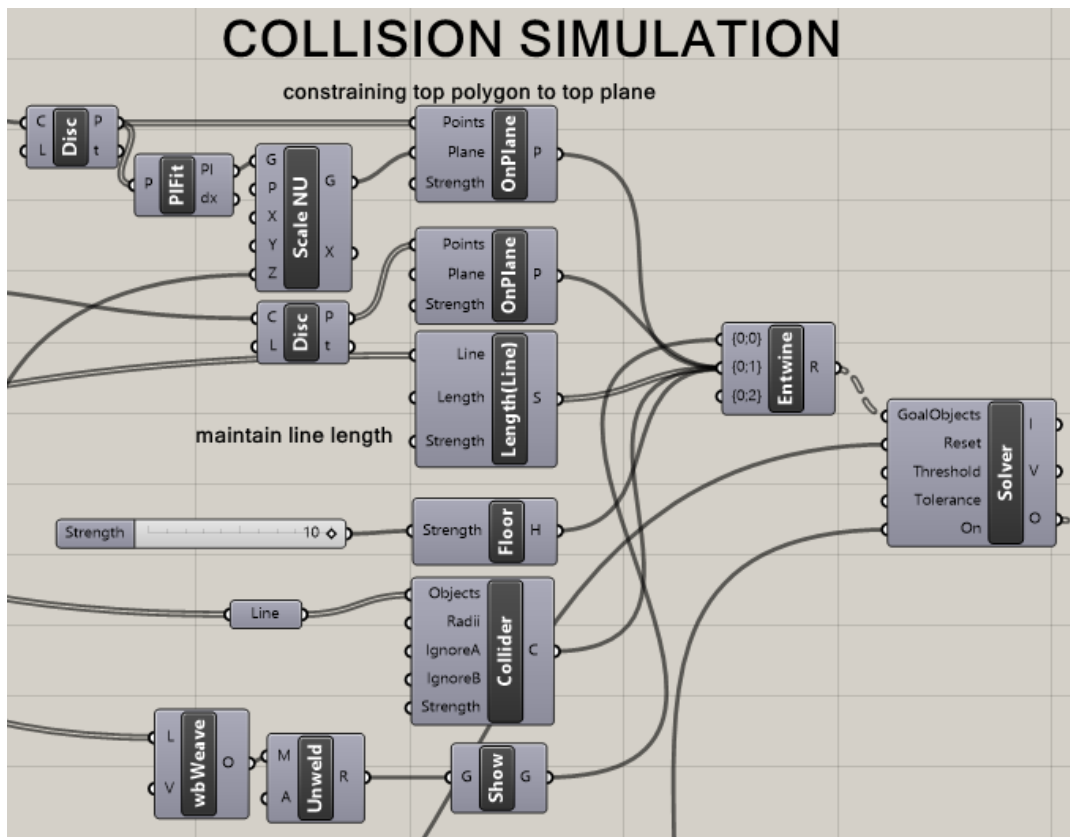


Figure 4.7: Kangaroo Constraints and Solver

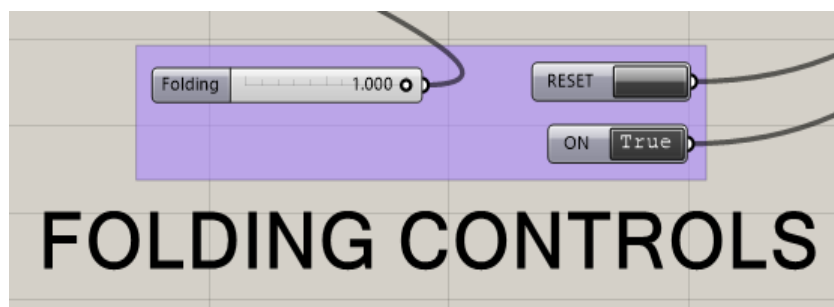


Figure 4.8: Folding Controls

The constraints, as depicted in Figure 4.7, are described below.

- Two planes are defined, one at the bottom of the first layer and another on top of the last layer. The topmost plane is scaled non-uniformly i.e. the plane will facilitate folding by scaling only in the Z direction using the Scale NU(Non-Uniform) module. To this module, a folding slider is attached, which forms the crux of the folding simulation. This slider can be used to fold and unfold the structure as required.
- An OnPlane constraint is used to ensure that the top plane remains attached to the vertices of the topmost polygon. This is repeated for its bottom-most counterpart.
- A length constraint is used to ensure all crease lines(mountains and valleys) remain the same length during the folding simulation. This is done in order to avoid warping, which will distort the overall structure and lead to an inaccurate representation of its behaviour.
- A floor constraint is used to ensure that while folding the structure, it remains on the XY plane and does not get pushed below it i.e., it defines a ground surface.
- A collider module is used to facilitate collision between all the line segments.

All of these constraints are combined and fed into the Kangaroo Physics solver. The solver is connected to a reset switch and a Boolean toggle to turn the solver on and off, as shown in Figure 4.8. The output of the solver is the meshed structure shown in Figure 4.9 with all the defined constraints applied to it, allowing folding and deployment of the origami structure.

To get accurate inner volume and stowed height, the mesh is thickened to a desired thickness of 0.3 mm to mimic the thickness of the prototype, as discussed in Chapter 7. To calculate volumes, it is necessary to have a closed structure. This is done using the CapEx module, which closes the thickened mesh by capping the top end, as can be seen in Figure 4.9c.

This concludes the pattern generation and simulation part of the algorithm.

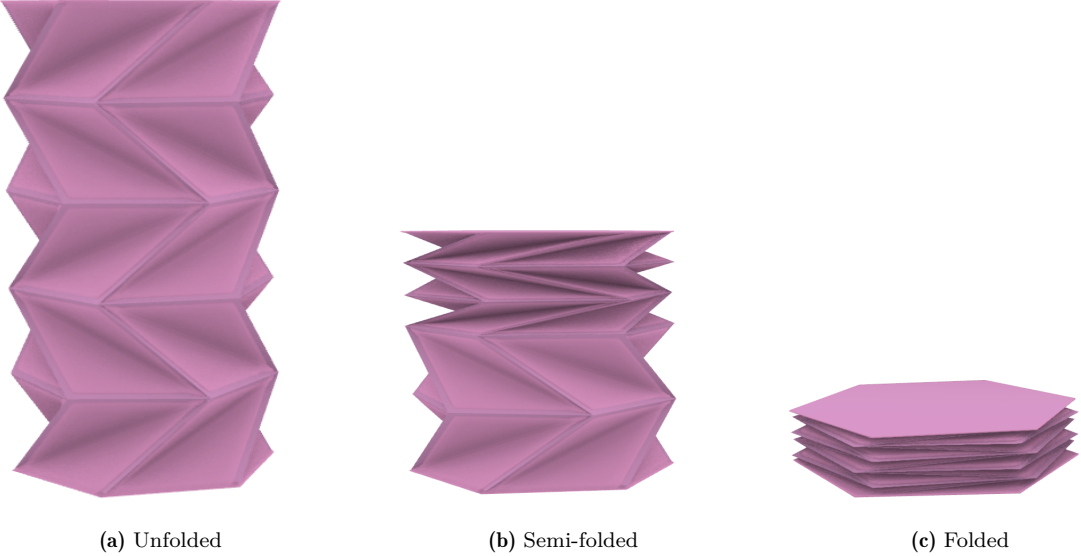


Figure 4.9: Folding Process

The next step is to extract the required outputs, as shown in Figure 4.10.

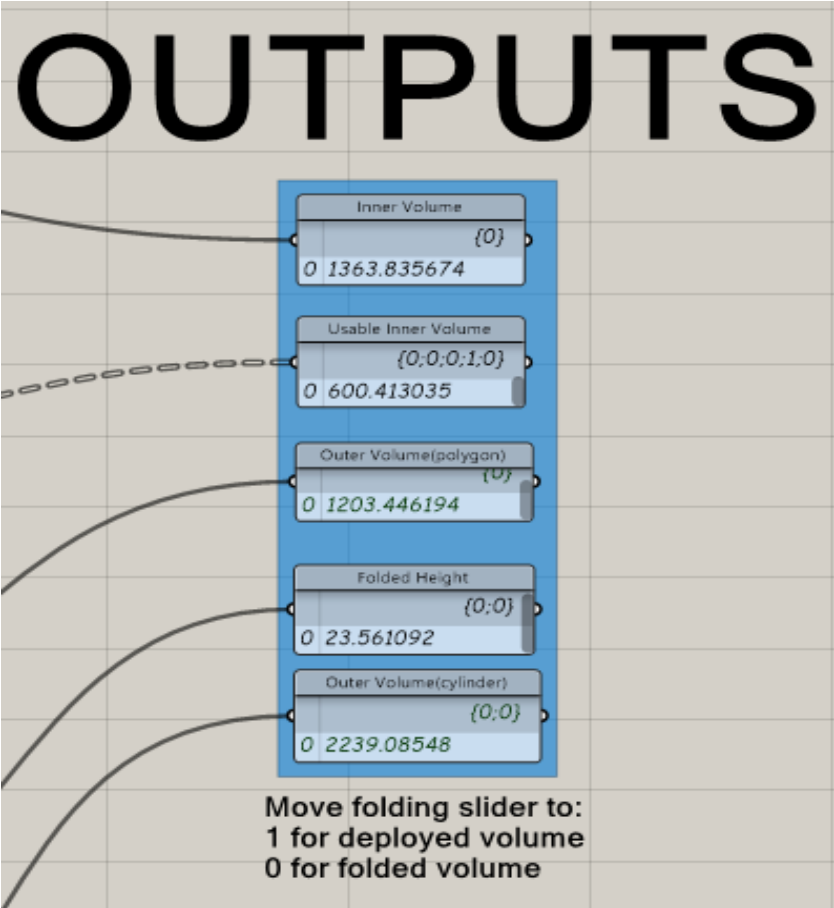


Figure 4.10: Outputs

The outputs are:

- **Outer Volume**
- **Total Inner Volume**
- **Usable Inner Volume**
- **Stowed Height**

To illustrate the functioning of the model, an example is provided below in Tables 4.1 and 4.2. The tables define the example input parameters and the generated outputs for the 3D structure and the flat pattern for manufacturing.

Table 4.1: Example - Input Parameters

INPUTS	
Parameters	Values
Radius	5 cm
No. of sides	6
Total height	22 cm
No. of layers	5

Table 4.2: Example - Output Parameters

3D OUTPUTS		FLAT PATTERN OUTPUTS	
Parameters	Values	Parameters	Values
Outer Volume	1726.3 cm^3	Twist angle θ	.7 rad
Total Inner Volume	1134.84 cm^3	Edge length	5 cm
Usable Inner Volume	591.09 cm^3	Mountain angle β	2.03 rad
Folded Height	1.93 cm	Vertical mountain fold length	5.57 cm

To conclude, this chapter outlines the key aspects of the modelling approach and the capabilities of the generated Rhino model. Before this model can be used for further steps in the design and optimisation process, its outputs have to be validated with physical prototypes. This is done in the following chapter.

5

Validation

With any digital model created to represent a physical system, it is necessary to validate its behavior, and the most reliable method to do so is to compare its properties and outputs with that of the physical system. This chapter discusses the validation process for the Rhino model. First, a brief description of the physical prototypes is provided, followed by a description of the measurement process. These measurements are compared with that of the Rhino model, along with an error analysis. These are represented in plots with error bars to show the discrepancies between the model and the prototypes. Following the validation process, it is determined if the model is adequately representative of the physical prototype.

Paper prototypes are created by laser-etching the origami creases onto 0.5 mm thick sheets of paper. The flat pattern is generated by laser cutting, and the pattern is then folded into a cylindrical structure, as shown in Figures 5.1 and 5.2. The complete procedure is detailed in Chapter 7 and will, therefore, not be elaborated upon here.

The validation process is conducted for a number of cases as listed below:

1. Three cases of varying number of polygon sides for a fixed radius(see Figure 5.1)
2. Three cases of varying radii, for a fixed number of sides(see Figure 5.2)

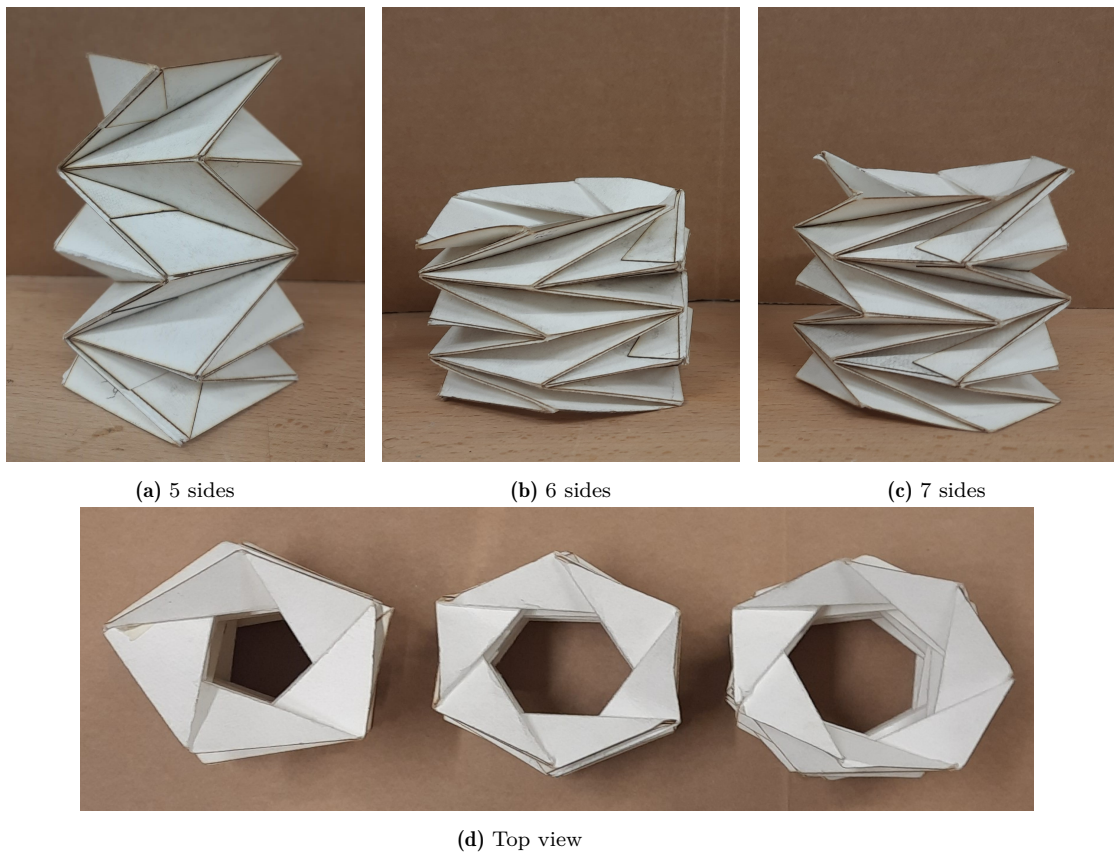


Figure 5.1: Three cases with varying number of sides and fixed radius, $r = 5$ cm

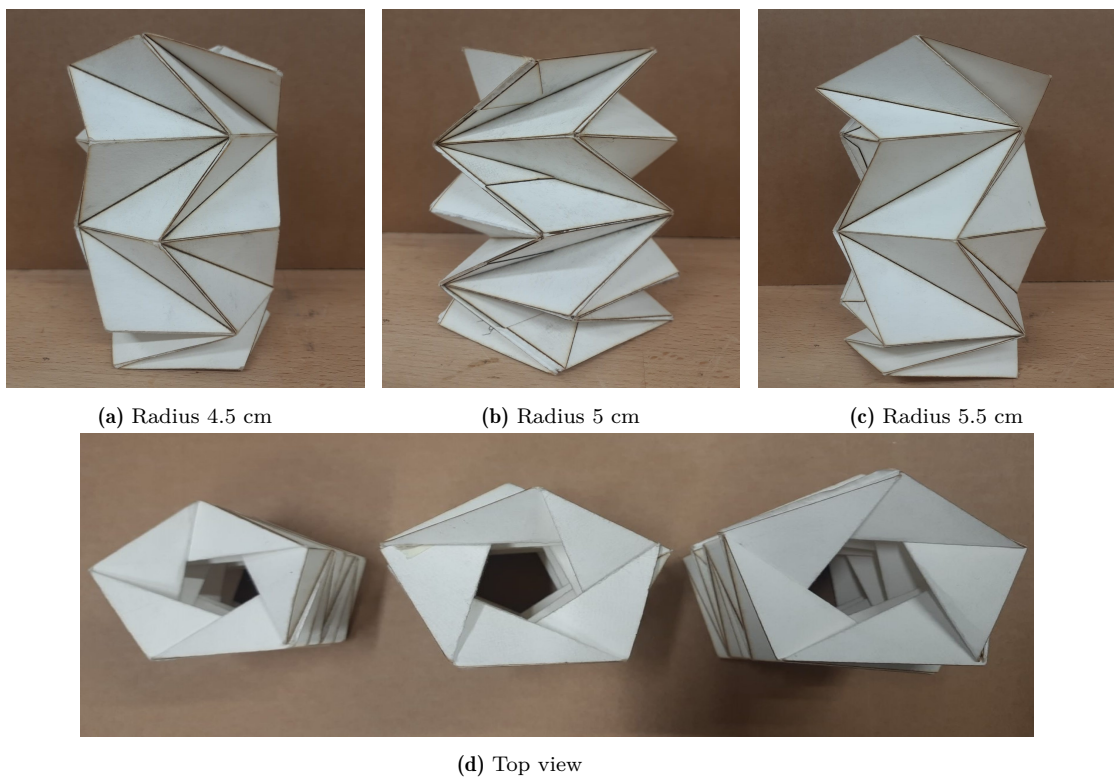


Figure 5.2: Three cases with varying radius and fixed number of sides, $n = 5$

For each case, the outer volume is calculated using the below equation with the design radius i.e., the radius of the polygon. The height of the structure is measured using a ruler.

$$\text{Outer Volume} = \pi r_1^2 H_D \quad (5.1)$$

where,

$r_1 =$ inscribed polygon radius

$H_D =$ total deployed height of the structure.

The usable inner volume is calculated using the volume formula for a polygon, as shown below.

$$\text{Usable Inner Volume} = \text{Inner Polygon Volume} = \frac{1}{2} n a r_2 H_D \quad (5.2)$$

where,

$n =$ number of polygon sides,

$a =$ edge length,

$r_2 =$ inner radius of the polygon (apothem)

In this case, the inner polygon is considered as the folds of the Kresling pattern, which protrude inwards, rendering the available volume lesser than the total volume of the structure. The radius of the inner polygon, r_2 is measured by rolling up a sheet of paper tightly and inserting it into the hollow structure. The paper is allowed to fill up the interior of the structure as shown in Figure 5.3, and the diameter is measured with a ruler.

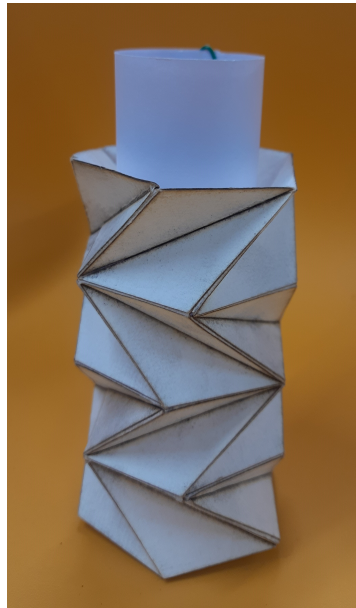


Figure 5.3: Measurement of inner radius

To properly report an experimental result such as the ones above, it is essential to include an estimate of error or level of confidence with the values. Generally, an experimental value can be reported as such:

$$\text{Measurement} = (\text{measured value} \pm \text{uncertainty}) \text{ units}$$

Where uncertainty accounts for both the accuracy and precision of the measurement. The accuracy is the level of agreement between a measured value and a true value. A measurement error is the amount of inaccuracy. Precision is the degree of consistency and agreement among independent measurements of the same quantity.

For this study, only accuracy is taken into account for uncertainty calculations because in order to report the precision level, repeated measurements of the prototype need to be taken, which is not done in this case.

For all of these height and inner radius measurements, a standard ruler with an accuracy of 0.5 mm is used. This means that there is some scope for an error in measurement. Human error can also add to discrepancies in measurements, but this cannot be quantified accurately.

For the radius and height measurements, the uncertainty is taken to be 0.5 mm as this is the smallest unit of the ruler used in measurements.

For all further calculations that the measured radius and height feed into, the associated uncertainties must be propagated. This is done using some laws of uncertainty propagation.

1. When adding (or subtracting) independent measurements, the absolute uncertainty of the sum (or difference) is the root sum of squares (RSS) of the individual absolute uncertainties. When adding correlated measurements, the uncertainty in the result is simply the sum of the absolute uncertainties, which is always a larger uncertainty estimate than adding in quadrature (RSS). Adding or subtracting a constant does not change the absolute uncertainty of the calculated value as long as the constant is an exact value.
2. When multiplying (or dividing) independent measurements, the relative uncertainty of the product (or quotient) is the RSS of the individual relative uncertainties. When multiplying correlated measurements, the uncertainty in the result is just the sum of the relative uncertainties, which is always a larger uncertainty estimate than adding in quadrature (RSS). Multiplying or dividing by a constant does not change the relative uncertainty of the calculated value.

Using these laws, the uncertainty propagation for the inner volume is derived as follows.

In the volume formula given in Equation 5.2, only the radius r_2 and height H_D are susceptible to measurement errors. The rest of the equation is considered to be an exact value or a constant for the purpose of the error propagation calculations.

$$\text{Constant} = \frac{1}{2}an$$

$$\text{Variable} = r_2H_D$$

$$\sigma_{r_2} = \sigma_{H_D} = 0.05 \text{ mm}$$

$$\frac{\partial(r_2H_D)}{r_2} = H_D \quad \frac{\partial(r_2H_D)}{H_D} = r_2$$

Since the radius and height measurements are not correlated to one another, the total uncertainty for the inner volume is calculated as,

$$\begin{aligned}\sigma_f &= \sqrt{\frac{\partial(r_2 H_D)^2}{r_2} \sigma_{r_2}^2 + \frac{\partial(r_2 H_D)^2}{r_2} \sigma_{H_D}^2} \\ \sigma_f &= \sqrt{H_D^2 0.05^2 + r_2^2 0.05^2} \\ \sigma_f &= 0.05 \sqrt{H_D^2 + r_2^2}\end{aligned}\quad (5.3)$$

Similarly, the uncertainty propagation for the outer volume is derived as follows.

$$\begin{aligned}\text{Constant} &= \pi \\ \text{Variable} &= r_1^2 H_D \\ \sigma_{r_2} &= \sigma_{H_D} = 0.05 \text{ mm} \\ \frac{\partial(r_1^2 H_D)}{r_1} &= 2r_1 H_D \quad \frac{\partial(r_1^2 H_D)}{H_D} = r_1^2 \\ \sigma_f &= \sqrt{\frac{\partial(r_1^2 H_D)^2}{r_1} \sigma_{r_1}^2 + \frac{\partial(r_1^2 H_D)^2}{H_D} \sigma_{H_D}^2} \\ \sigma_f &= \sqrt{(2r_1 H_D)^2 (0.05)^2 + r_1^4 (0.05)^2} \\ \sigma_f &= 0.05 r_1 \sqrt{4H_D^2 + r_1^2}\end{aligned}\quad (5.4)$$

It is to be noted that all uncertainties are reported with two significant digits, as the measurements taken by the rule only have a precision of two decimal places.

For the Rhino model, the only source of uncertainty is the assumption made regarding the twist. Here, for a twist angle below 0.55 radians, the model rotates each polygonal plane in alternating directions, and for angles greater than 0.55 radians, rotates only alternate planes in a single direction. This is considered to closely mimic the real behaviour of the structure in most cases, but it does contribute to the uncertainty. However, this uncertainty is negligible and not quantifiable and is, therefore, not considered in the uncertainty calculations.

The next step is to determine if the Rhino and prototype values agree with each other. Generally, the values are considered to be in agreement if the theoretical predictions (in this case, Rhino calculations) lie within the range of experimental uncertainty (paper prototype).

If they do not agree, then an error % is reported, calculated as follows.

$$\text{Error \%} = \frac{|Prototype\ measurement - CAD\ Model\ measurement|}{Average(Prototype\ measurement - CAD\ Model\ measurement)} \quad (5.5)$$

Following are the findings for each of the aforementioned cases with their uncertainties and error percentages, listed in Tables 5.1 and 5.2. The number of layers for all cases is 4.

Table 5.1: Measurements and Uncertainties - Varying Number of Sides, Fixed Radius = 5 cm

5-sided Polygon				
Measurements (in cm and cm ³)	Prototype	Uncertainty	CAD Model	Error%
Deployed Height	21.5	0.05	21.5	0.0
Folded Height	1.6	0.05	1.56	2.6
Usable Inner Volume	413.2	15.89	461.26	10.4
Outer Volume	1688	10.82	1689.67	0.1
6-sided Polygon				
	Prototype	Uncertainty	CAD Model	Error%
Deployed Height	15.6	0.05	15.6	0.0
Folded Height	1.2	0.05	1.54	28.3
Usable Inner Volume	362.5	11.86	359.6	0.8
Outer Volume	1225.2	7.90	1227.03	0.1
7-sided Polygon				
	Prototype	Uncertainty	CAD Model	Error%
Deployed Height	17.6	0.05	17.59	0.1
Folded Height	1.5	0.05	1.56	4.0
Usable Inner Volume	534.0	13.56	530.58	0.6
Outer Volume	1382.3	8.89	1381.20	0.1

Table 5.2: Measurements and Uncertainties - Varying Radius, Fixed Number of Sides = 5

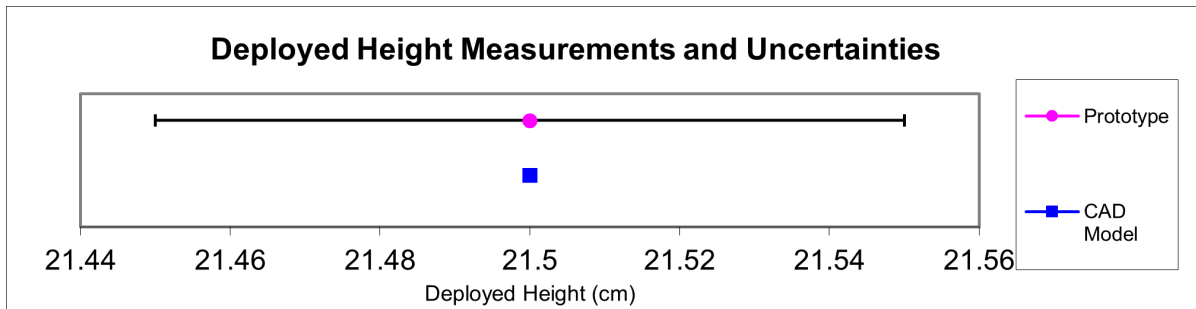
Polygon with Inscribed Radius = 4.5 cm				
Measurements (in cm and cm ³)	Prototype	Uncertainty	CAD Model	Error %
Deployed Height	19.4	0.05	19.41	0.07
Folded Height	1.7	0.05	1.65	3.03
Usable Inner Volume	356.8	12.91	339.9	4.96
Outer Volume	1234.2	8.79	1234.79	0.05
Polygon with Inscribed Radius = 5 cm				
	Prototype	Uncertainty	CAD Model	Error %
Deployed Height	21.5	0.05	21.5	0
Folded Height	1.6	0.05	1.64	2.5
Usable Inner Volume	413.2	15.89	461.26	10.41
Outer Volume	1688	10.82	1689.67	0.10
Polygon with Inscribed Radius = 5.5 cm				
	Prototype	Uncertainty	CAD Model	Error %
Deployed Height	23.5	0.05	23.5	0
Folded Height	1.8	0.05	1.64	9.76
Usable Inner Volume	669.3	19.11	604.97	10.63
Outer Volume	2233.2	13.01	2234.24	0.05

Large discrepancies are shown for the usable inner volume, up to 10.6%. This is attributed to the assumption made for the plane rotations based on the twist. The values in Tables 5.1 and 5.2 are visualised in Figures 5.4 to 5.8. The graphs help visualise if the prototype and CAD model values are in agreement with each other i.e., if the CAD model data points fall within the range of the prototype's error bars.

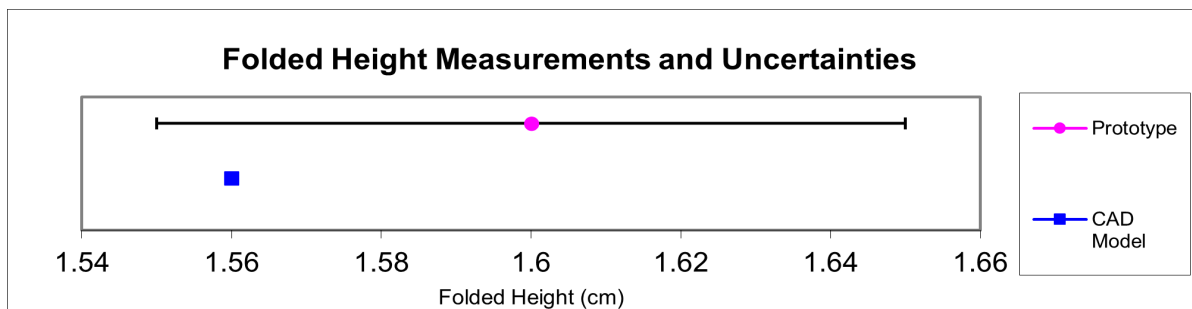
It is seen that, in some cases, the usable inner volume measured by the Rhino CAD model falls outside the range defined by the error bars i.e., they are not in agreement. To reduce the error, further study must be undertaken to accurately represent the relationship between the twist angle and the inward 3D projection of the valley folds that determine how much inner volume is obstructed.

There are also some errors with the folded height outputs from the Rhino model, with the model producing a higher height than the prototypes. This could be due to human error in the height measurement technique of the prototype. The structure is manually folded down, and depending on the force applied to keep it folded while measuring, the measurements might vary slightly. While the percentage errors seem large (up to $\approx 28\%$), the actual difference in values is less than a centimetre.

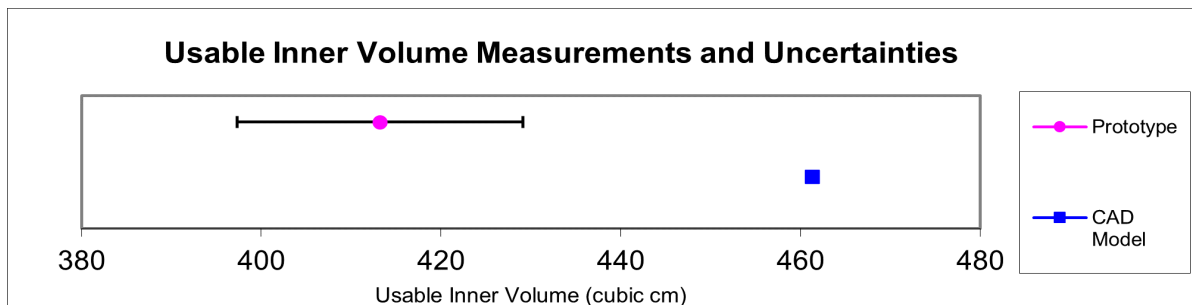
For the present work, the aforementioned errors are considered acceptable to some extent as the model is a simplification of reality, and at such a preliminary design stage, a balance must be found between simplicity and having the most accurate model. While the errors do affect some data points, the model is still capable of depicting trends in the behaviour of the cylindrical Kresling origami structure, which helps guide design decisions. Chapter 9, for example, defines design guidelines that are determined based on trends observed in the model and prototypes, which remain valid even if the numbers do not perfectly match up. Also, for manufacturing, the model provides accurate flat pattern parameters that can be used to fabricate the desired structure.



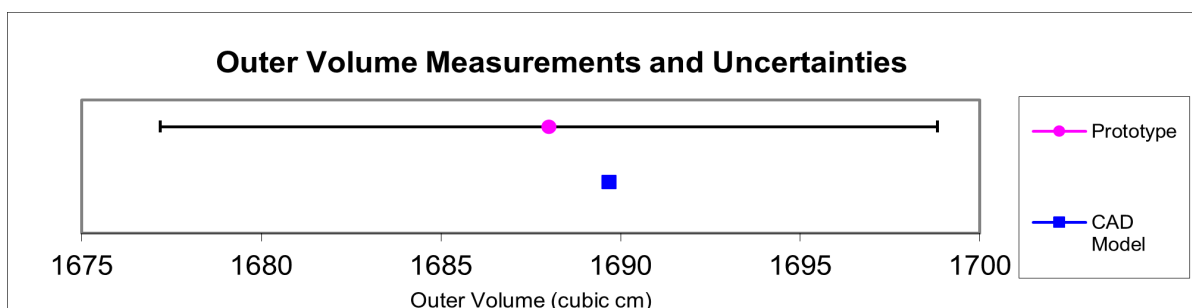
(a) Deployed Height



(b) Folded Height

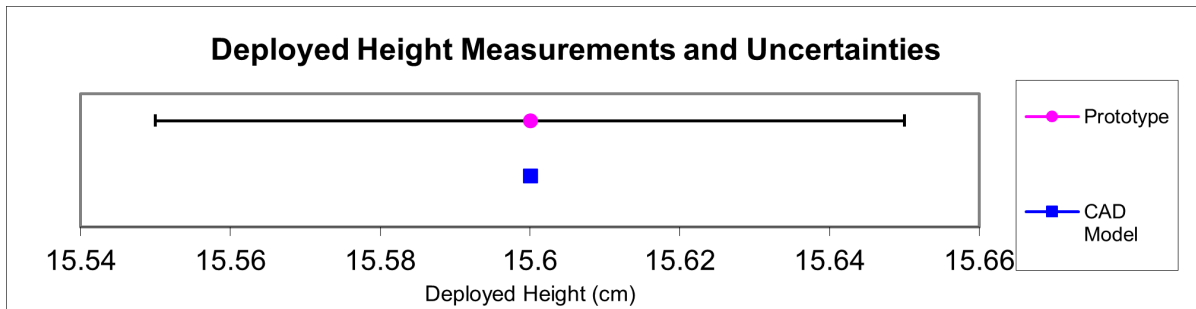


(c) Usable Inner Volume

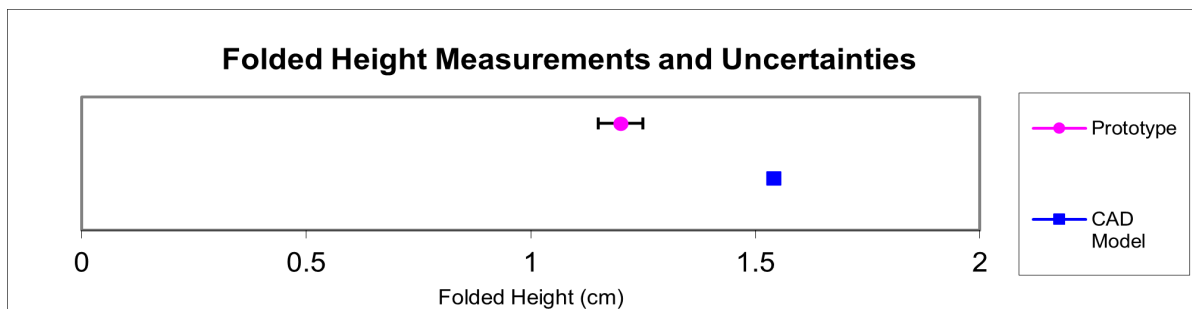


(d) Outer Volume

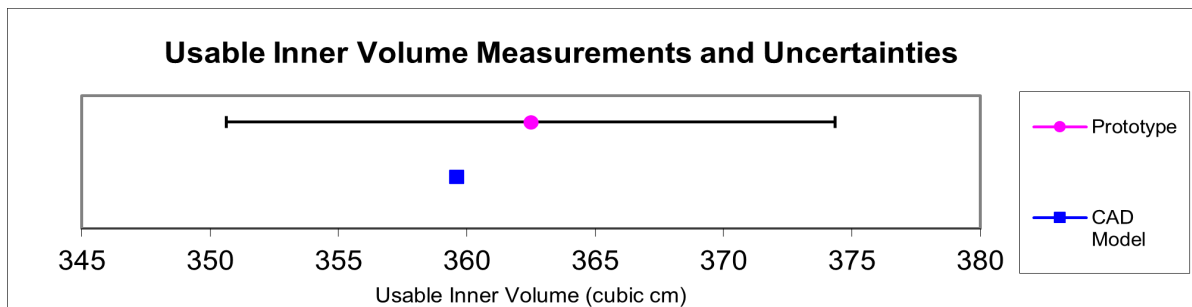
Figure 5.4: Measurements and Uncertainties - 5-sided polygon with fixed radius



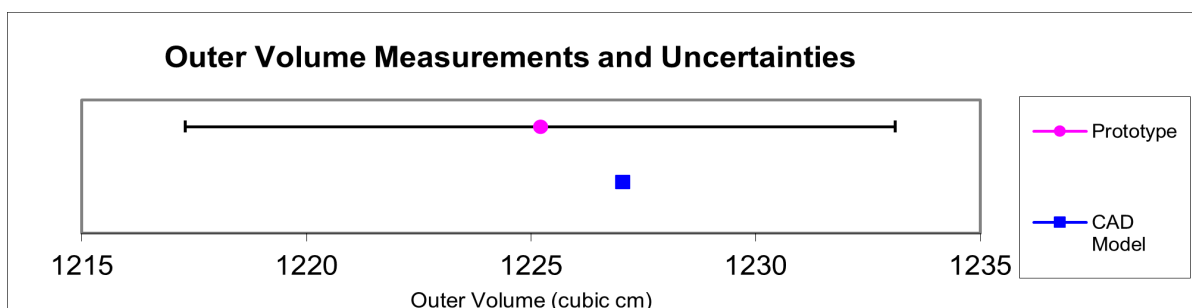
(a) Deployed Height



(b) Folded Height

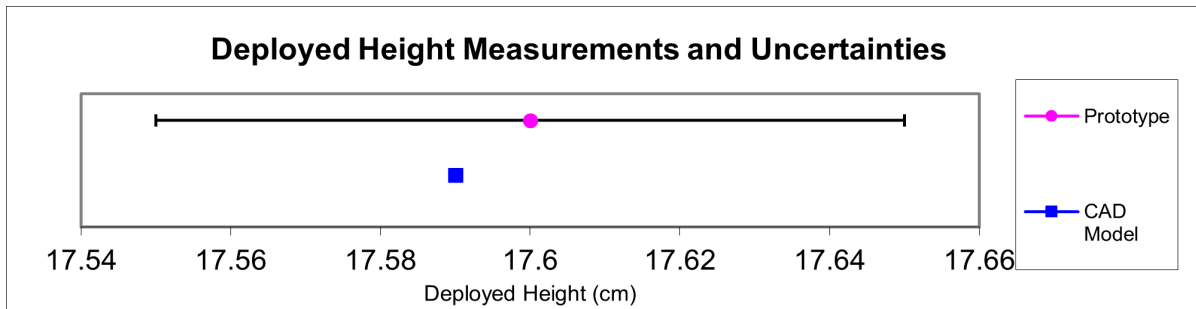


(c) Usable Inner Volume

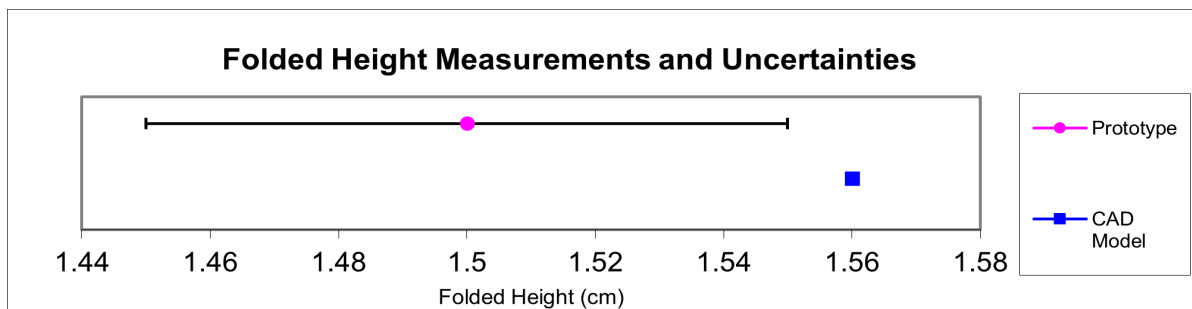


(d) Outer Volume

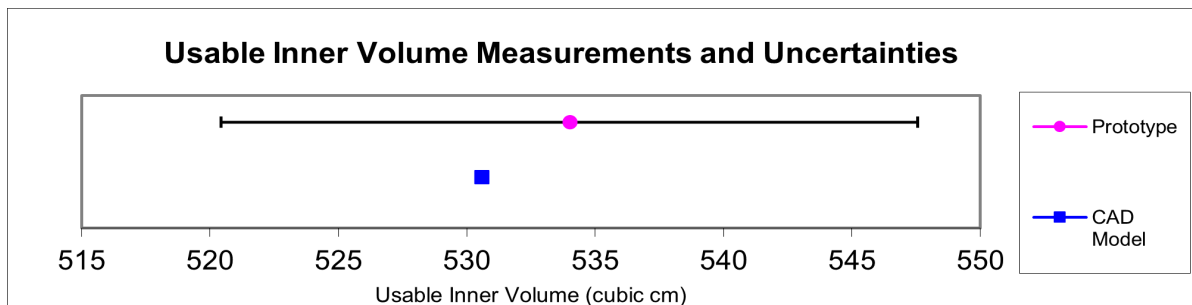
Figure 5.5: Measurements and Uncertainties - 6-sided polygon with fixed radius



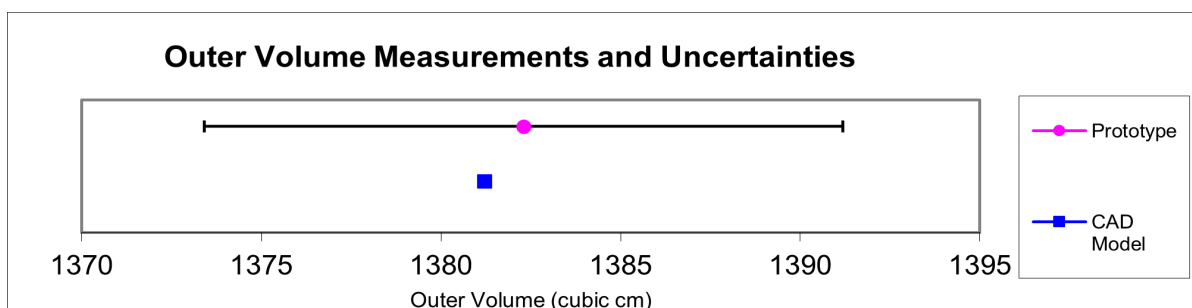
(a) Deployed Height



(b) Folded Height

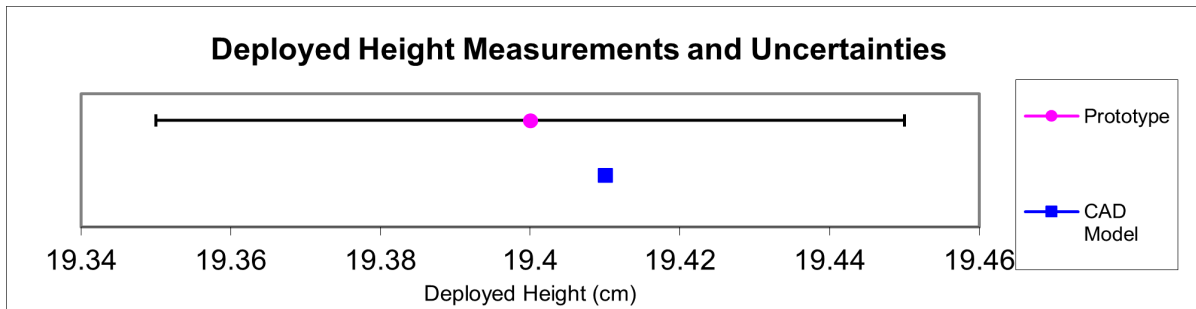


(c) Usable Inner Volume

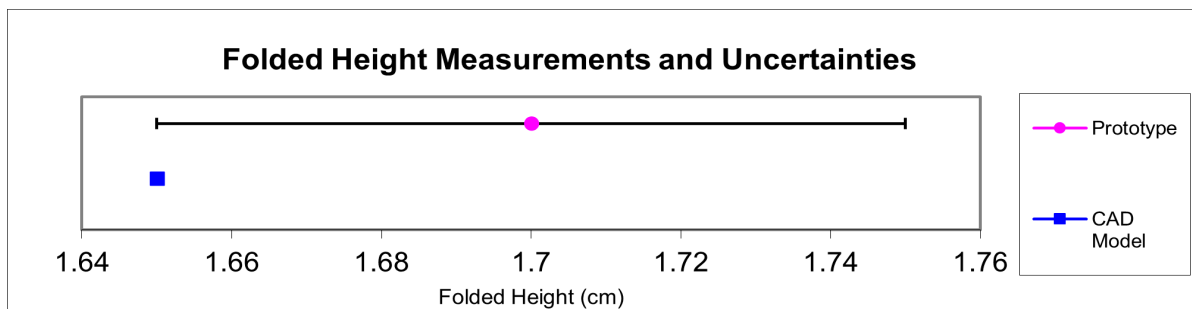


(d) Outer Volume

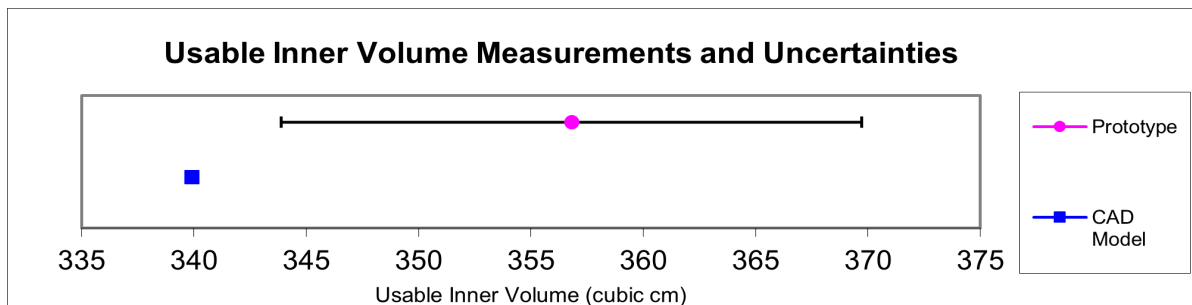
Figure 5.6: Measurements and Uncertainties - 7-sided polygon with fixed radius



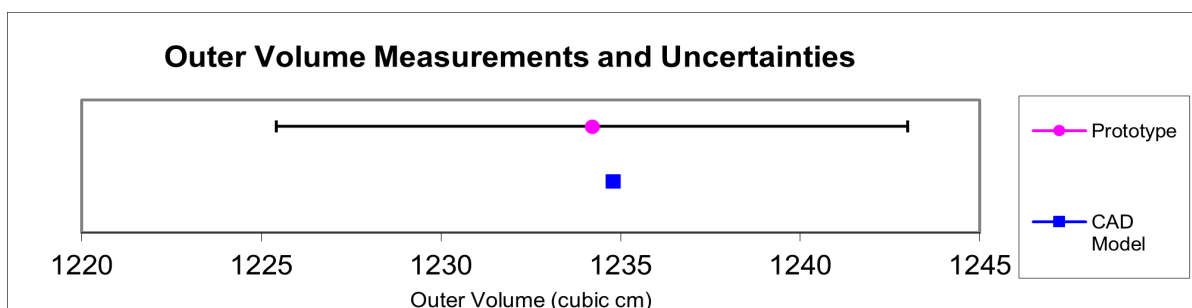
(a) Deployed Height



(b) Folded Height

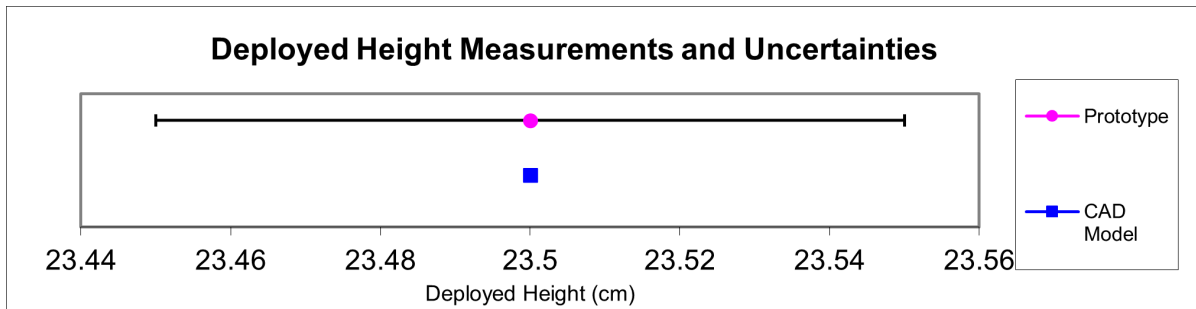


(c) Usable Inner Volume

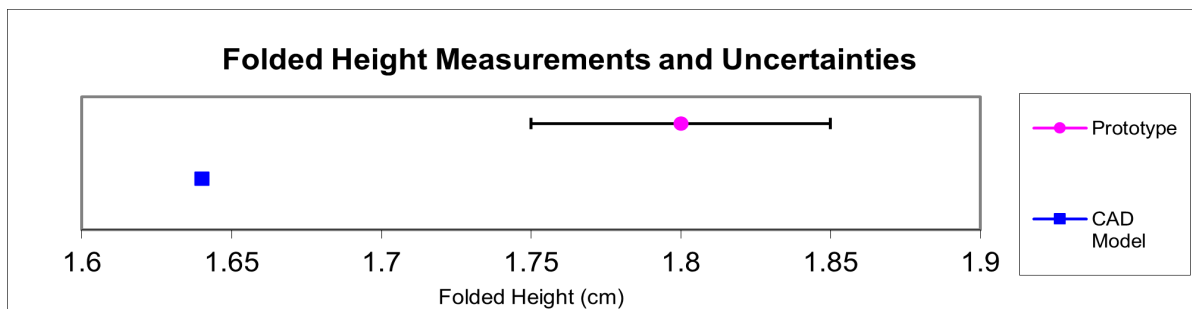


(d) Outer Volume

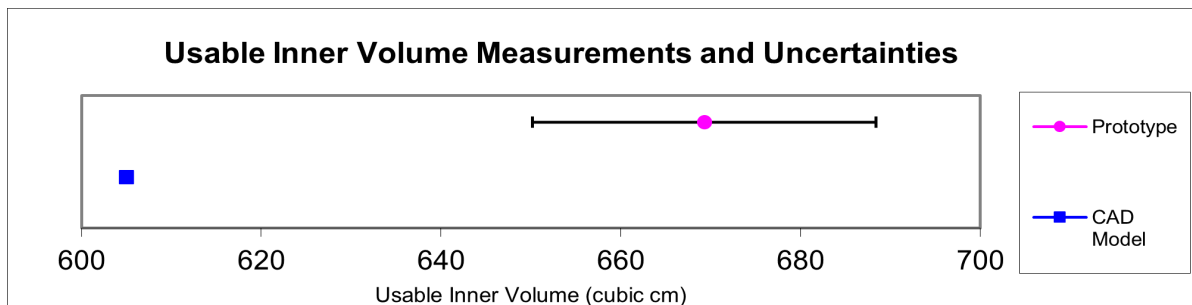
Figure 5.7: Measurements and Uncertainties - Polygon with fixed sides and radius = 4.5 cm



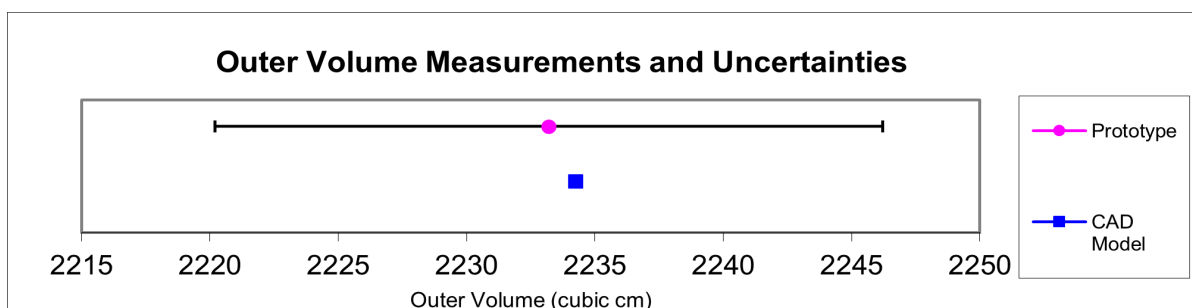
(a) Deployed Height



(b) Folded Height



(c) Usable Inner Volume



(d) Outer Volume

Figure 5.8: Measurements and Uncertainties - Polygon with fixed sides and radius = 5.5 cm

6

Parametric Study and Optimisation

The design and analysis of origami deployable structures entail a myriad of intricate variables and parameters that determine the performance and behavior of the structures. This chapter delves into the domain of parametric study to help understand the impact of various parameters on the main design objectives. In this project, the aim is to optimise for maximum usable inner volume and minimum packaging ratio i.e., ratio of folded height to deployed height.

In the previous chapter, the Rhino model was validated with physical prototypes. Therefore, it is now appropriate to use it for all further processes, such as parametric studies and optimisation.

First, a simple approach is taken. Parameters(number of sides, number of layers, total height) are varied manually and individually to assess their effects on the usable inner volume and the packaging ratio. The following graphs show the variation of the usable inner volume and packaging ratio with variations in the number of base polygon sides, number of origami layers, and height of the total structure.

For this study, the radius is fixed at 5 cm. Other fixed and varying parameters are as follows:

- **Varying Number of Sides**

For a fixed height and number of layers, the number of base polygon sides is varied from 6 to 10.

From Graph 6.1a, it is seen that the usable inner volume increases with an increase in the number of sides. This is expected as with more polygon sides, the base area tends closer to a circle and thereby leads to an increase in cross-sectional area. However, the difference in packaging ratio(Graph 6.2a) is negligible, likely due to the fact that increasing the number of sides contributes minimally to the height.

- **Varying Number of Layers**

For a fixed height and number of sides, the number of layers is varied from 6 to 10.

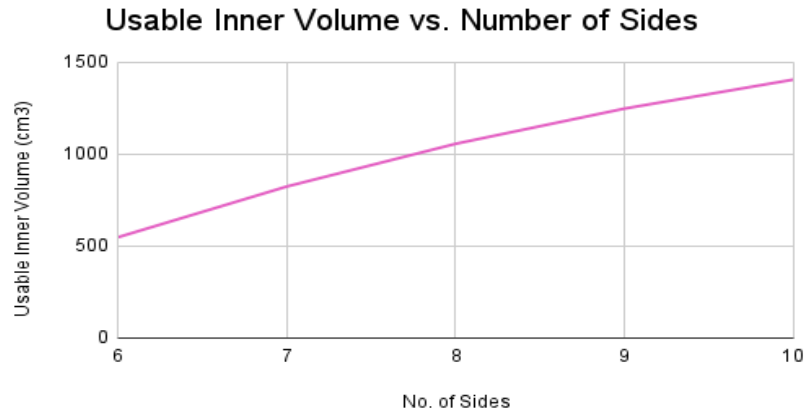
The effect of varying the number of origami layers on the usable inner volume is not clear. There is a brief increase followed by a gradual decrease, as shown in Graph 6.1b. The trend expected is a slight decrease in the volume as with more layers, there are more valley folds protruding inwards, thereby obstructing the available volume. For the effect on packaging ratio, the behaviour depicted in Graph 6.2b is as expected—gradual increase due to the increased number of folds contributing to the folded height.

- **Varying Height**

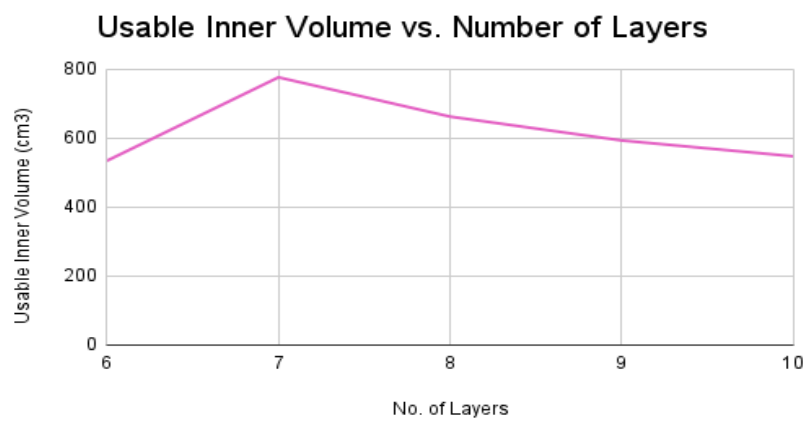
For a fixed number of sides and layers, the deployed height is varied from 35 cm to 50 cm.

It is seen in Graph 6.1c that the usable inner volume increases gradually before dipping again. It is likely that this behaviour is observed for this particular set of fixed parameters but it may not necessarily always be the case. The dip in volume can be attributed to an increased twist angle that is derived from the fixed parameters. For the packaging ratio, only a slight decrease is observed in Graph 6.2c even though intuitively, it seems that a larger height would result in a larger folded height. This is attributed to the fact that though the height increases, the number of layers remains the same, so the folded height, which is essentially the layers folded one on top of the other, does not vary much.

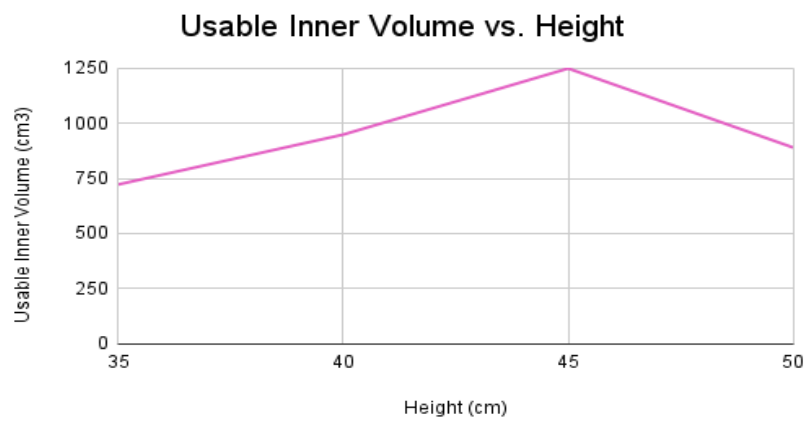
Studying the effects of these parameters individually on the optimisation criteria offers an understanding of the origami structure's behaviour and helps identify trends that may not be as intuitive or straightforward as expected.



(a) Variation of usable inner volume with number of polygon sides

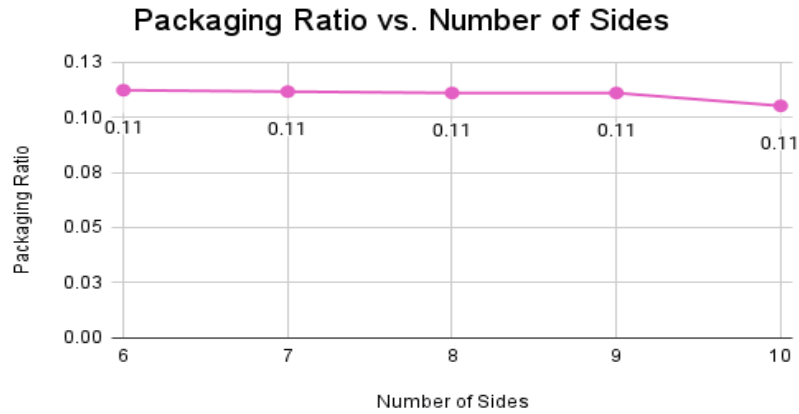


(b) Variation of usable inner volume with number of origami layers

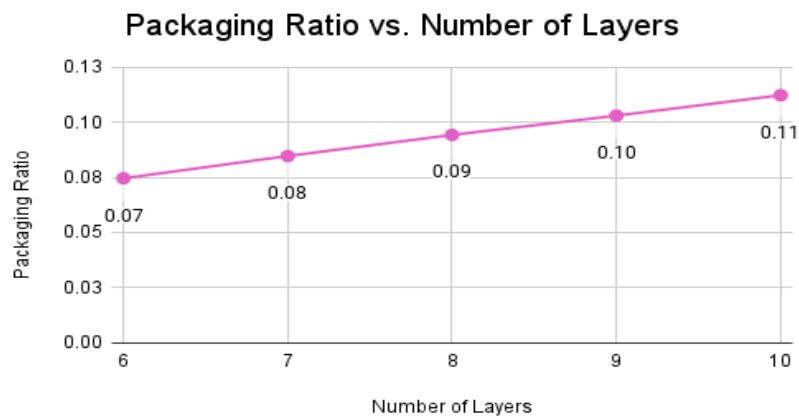


(c) Variation of usable inner volume with total height

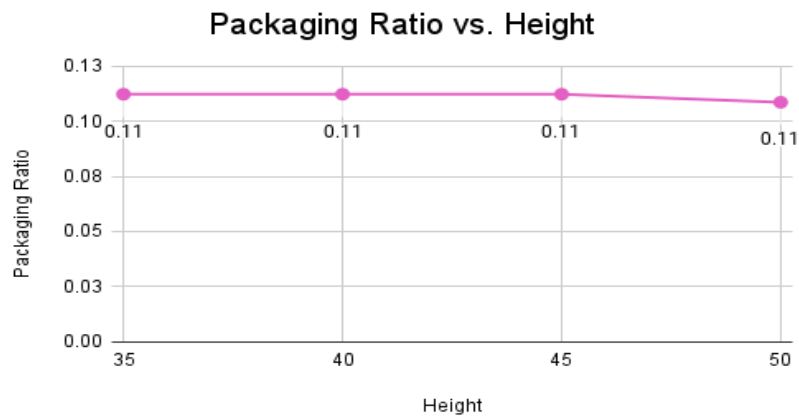
Figure 6.1: Effect of origami structure parameters on usable inner volume



(a) Variation of packaging ratio with number of polygon sides



(b) Variation of packaging ratio with number of origami layers



(c) Variation of packaging ratio with total height

Figure 6.2: Effect of origami structure parameters on packaging ratio

Next, a suitable balance must be found for all parameters to get an optimal solution for both objectives combined. While ideally, it is desired to use multi-objective optimisation for the two main objectives: maximising usable inner volume and minimising packaging ratio, the current

structure of the Grasshopper algorithm is such that the folded height cannot be obtained while running an iterative optimisation loop.

This is due to the fact that the folded height can only be obtained when the folding slider, pictured in Figure 4.8, is manually slid down to 0. This cannot be done manually when the optimisation loop is running hundreds of iterations at high speed. This results in wrong outputs for folded height, rendering the entire procedure useless. Therefore, it is decided to only optimise for maximum usable inner volume and then verify if the folded height and packaging ratio meet design goals, as specified in the requirements **ORI-CON-1** and **ORI-DRI-4**.

For the single-objective optimisation, the in-built Galapagos evolutionary solver is used. Inspired by genetic algorithms, Galapagos facilitates optimisation and exploration of design solutions by iteratively evolving a population of potential solutions based on defined fitness criteria. By defining variables and objectives, Galapagos automatically generates and evaluates multiple design alternatives, iteratively refining them towards the desired outcome.

However, Galapagos does have its limitations. The ones relevant to the current design problem are :

- **Sensitivity to initial parameters:** The performance of Galapagos can be highly dependent on the initial population and parameter settings. Choosing appropriate initial values and setting up fitness functions can be challenging, and inadequate selections may lead to suboptimal or biased results.
- **Lack of Global Optimality Guarantee:** Galapagos utilizes an evolutionary algorithm, which is a heuristic approach that does not guarantee finding the global optimum. Depending on the problem complexity and parameter settings, Galapagos may converge to a local optimum instead of the best possible solution.
- **Limited Convergence Criteria:** Galapagos uses convergence criteria to determine when to stop the optimization process. However, selecting appropriate convergence criteria can be subjective and may require manual adjustment, leading to potential premature convergence or excessive computation time.

Following are some methods used to mitigate the impact of these limitations.

- **Multiple Runs and Random Seed Variation:** Run Galapagos multiple times with different random seeds to explore different regions of the solution space. This can help overcome the issue of potential bias introduced by the initial population. Analyze the results from multiple runs to identify common trends or solutions that consistently perform well.
- **Population Size Modification:** Adjust the size of the population in Galapagos. Increasing the population size can enhance exploration capabilities and reduce the likelihood of premature convergence. Increasing the exploration space also reduces the risk of getting trapped in a local optima.

For the initial run, the default settings of the Galapagos solver are retained, as shown in Figure 6.3. Below is a description of each setting.

The image shows the Galapagos Editor interface with the following settings:

Section	Parameter	Value	Unit/Label
Generic	Fitness	Maximize	
	Threshold		
	Runtime Limit	<input type="checkbox"/> Enable	
	Max. Duration	01 Hours 30 Minutes	Hours Minutes
Evolutionary Solver	Max. Stagnant	00100	
	Population	00020	
	Initial Boost	00001	x
	Maintain	005	%
	Inbreeding	+075	%

Figure 6.3: Galapagos Solver settings

- **Fitness:** Specifies the optimization objective, whether it is to maximize or minimize a particular fitness function. The fitness goal guides Galapagos towards improving solutions based on the defined objectives. A threshold can also be specified such that if it is achieved, the solver aborts. By default, it is left blank.
- **Runtime Limit:** A maximum runtime can be specified. This is useful if the process is foreseen to be very long, has many objectives and parameters, but is disabled by default.
- **Max. Stagnant:** Indicates the maximum number of stagnant generations without significant improvement before the solver aborts. This is set to 100, by default.
- **Population Size:** Specifies the number of individuals or potential solutions in each generation of the evolutionary process. A larger population size can enhance the exploration capability but may increase computation time. The default is 50.
- **Initial Boost:** Indicates the population multiplication factor for the first generation. Boosting the initial population provides a larger exploration space to start with without increasing the computation time too much. The default is twice the population size.
- **Maintain:** Specifies what percentage of individuals with the highest fitness values in a population are carried over to the next generation without any modifications. This preservation of individuals helps to maintain a level of genetic diversity and prevents the loss of potentially good solutions from one generation to the next. The default is 5%.
- **Inbreeding:** This setting determines the percentage of individuals within the population that undergo genetic operations with other individuals from the same generation. Higher percentages encourage more genetic diversity as individuals exchange genetic information with a larger number of peers. However, excessive inbreeding can lead to a loss of diversity and reduce the exploration capabilities of the optimization process. The default is 75%.

The annealing solver settings shall not be discussed as it is out of the scope of the current work.

The Fitness input, i.e., the parameter to be optimised here, is the usable inner volume. The genomes are the number of sides of the base polygon, the fully deployed height of the structure, and the number of origami layers. These are the variables that are varied to determine an optimum fitness value. The radius of the base polygon could also be a genome but, in this case, is a fixed value of 5 cm to suit the design criteria of the demonstrator being built.

On running the model with the current settings, the process was found to be computationally expensive and time-consuming. This is due to the fact that the algorithm created to generate the origami structure is extremely dense. When this needs to repeat for many iterations at high speed, it does not perform very well.

To solve this issue, a reduced model is used, as shown in Figure 6.4. In the reduced model, the entire folding algorithm is removed along with the Kangaroo solver constraints and components, as well as the thickened closed mesh. The only components retained are the ones used to generate the fully deployed origami structure, the flat pattern parameters, and the output modules with the calculated volumes and height. This reduction greatly simplifies the model and allows it to run at high speed without breaking down.

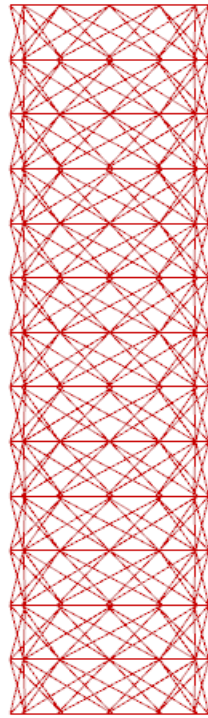


Figure 6.4: Reduced Rhino-Grasshopper model

Running the optimisation process results in the generation of a number of optimal solutions in descending order of fitness, as shown in Figure 6.5. It is to be noted that, often, the top few solutions, while having highest available inner volumes, are also very nearly cylindrical i.e., the pattern generated is such that it cannot be folded down to a smaller height and volume.

Therefore, discretion must be used to find the true optimal solution that not only has a high volume but can also compress sufficiently. This can be tested by extracting the genome values and using them as input in the full model to check if they generate a structure that can fold. At this point, the folded height must also be noted so the packaging ratio can be calculated.

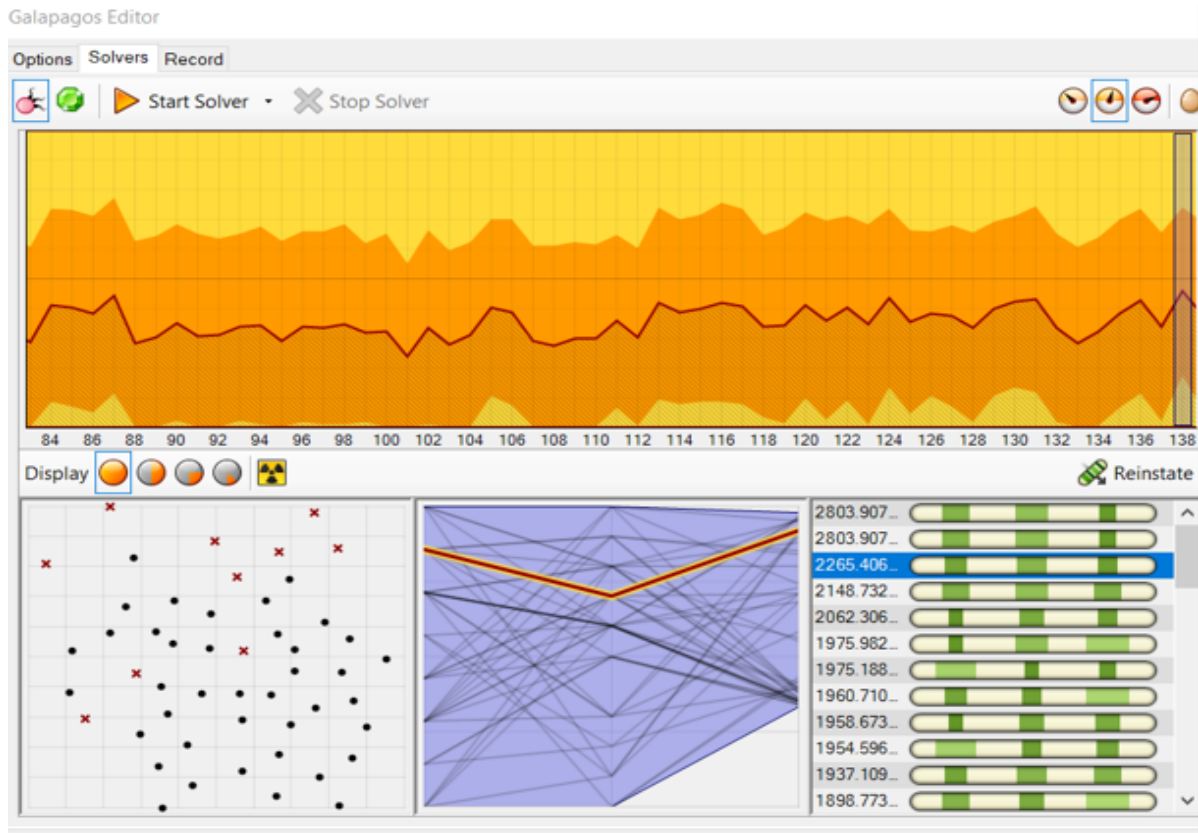


Figure 6.5: Galapagos Solver - Optimisation

The optimal configuration thus obtained for a radius of 5 cm is as shown in Table 6.1.

Table 6.1: Optimised Parameters

Optimised Parameters	Number of Sides	Number of Layers	Height (cm)
	14	11	39.2

The optimal outputs obtained with the aforementioned parameters are shown in Table 6.2.

Table 6.2: Optimal Outputs

Outputs	Stowed Outer Volume (cm^3)	Usable Inner Volume (cm^3)	Packaging Ratio	Deployment Ratio
	314.15	2265	0.102	9.72

The deployment ratio is calculated as the ratio of the deployed height to the folded height and is found to be $9.72 \approx 10$ i.e., the structure can be folded down to about **one-tenth of its deployed height**. However, it should be noted that this value could vary for a physical model because, in reality, some sections are twice as thick as the rest due to additional flaps used to join two halves of the structure.

Now that an optimal configuration is identified for maximum usable inner volume that also has a satisfactory packaging ratio, the structure must be manufactured. This will be discussed in the next section.

7

Prototyping

Prototyping is a crucial step in the development of new technologies. It is the bridge between conceptualisation and realisation of a design concept that allows one to explore, test, and refine ideas before reaching the final production stage. This chapter delves into the prototyping phase of the thesis project, which involves fabricating models to validate the digital Rhino model developed in Chapter 4 as well as identifying a suitable material and manufacturing technique combination to develop a functional prototype.

7.1. Prototypes for Model Validation

To be able to use the Rhino-Grasshopper model as a reliable tool for parametric studies, it is essential to validate its outputs. This is done by comparing the outputs of the model with those obtained from a physical prototype.

To create a physical prototype, multiple options are considered, such as acetate sheets, cardstock, and watercolour paper, all of which have been used for origami prototypes in the past for their pliability[24][63]. Watercolour paper is chosen for its thickness (0.5 mm), pliability, and easy availability. The thickness provides sufficient rigidity to the structure while the pliability makes it easy to fold at the creases.

The origami pattern has to be transferred onto the paper such that it folds at the creases like the desired Kresling pattern. This is done using a laser cutting and engraving procedure.

First, the flat origami pattern has to be prepared in a format that is readable by the laser cutting machine used i.e., the Snapmaker, pictured in Figure 7.1. The pattern is first drawn on Solidworks and then transferred to the LightBurn software which is used to generate the G-code file readable by the machine.

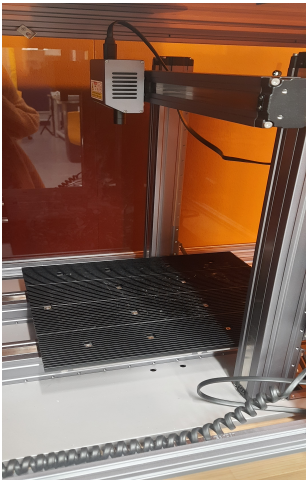


Figure 7.1: Snapmaker laser bed

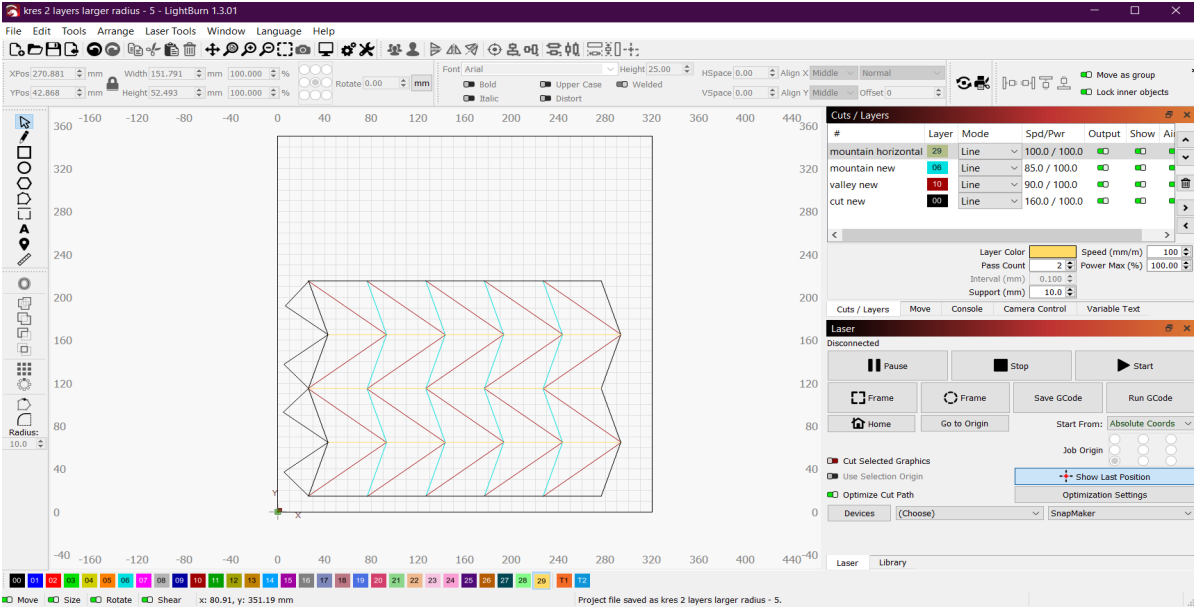


Figure 7.2: Lightburn Interface

In Lightburn, the different parts of the origami pattern i.e., the horizontal and vertical mountains, and valleys, can be assigned different laser setting procedures with variations in cutting speed, laser power, perforation mode, and number of passes.

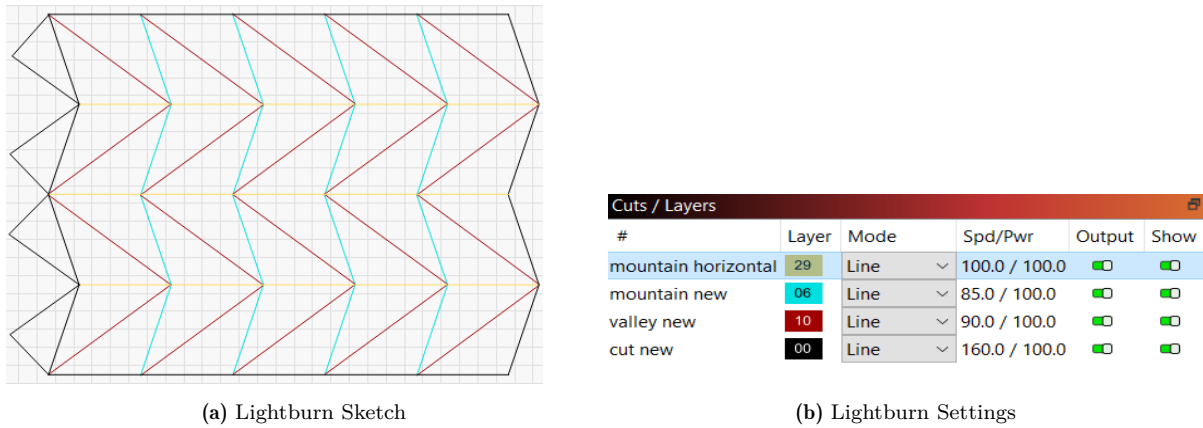


Figure 7.3: Lightburn - Flat Pattern

The sheet of paper is cut to the size of the laser bed (300 mm x 320 mm) and held in place by taping all four edges down to the bed.

To arrive at the optimal settings for each element, a trial-and-error procedure was used, gradually varying a single parameter at a time to observe its performance. The pattern used to test various settings is double Kresling units, as shown in Figure 7.4. This allows observation of the impact of cutting parameters as well as settings for the mountains and valleys.

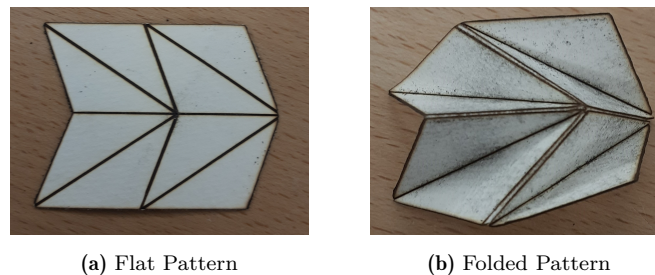


Figure 7.4: Kresling double units

7.1.1. Cutting - Outer Silhouette

To cut out the outer silhouette of the pattern, initially, three passes were tried, with a cutting speed of 140 mm/min at 100% laser power. This seemed to do the job sufficiently, but it was decided to increase the cutting speed a little more to reduce overall job time. The final chosen cutting speed is 160 mm/min.

The cutting step is done last to prevent the pattern from entirely detaching from the sheet and moving on the laser bed during the engraving procedures.

7.1.2. Engraving - Mountains and Valleys

To create the mountain and valley folds, we aim to remove some material to make the fold region more flexible without cutting. The perforation settings used for each iteration are listed in the table below.

Table 7.1: Laser engraving iterations

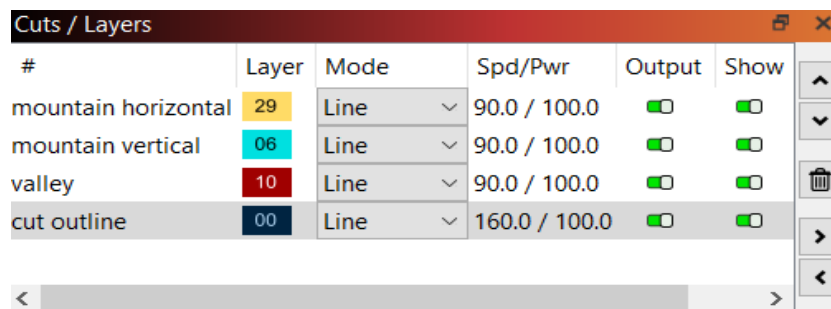
Design Features	Cuts (mm)	Skips (mm)	Number of Passes
Iteration Number			
1	0.2	0.1	1
2	0.1	0.2	1
3	0.1	0.1	1
4	0.1	0.2	2

The results obtained for each of these iterations are as follows.

- **Iteration 1:** A single pass with these settings removes almost all material and, therefore, is unsuitable.
- **Iteration 2:** These settings result in a stiff crease that is not sufficiently flexible.
- **Iteration 3:** Results similar to Iteration 1.
- **Iteration 4:** These settings are similar to Iteration 2 but with an extra pass. The added pass improves the flexibility of the fold lines while maintaining sufficient stiffness.

The settings from Iteration 4 are finalised. However, it was noted that, at times, the laser misses portions of the pattern entirely, leaving the paper unetched. To solve this problem, the engraving speed was reduced slightly from the default 100 mm/min to 90 mm/min. The slower speed ensures the laser does not glaze over any part of the pattern.

The final settings chosen are as seen in Figure 7.5, which is used to create a flat pattern that can then be folded into a 3D origami structure.



#	Layer	Mode	Spd/Pwr	Output	Show
mountain horizontal	29	Line	90.0 / 100.0	<input type="checkbox"/>	<input type="checkbox"/>
mountain vertical	06	Line	90.0 / 100.0	<input type="checkbox"/>	<input type="checkbox"/>
valley	10	Line	90.0 / 100.0	<input type="checkbox"/>	<input type="checkbox"/>
cut outline	00	Line	160.0 / 100.0	<input type="checkbox"/>	<input type="checkbox"/>

Figure 7.5: Lightburn final settings

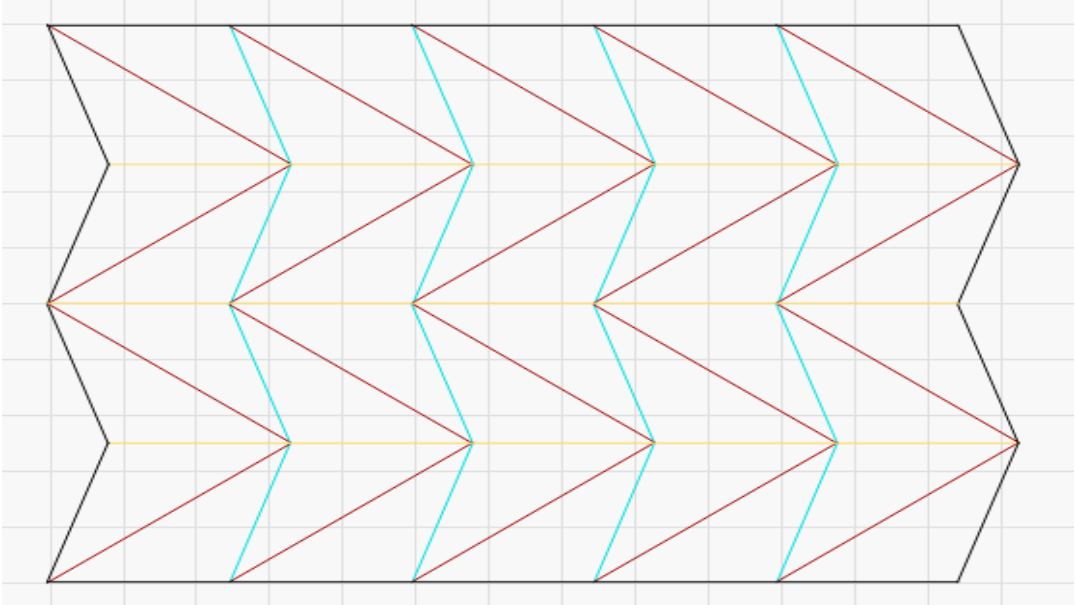


Figure 7.6: Lightburn sketch

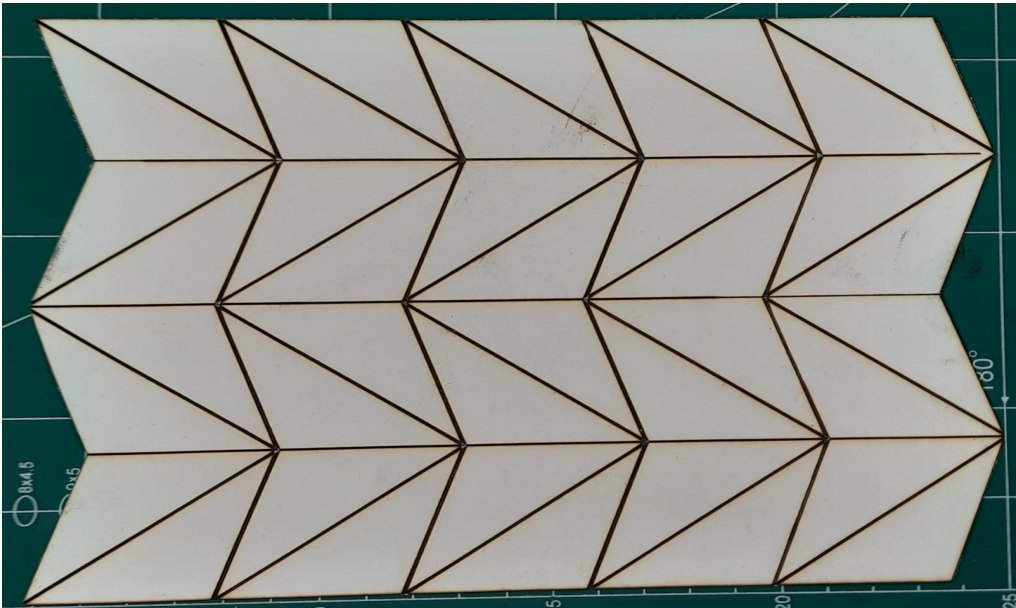


Figure 7.7: Laser cut Kresling flat pattern

7.1.3. Forming the 3D structure

The next step is to form the 3D Kresling origami structure from the flat pattern.

To enable radial attachment of two ends of the structure, additional tabs in the shape of half an origami unit are added, as shown in Figure 7.8. These tabs can be glued onto their counterparts on the other end to form a closed tube.

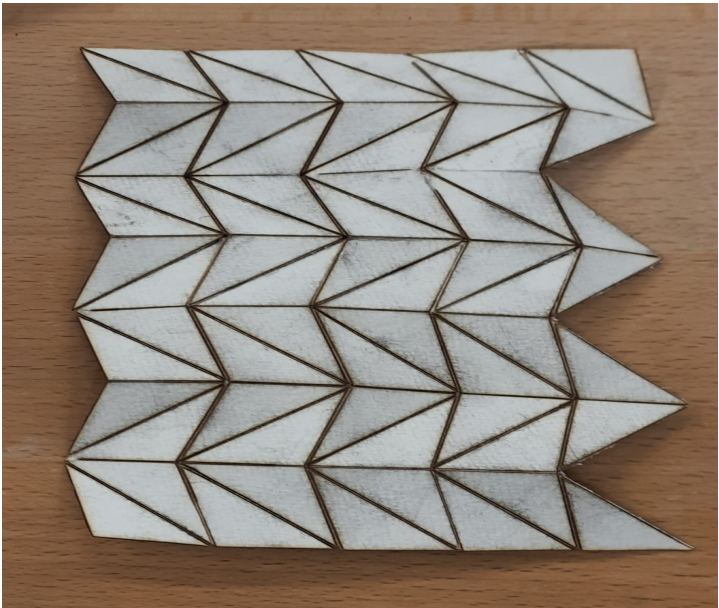


Figure 7.8: Original tab design - half an origami unit

The tabs started as half units but were later optimised to enable better folding and lesser overlap of material. The transition of the tab design can be seen in Figure 7.9. Similar tabs were also used for vertical attachment of origami layers to create longer structures, as shown in Figures 7.9 and 7.10.

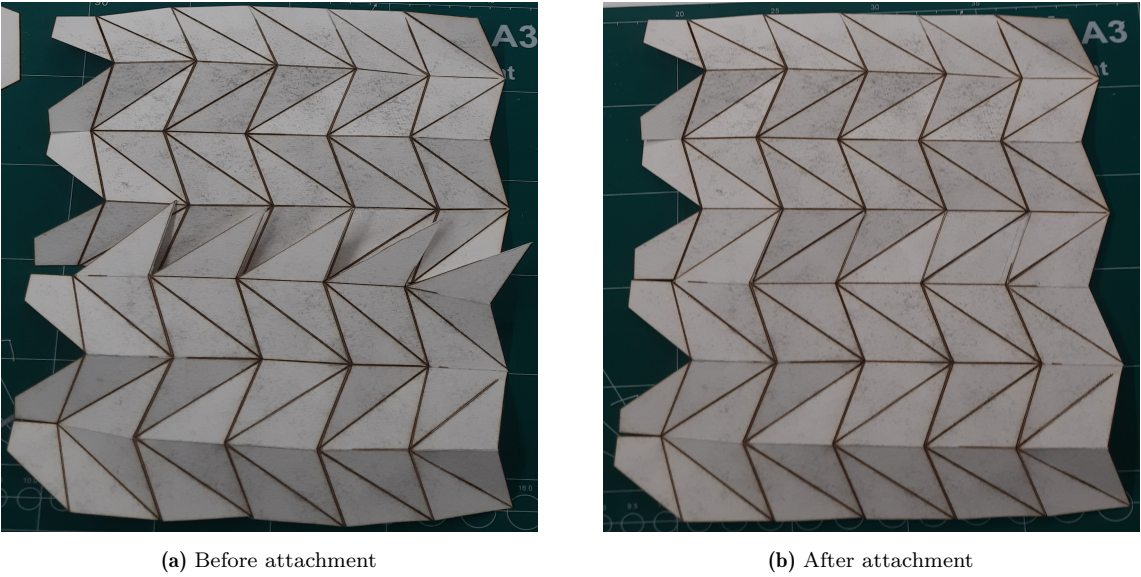


Figure 7.9: Tabs created for attachment



Figure 7.10: Closed origami structure

At this stage, it was noticed that when the 3D structure is formed, small holes are present at the vertices. This is due to the laser slowing down at the end of each pass, allowing for a deeper cut and hence, a hole. While this does not pose a problem at present, it will cause issues during deployment of the structure by inflation.

To solve this issue, initially, a thin layer of tissue paper was pasted onto the back of the pattern, covering all holes. This, however, became messy due to the multiple tissue plies separating while folding. As an alternative, masking tape was pasted across just the horizontal mountain creases, covering all the holes and not unravelling during deployment. This approach slightly increases stiffness at the folds.

Finally, to be able to deploy the structure via inflation, it is necessary to have a structure that is closed on one end. The other end is attached to the gripper and inflation setup, as discussed in Section 7.1.4. To achieve this, two methods were tried.

- Cutting a piece of paper in the shape of the polygonal cross-sectional area and taping it to the top end of the 3D structure.
- Cutting the top polygon covering as part of the flat origami pattern and taping down as before, as shown in Figure 7.11.

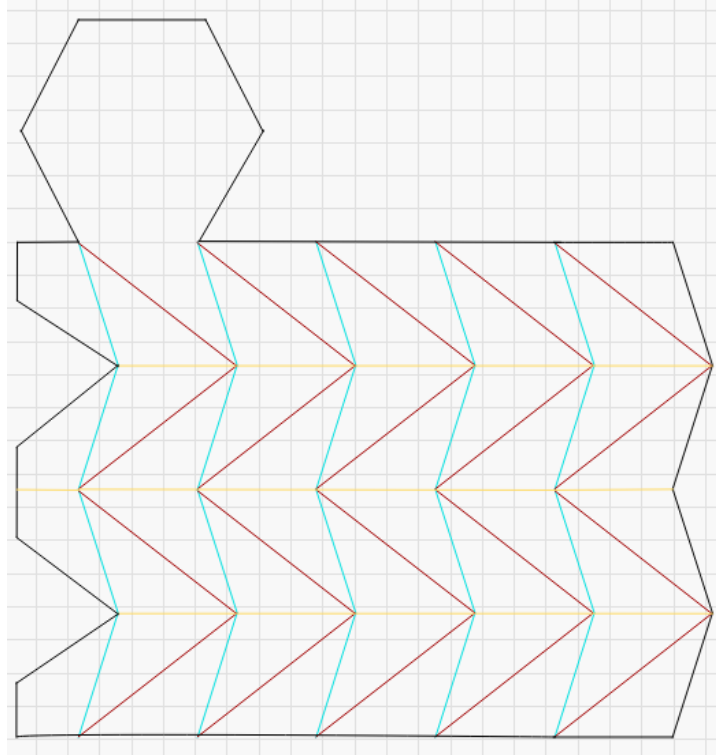


Figure 7.11: Attached covering

Both methods serve the purpose though the latter option could be considered better as it is completely attached on one edge, and therefore, absolutely no air can escape from that edge during inflation.

7.1.4. Inflation of paper model

In the early stages, a makeshift inflation setup was used to inflate the model, as shown in Figure 7.12. This included an uncontrolled air supply that was routed through a Bowden tube into the bottom of the origami structure, causing it to inflate and thereby, go from its fully folded configuration to its fully deployed configuration. It is also possible to observe intermediate states as each origami layer unravels separately.



Figure 7.12: Inflation setup

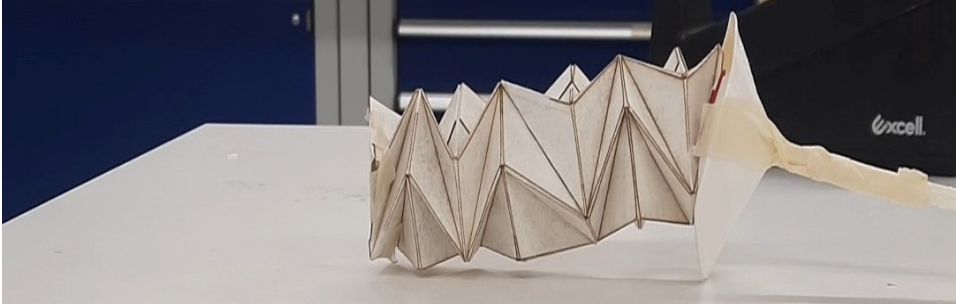
To attach the Bowden tube to the structure, a funnel-shaped gripper is 3D printed as shown in Figure 7.13. The flaps secure the bottom oris in place so the structure does not detach from the inflation setup.



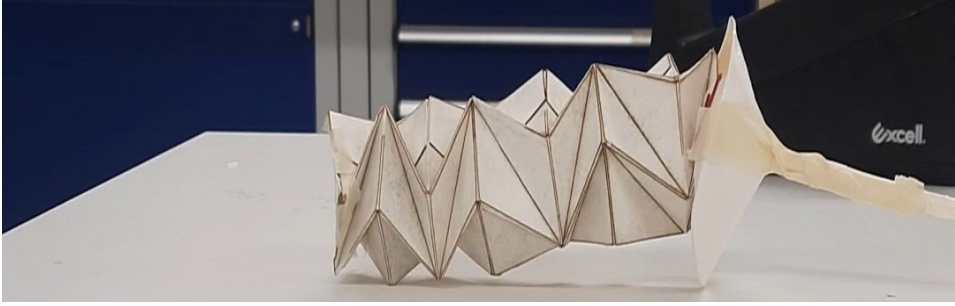
Figure 7.13: 3D printed gripper

Other inflation methods that were tried are a bike pump, a balloon, and a pipe with a valve. These methods were ruled out due to missing parts and/or malfunctioning devices.

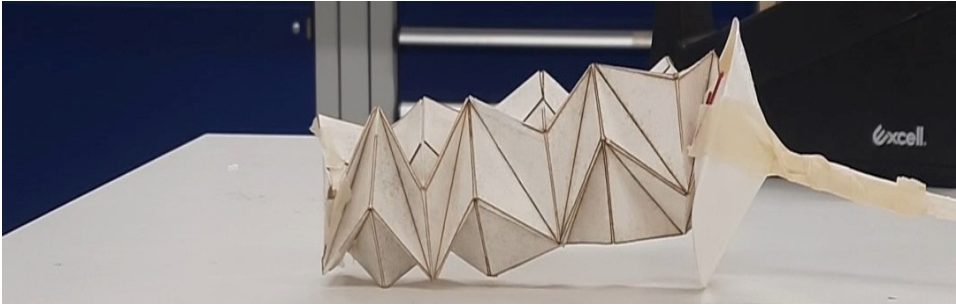
The inflation, as shown in Figure 7.14, was successful for different lengths and sizes of the origami structure and is therefore considered a viable deployment technique.



(a)



(b)



(c)



(d)

Figure 7.14: Inflation of paper prototype

7.2. Materials and Manufacturing

So far, the pattern and deployment concept has been validated with paper prototypes and a temporary inflation setup. It is also necessary to consider how the concept might translate to different materials that are more likely to be used in the end product - an in-orbit technology demonstrator. To do so, a selection of materials and associated fabrication methods are studied, as described in the literature review, in section 2.1.3. Fabrics are not included in this assessment as they are not suitable for the intended applications. The remaining options are traded off in Table 7.2 based on three main criteria, as described below.

Table 7.2: Prototyping Options Trade-off

Tradeoff Criteria Prototyping Options	Resource Availability	Manufacturing Time	Novelty of Approach
Metals - Manual Folding w/ Master Sheet			
Dual Matrix Composites - Hand Fabrication			
Thermoset SMPs - Hand Fabrication			
Thermoplastics - 3D Printing			



- Resource Availability:** Keeping in mind the available time and budget for the project, it is necessary to consider how easily accessible the required materials are. Additionally, they must be manufacturable with the facilities available at the site of the project i.e., the university or in its vicinity.

3D printing with thermoplastics performs very well in this regard as there is a dedicated additive manufacturing lab at the TU Delft Department of Aerospace Engineering with commonly used materials already available. Composites and metals are a little harder to procure and require more training from technicians to get started with fabrication, which adds extra time to the project. Shape memory polymers are also not easy to procure, and training for the fabrication of these materials is not easily available within the department.

- Manufacturing Time:** Since the project follows a strict timeline, a fast turnaround time is desired so multiple iterations can be done to achieve the optimal manufacturing parameters.

Metals, DMCs, and SMPs, all require manual effort, which is time-consuming. DMCs and SMPs also need curing time which can take several hours to days. For a structure of similar dimensions, 3D printing takes far lesser time and also does not require hands-on work; it is almost entirely computerised.

- Novelty of Approach:** With the current research, it is expected to contribute to the existing body of knowledge with a novel design concept in the field of large deployable

space structures. This novelty can be brought about by the prototyping options chosen, in addition to the concept of origami in space.

DMCs, SMPs, and 3D-printed structures all have promising capabilities but are lesser explored in the space industry. Metals, on the other hand, already possess extensive spaceflight heritage, having been used for decades in various capacities.

Taking these criteria into account, it is clear that 3D printing is the most suitable option for the prototyping of a deployable technology demonstrator. This option will be further explored in the following section.

7.3. 3D Printing

As described in Section 2.1.3, 3D printing or Fused Deposition Modeling is the most commonly used additive manufacturing technique. It is chosen for this project due to its relatively low manufacturing time and easily available material and facilities, making it highly suitable for the early design phase, where rapid prototyping is required.

It is important to note that while 3D printing is used currently for rapid testing of the deployable origami structure's functionality and can potentially be used for the final demonstrator as well, it may not necessarily be scalable to ultra-large structures like habitats. The scalability of the materials and manufacturing technique combination must be considered in future studies.

To manufacture a structure that represents foldable origami, it is necessary to have rigid parts for the panels and flexible parts at the creases. For the rigid sections, polylactic acid (PLA) is chosen. This thermoplastic polymer is the most commonly used material for 3D printing rigid structures. For the flexible parts, thermoplastic polyurethane (TPU) is chosen. TPU is known for its elastic properties and high mechanical strength. With these two materials together, adequate rigidity and flexibility are obtained as required in different parts of the structure. The material properties are listed in 7.3.

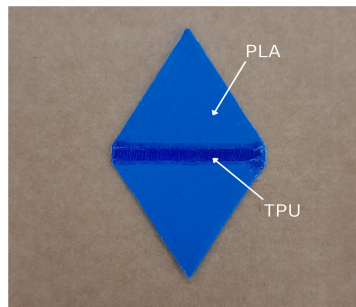
TPU's ability to undergo significant deformation or stretching before failure is indicated by its high elongation at break and low Young's modulus. The high Poisson's ratio is characteristic of rubbery materials that can undergo high deformation and return to their original dimensions on unloading. Therefore, TPU is a suitable option for the creases of the origami structure, which undergo significant strains during folding.

The strength and rigidity of the structure, on the other hand, are obtained from the PLA panels, which possess a high tensile strength of 49.5 MPa and a Young's Modulus of 2346.5 MPa. These parts are brittle and cannot be subjected to plastic deformation in the way the TPU creases can.

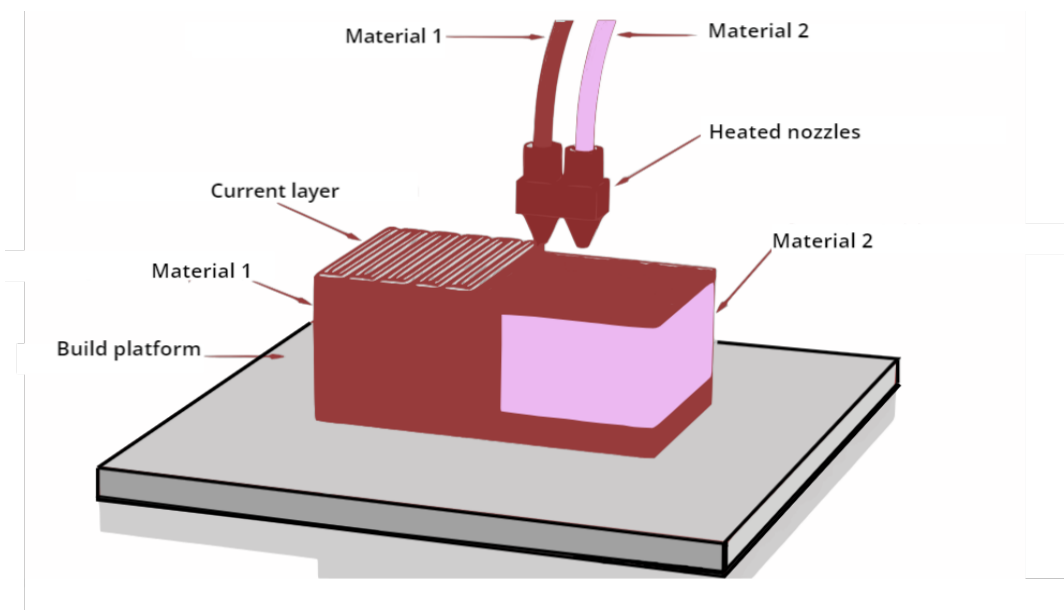
Table 7.3: PLA and TPU Material Properties[64]

Materials	Thermoplastic Polyurethane (TPU)	Polylactic Acid (PLA)
Properties		
Young's Modulus(MPa)	26	2346.5
Tensile Strength(MPa)	8.6	49.5
Elongation at Break(%)	580	5.2
Poisson's Ratio(-)	0.45	0.35

The proposed concept is depicted in Figure 7.15.

**Figure 7.15:** Feasibility check of proposed material choice and manufacturing technique

The specific 3D printing method used for this application is dual hot end extrusion, see Figure 7.16. This involves using a printer with two nozzles extruding two different materials, PLA and TPU in this case. According to the G-code file, the printer alternates between nozzles to extrude the required material. The printer used for this project is the Ultimaker 3+.

**Figure 7.16:** Dual hot end extrusion technique

It was decided to print the origami structure flat, like the paper prototype, and then fold it manually along the creases. It could have been useful to print the 3D structure directly as is, but the creation of the CAD file for the 3D structure is an added hassle. Every single crease and panel has to be created as a separate part and assembled together which is a time-consuming task.

As with the laser cutter, print parameters were gradually varied to identify ideal conditions.

The first step is to ensure the print bed is clean and levelled correctly. The bed is cleaned with isopropyl alcohol and sprayed with an adhesive so the materials stick to the bed. Bed leveling is done manually by following the printer's inbuilt instructions.

The origami flat pattern is first prepared in Solidworks Assembly. Each crease and each panel is a separate part that form the whole assembly, as shown in Figure 7.17. This file is saved as an STL that can be opened in the 3D printer's slicer software, Cura.

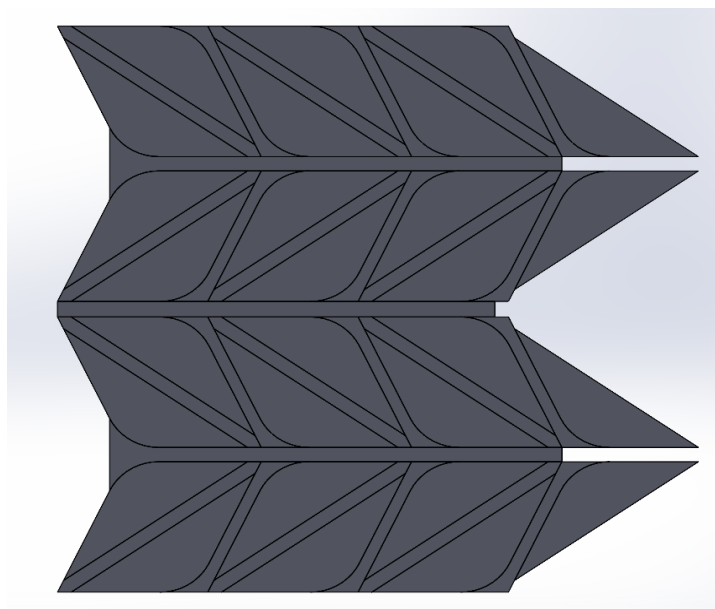


Figure 7.17: Solidworks Assembly

Cura imports all the parts and allows the user to assign different extruders to different parts, depending on the material it needs. The parts are then joined together using the 'Merge model' command and are automatically aligned in the same configuration as in Solidworks, as shown in Figure 7.18. If necessary, the model is resized and rotated to fit the print bed dimensions.

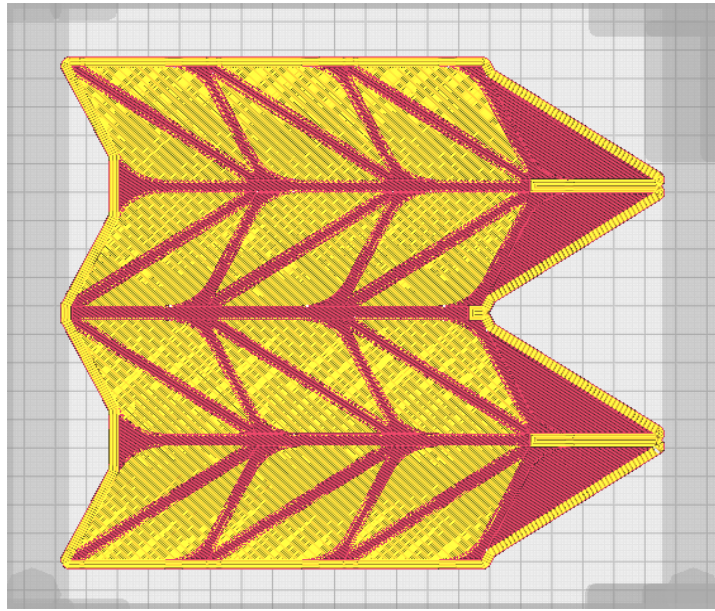


Figure 7.18: Cura preview

The following settings are set initially:

- **Infill density** - Refers to the amount of internal support structure or material that is used to fill the empty space within a printed object. It is expressed as a percentage, where 0% is completely hollow and 100% is solid. High densities provide maximum strength but take a long time to print and vice versa for lower densities. Here, the infill density is set to 100% for both materials.
- **Initial layer height** - This is the height of the first layer of material deposited on the bed. This layer is thicker to ensure proper bed adhesion and compensate for any unevenness on the bed surface. It has been set to 0.2 mm for both materials.
- **Printing temperature** - the nozzle temperature must be higher than the melting point of the material for it to flow through. This is set to 220° C for PLA and 223° C for TPU.
- **Bed temperature** - It is necessary to have a heated bed to prevent warping of the material. It is set to 60° C by default.
- **Print speed** - Refers to the rate at which the 3D printer's nozzle or extruder moves along the X, Y, and Z axes to deposit material and build up the layers of a 3D printed object. Printing too fast can result in imperfections and poor quality, so, a balance must be found between printing speed and time. PLA has been set to print at 50 mm/s, while TPU prints at 25 mm/s. These values are obtained by starting from a higher speed and gradually decreasing it until the print is of sufficient quality.
- **Adhesion** - To ensure adhesion of the structure to the print bed during printing, an adhesion component can be added—brim, skirt, or raft—depending on the print object and printer and bed conditions. In this case, the brim is used which adds a single layer of flat material around the print to prevent warping. The brim is created with PLA.
- **Top/bottom line directions(TPU)** - Refer to the orientation in which the layers of the top and bottom surfaces of a 3D printed object are printed. These settings impact the visual appearance and structural integrity of these surfaces. The default printing direction is

45° and 135° but is changed to 100° to align as close as possible with the direction of folding for maximum pliability.

- **Mesh overlap** - This is one of the most important settings for the current application. The mesh overlap allows the panels and creases to slightly overlap to create a bond in every layer, see Figure 7.19. This aids in creating a cohesive unit rather than printing separate elements next to each other that will fall apart. This is a simple method to ensure bonding without needing any post-manufacturing procedures.

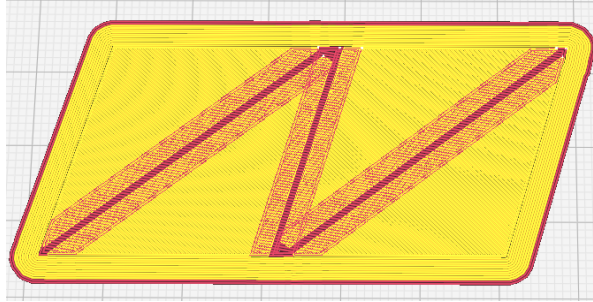


Figure 7.19: Mesh overlap at creases

The printed flat pattern is as shown in Figure 7.20 below, for one half of a 6-sided Kresling origami structure. The pattern was initially printed with a thickness of 0.5 mm which proved to be too thick to fold. The thickness was gradually reduced to 0.3 mm at which point the structure can fold much more easily.

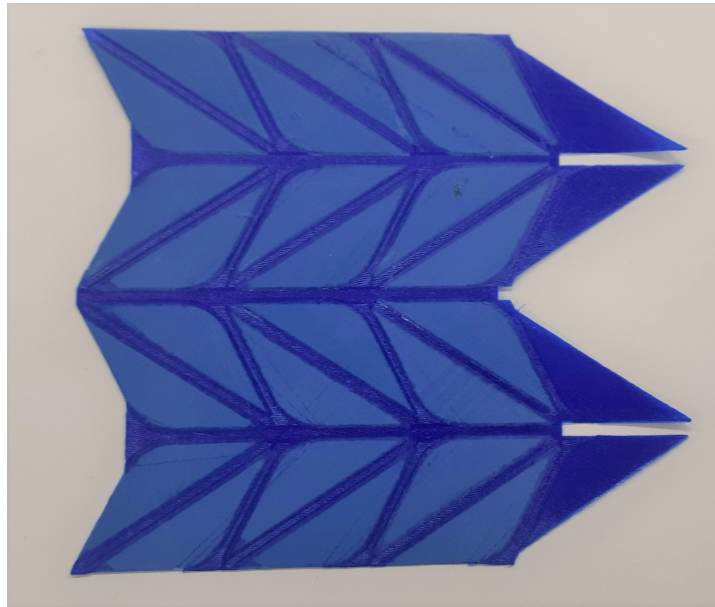


Figure 7.20: Printed flat pattern

Once again, the structure has to be closed using the additional tabs provided on the sides. These are made from TPU and are slightly thinner than the rest of the structure.

To attach these tabs, multiple methods were tried. Cyanoacrylate glue and shoe glue were used but did not hold up during folding. As a temporary solution to close the structure and test its folding capability, the tabs were stapled onto the rigid PLA panels.

Later, plastic soldering was considered as a permanent solution. Here, the TPU tabs are held against the PLA on a hard surface, and welded to it, as shown in Figures 7.21 and 7.22.

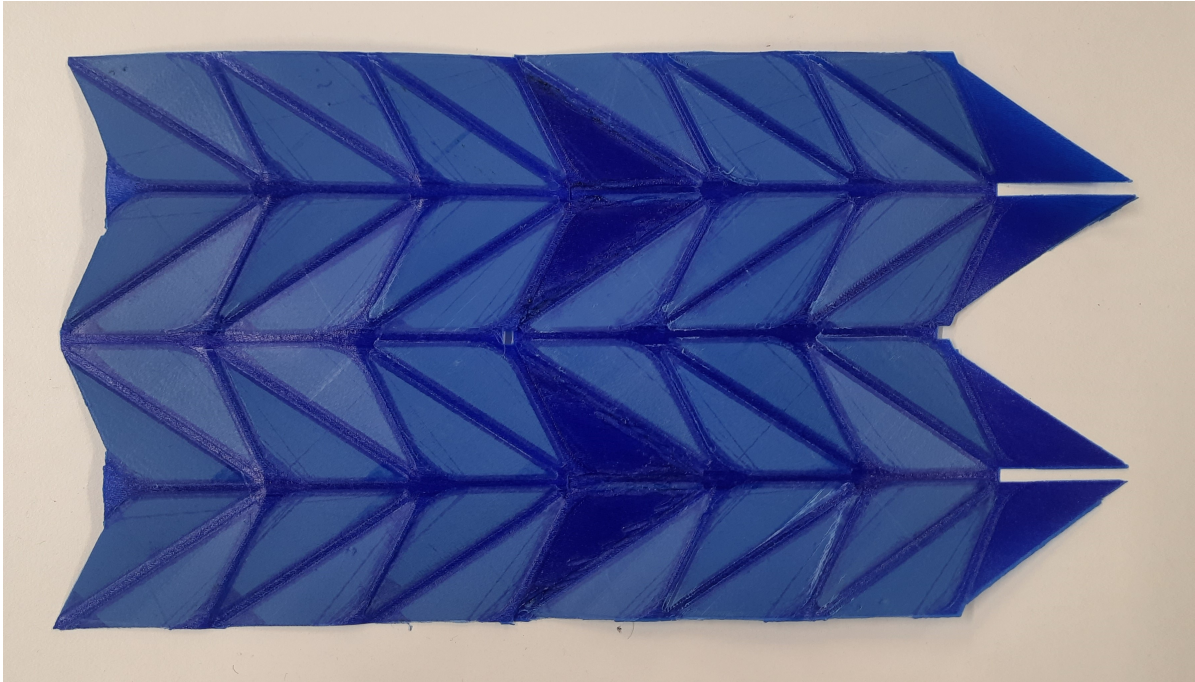


Figure 7.21: Welded tabs - flat pattern



Figure 7.22: Closed 3D printed origami structure

Lastly, to enable load application on the top surface, a hexagonal cover is printed and welded, as shown in Figure 7.23.

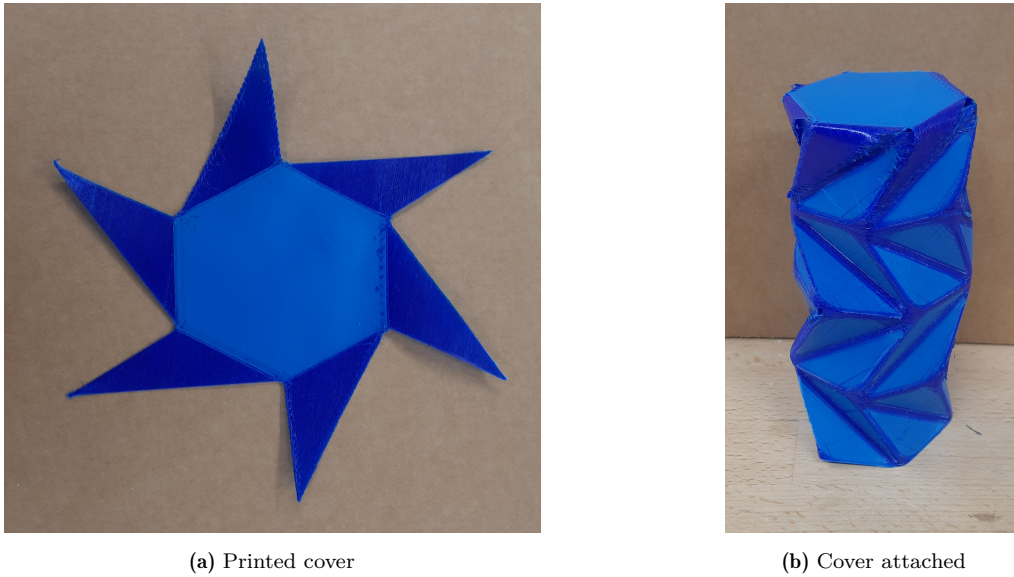


Figure 7.23: Printed top covering

While some of the paper prototypes exhibit bistability, for the same configurations, this behaviour is not exhibited in the 3D printed model, even though bistability is independent of the materials used. This could possibly be due to very nature of the manufacturing method. The layers in the 3D printed model could potentially affect how the structure behaves. Another potential cause could be due to the relatively lesser degree of control in the folding of the 3D structure to form the cylinder. In paper, the creases are formed more uniformly and precisely, enabling bistability. These issues are recommended for further investigation in future work.

7.4. Packaging Ratio and Deployment Ratio

Next, the packaging ratio of the structure is to be determined. Its height is measured with a ruler and is found to be 170 mm. On applying force manually, the structure can be folded down to a height of approximately 22 mm. The packaging ratio is then calculated as follows.

$$\eta = \frac{H_F}{H_D} = \frac{22}{170} = 0.1294$$

The deployment ratio, calculated as the inverse of η , is 7.7 i.e., the structure can be deployed to 7.7 times its folded height.

This concludes the prototyping section of the thesis. Further attempts to manufacture the optimal configuration found in Chapter 6 are not made as first, the problem regarding bringing out the bistability of the structure with the proposed manufacturing technique is to be solved. With the current prototype, an assessment of the structural behaviour is done, as detailed in the next chapter.

8

Structural Performance

In this chapter, the structural performance of the origami structure is investigated with ABAQUS simulations. The intricate modelling work was undertaken by Ester Velazquez Navarro[65], working on the development of a computational representation of the origami structure's behaviour. This thesis builds upon her work to extract meaningful results that provide insights into the origami structure's response to folding and deployment loads.

First, the modelling approach is described to the extent that is necessary to grasp the key factors that define the origami model. This is followed by the results obtained, the conclusions drawn from them, and finally, a discussion of their implications.

8.1. Origami Model Generation

The Python script developed by Velazquez Navarro[65] is used to generate an ABAQUS input file. This script takes the following inputs to define the 3D origami geometry– radius of the 3D structure, height of the flat pattern, number of origami layers, and number of sides of the base polygon.

The materials used in the Property module are the same as chosen in Chapter 7 i.e., PLA and TPU, as shown in Figure 8.1, defined with a thickness of 0.3 mm as in the 3D printed prototype.

Next, loads are defined in the model as described below.

- **Pinned:** The bottom vertices of the structure are pinned to constrain their motion in each axis.
- **Displacement:** The displacement boundary condition is used to facilitate folding. It is applied to the top covering of the origami structure.
- **Pressure:** Pressure is applied to the inner surfaces of the structure to emulate inflation to its final deployed configuration.

The Quad-Tri mesh type is used, which has both quadrilateral and triangular elements. The mesh size is defined by the number of elements along the length of each polygon side(a), with

a maximum mesh size of $\frac{a}{20}$. To reduce simulation time, an inner triangle with fewer elements (larger mesh size) is created in each panel as shown in Figure 8.1a.

The origami structure taken into consideration for this analysis is the same configuration as the prototype i.e., a four-layered, six-sided Kresling structure with an inscribed polygon radius of 5 cm.

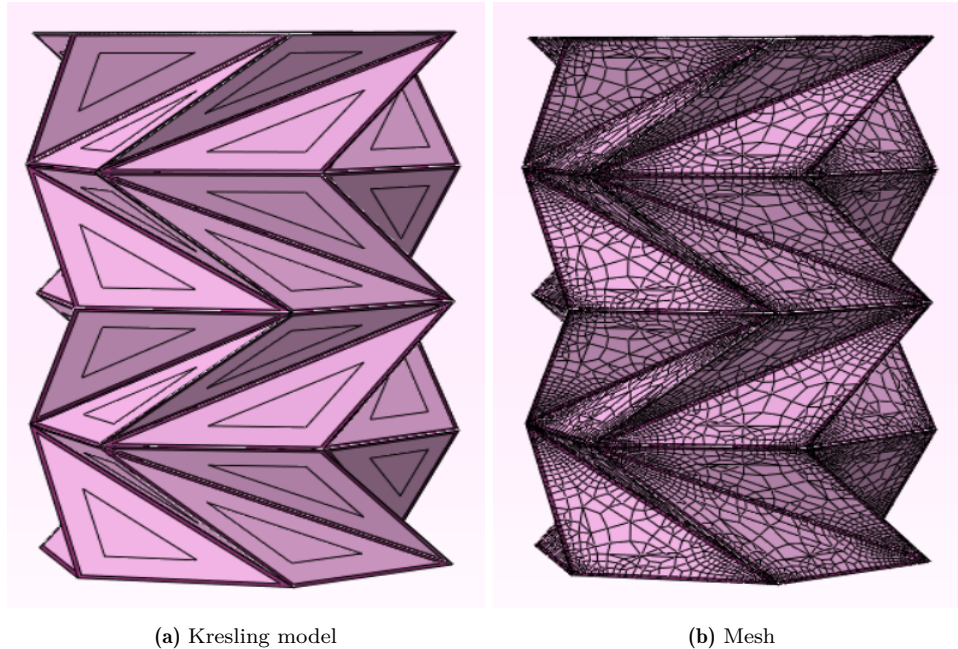


Figure 8.1: ABAQUS origami model generation

8.2. Analysis Procedure

For the simulations, the script accepts "FOLD" or "INF" as the step name, depending on if folding or deployment (inflation) is being simulated. The script performs an Explicit analysis which is generally used for complicated three-dimensional contact problems. In explicit analysis, the displacements and velocities are calculated with quantities known at the start of each increment, thereby not requiring the formation of global mass and stiffness matrices.

The amplitude of the displacement and pressure boundary conditions are applied using a smooth step because then, the simulation is nearly time-independent, and the step time (and, therefore, simulation time) can be lowered. Therefore, the simulation period for each process is set to 0.01 seconds.

Three steps are defined: Folding, Bistable - where the folding force is released, and Inflation - where an internal pressure load is applied. Finally, the job file is created and submitted to obtain the results from history and field outputs. The requested outputs are:

- **Field Outputs (For the whole model):** Von Mises stresses
- **History Outputs:** Strain energy for the whole model, displacement and reaction forces at the top plate

8.3. Simulation Results

In this section, the simulation results are presented and discussed. These results help visualise how the origami structure behaves under folding and deployment loads.

8.3.1. Folding Force

Since the prototype built currently does not exhibit bistable behaviour, the amount of force required to hold it in its folded configuration has to be determined. To do so, a force-displacement curve is obtained. The reaction forces at the top plate are plotted against its displacement during the folding process. The two parameters are obtained by creating a reference point attached to the top plate to which a displacement boundary condition is applied.

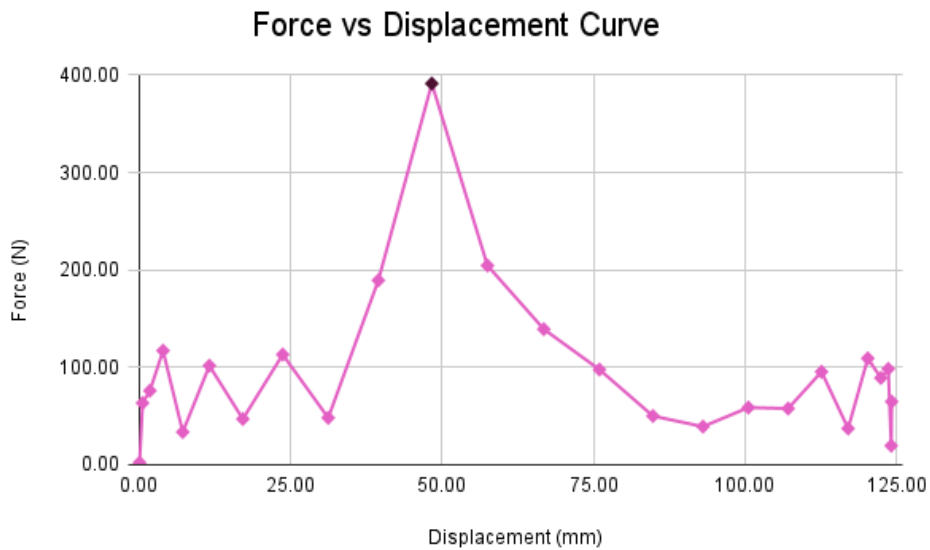


Figure 8.2: Force-Displacement Plot

From Figure 8.2, it is seen that the maximum force applied throughout folding is 391.3 N. Though the force required drops after it peaks at this value, the maximum force is still needed to cross the energy barrier at the peak location, without which the structure will not fold further. This peak in the curve indicates a section where the structure transitions from one stable state to another.

However, in the model, it is seen that for one panel, the contact definition between the crease material and the panel does not exist (see Figure 8.3), causing a split in the structure while folding. This could also possibly be the reason for the sudden spike in required force, as the structure's movement is restricted due to the unconstrained edge. In that case, a lower force would be required in reality to fold the structure. To verify this, a compression test must be done, and the force-displacement curve thus obtained should be compared with the simulation.

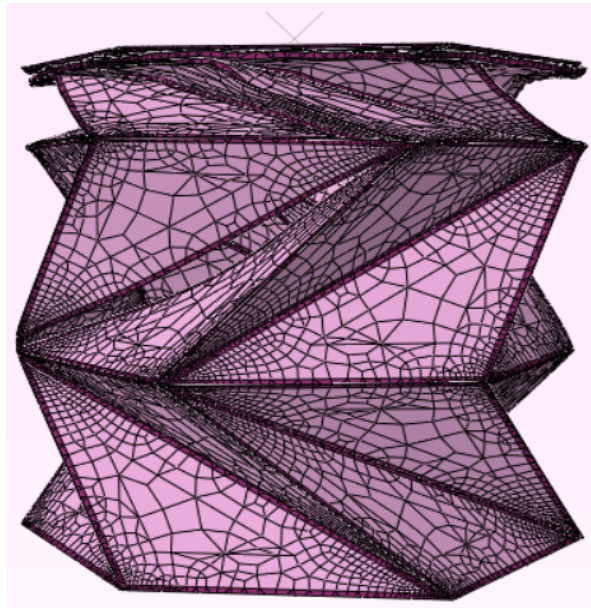


Figure 8.3: Contact definition error

8.3.2. Packaging Ratio

To calculate the packaging ratio, the total energy evolution during the folding process is considered. In Graph 8.4, though the negative energy values are not representative of how energy works in the physical world, the curve can help identify the height up to which it can be folded without accumulating internal energy, as indicated by the sharp spike. The minimum value of energy just before the peak indicates the lowest feasible folded height.

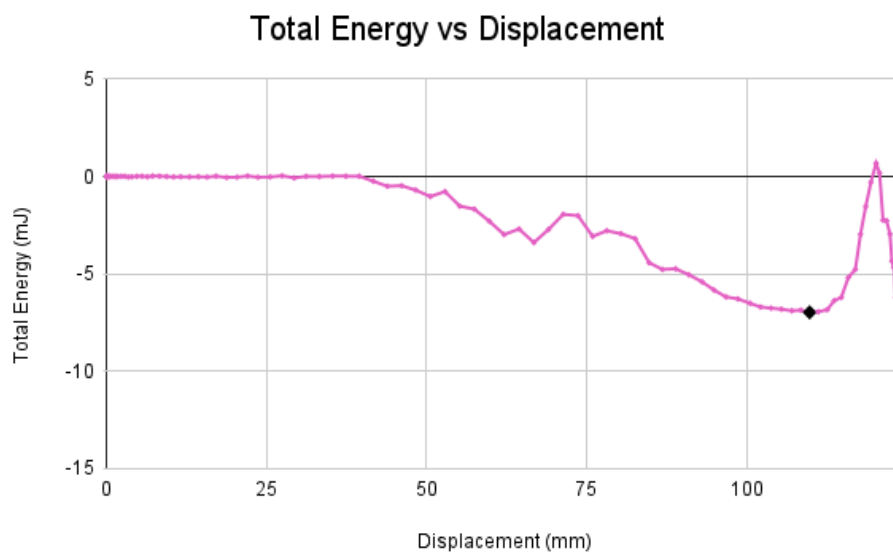


Figure 8.4: Total Energy-Displacement Plot for Folding

In this case, the minimum energy is observed at a displacement of 88.5% of the total deployed height of the structure i.e., 109.85 mm, or a folded height of 14.33 mm. The packaging ratio

is then calculated as follows.

$$\eta = \frac{H_F}{H_D} = \frac{14.33}{124.18} = 0.1154$$

Subsequently, the deployment ratio is calculated as the inverse of the packaging ratio i.e., $\frac{1}{0.1154} = 8.6$. This means that the structure can be deployed to 8.6 times its folded height.

In Chapter 7, the deployment ratio was found to be approximately 7.7, with a folded height of 20 mm or 2 cm. This can be attributed to the added material thickness at the seams where an extra TPU layer is used to form the closed structure. This is not accounted for in the ABAQUS model.

8.3.3. Strain Energy

Graph 8.5 depicts the strain energy in the whole structure during the folding process, though maximum strain energy is expected to be stored in the TPU creases. It is seen that strain energy gradually increases during folding(displacement). At about halfway through the displacement, a hill-like peak is formed. This is assumed to be due to the strain-softening non-linear behaviour of TPU, where it transitions from elastic to plastic deformation.

Shortly after, there is a significant rise in strain energy which means the structure is at equilibrium but is unstable i.e., requires very little displacement to switch to a stable state. Following this brief peak, the energy drops again, indicating another stable state. In addition to the two stable states, the initial configuration is also considered to be a stable state, thereby resulting in a multi-stable structure.

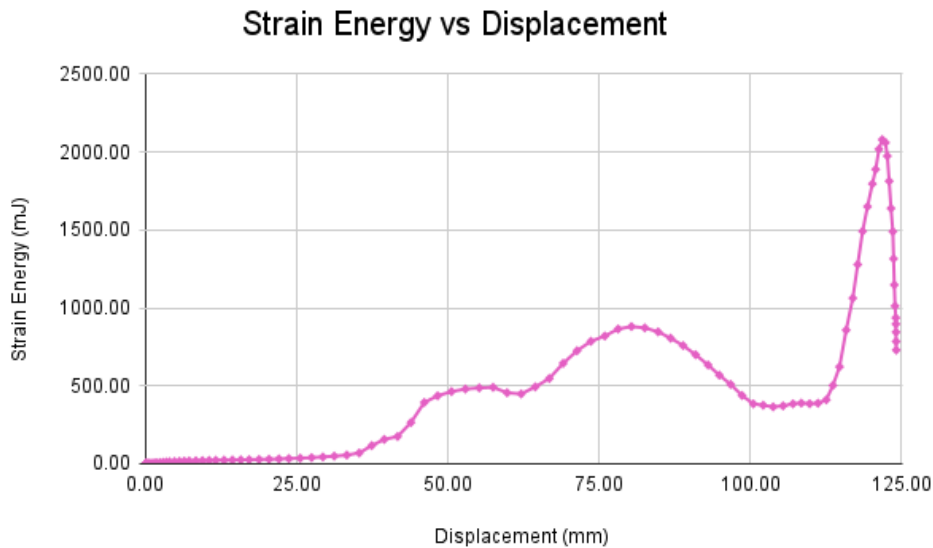


Figure 8.5: Strain Energy-Displacement Plot for Folding

This multi-stability is not observed in the prototype, as explained in Chapter 7, which could be due to a non-optimal manufacturing technique.

The next plot, Graph 8.6, the strain energy during the phase where the folding force is released, and the structure is allowed to settle into a stable state. It can be seen that it does not return to its initial fully deployed configuration with minimum strain energy but settles into a second stable state, indicated by the gradually reducing strain energy. In this phase, further displacement does not lead to a substantial change in strain energy.

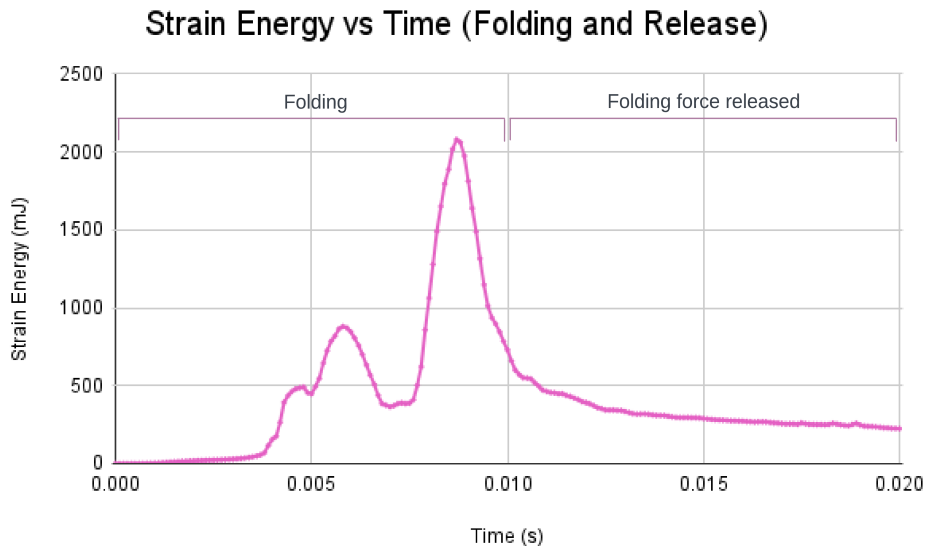


Figure 8.6: Strain Energy during folding and release

In Graph 8.7, it is seen that after the force used to fold the structure is released, it does not go back to its original height; instead, it stops unfolding at an intermediate displacement of 56.5 mm (or at a height of 67.68 mm which is likely a stable state).

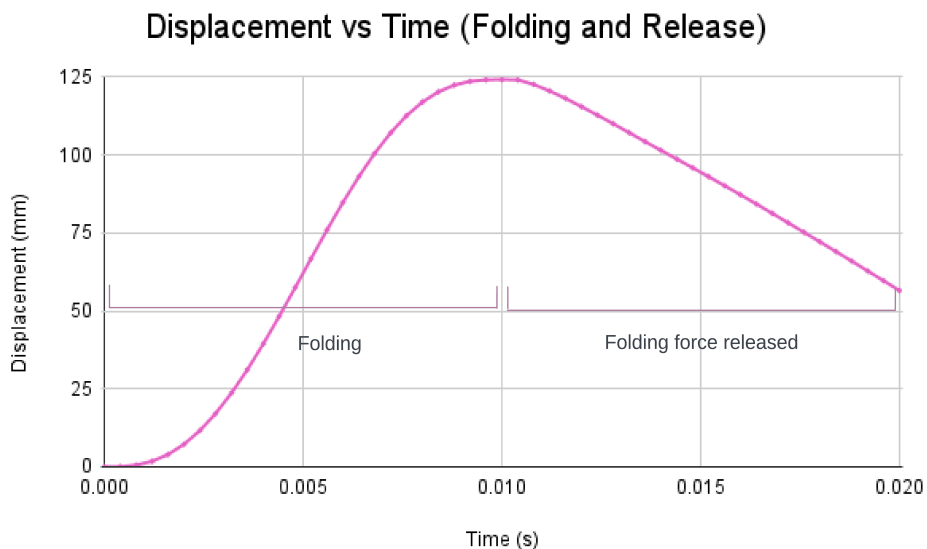


Figure 8.7: Displacement during folding and release

Finally, Graph 8.8 shows the strain energy evolution during inflation. It behaves as expected as the internal pressure is bound to result in strains, especially in the more flexible TPU creases, as the structure undergoes deformation to further change its configuration. As the inflation progresses, the material elements within the structure experience increasing levels of deformation due to the pressure load. This deformation leads to an increase in the strain energy stored within the material.

The displacement switches from negative to positive values, indicating that inflating it has caused it to surpass its initial height before folding to now form a large structure.

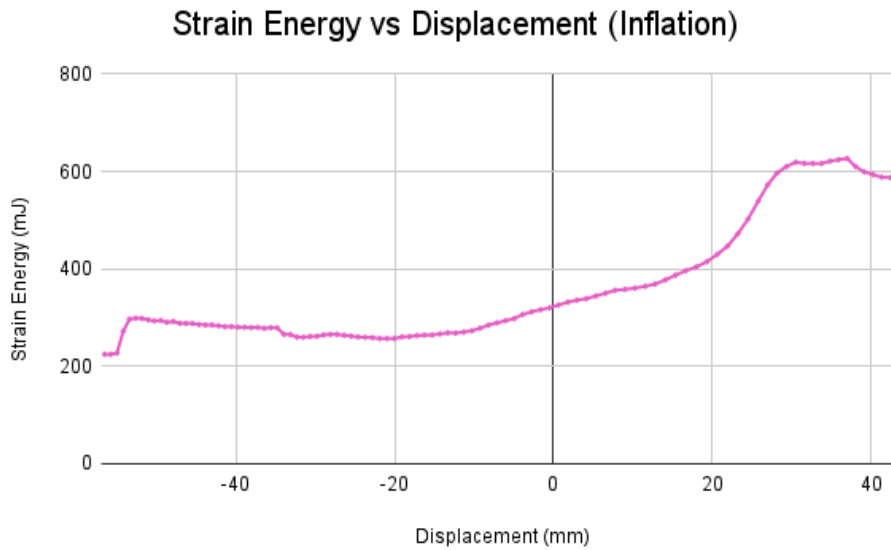


Figure 8.8: Strain Energy-Displacement Plot for Inflation

8.3.4. Contour Plots

Next, the Von Mises stress and strain contour plots are presented. As expected, the maximum stress is present in the PLA panels, near the vertices or along the fold lines. Due to PLA's lower ability to deform plastically, it undergoes higher stresses at the sharp edges i.e., the folds. The maximum stress is 774.5 MPa which is well above the yield strength of PLA. However, this occurs only at one location. In the rest of the structure, the stresses experienced are quite low, below the yield strengths of the materials.

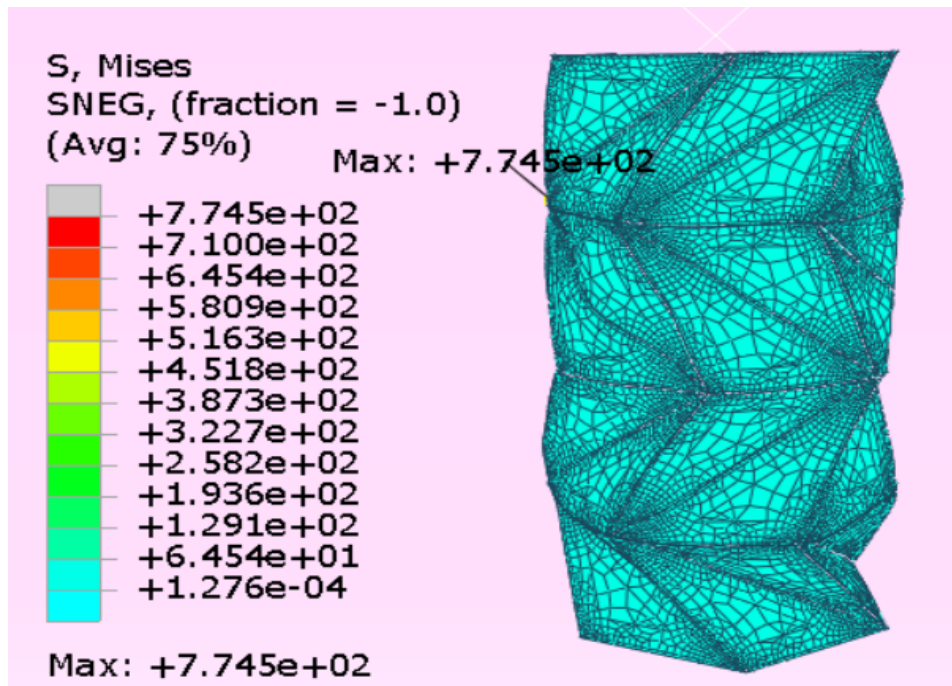


Figure 8.9: Stress Distribution

Similarly, the strain distribution is also as expected, with the highest strains at the fold lines made of TPU. The stresses at the creases induce stretching and deformation, resulting in high strains, as indicated by the pink colouring of the creases (Figures 8.10, 8.11, and 8.12), which are accommodated by the TPU material's flexibility.

While the simulation results allow us to obtain an understanding of the structure's behaviour under folding and deployment loads, they are yet to be validated with results from experimentation, after which the model can be used for further prediction of the structure's behaviour for different configurations. This task can be undertaken in the future as an extension of this project.

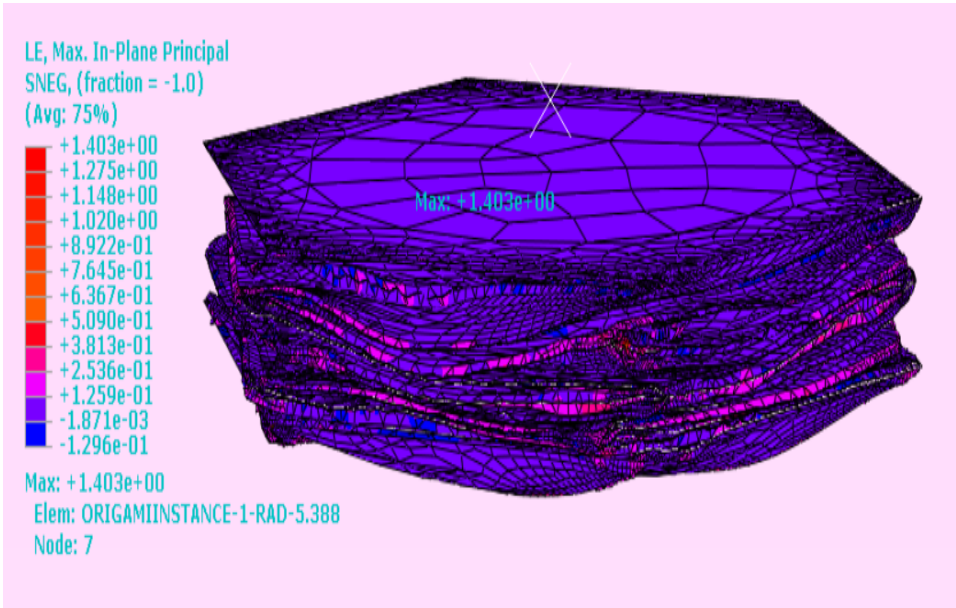


Figure 8.10: Strains after folding

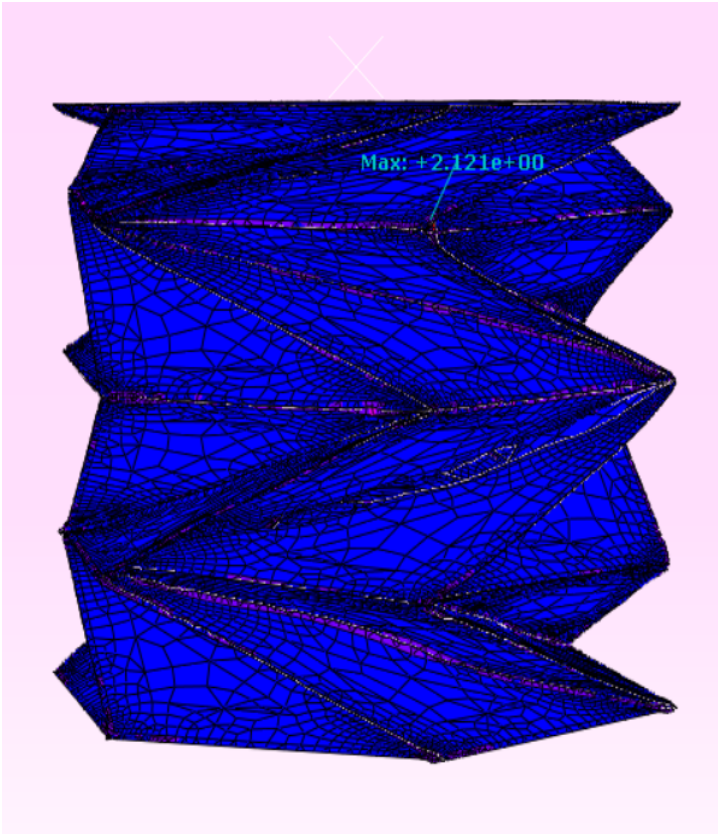


Figure 8.11: Strains after folding force is released

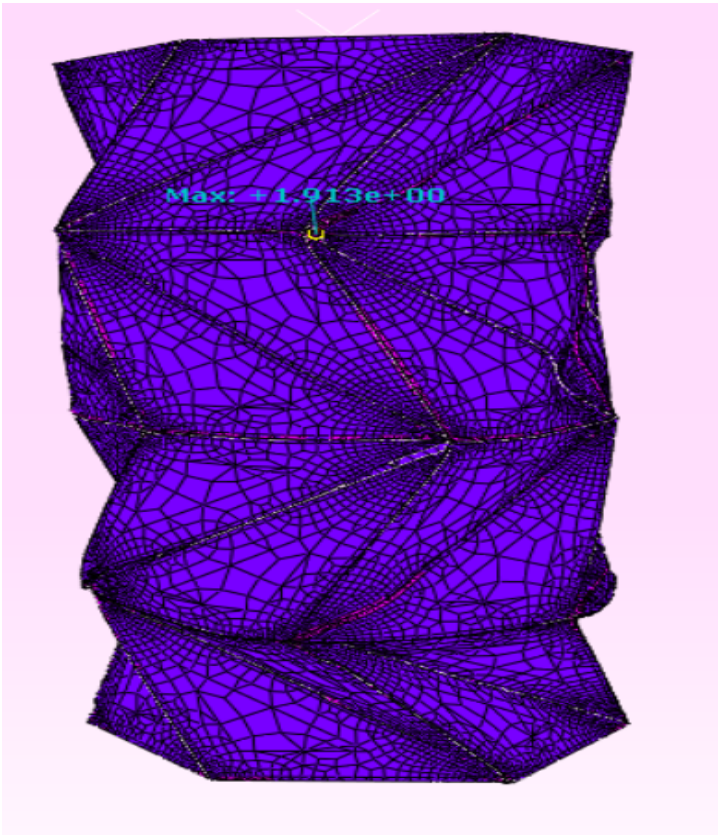


Figure 8.12: Strains after inflation

9

Design Guidelines

As the field of engineering origami is relatively new, the design possibilities are seemingly endless. However, it is prudent to have a set of guiding principles to help navigate the complex relationships between origami patterns, their foldability, manufacturability, and other important aspects. With a common framework, it is easier to ensure consistency and reliability, while narrowing down the design space by eliminating solutions that may seem feasible but break down upon further examination.

The current work aims to provide a set of guidelines for designing Kresling origami deployable structures. These guidelines were derived as a result of Rhino optimisation studies for maximum usable inner volume, prototyping, and its foldability in Rhino and the physical prototype. This is done because, sometimes, the optimal configuration output by Rhino cannot necessarily fold and act as a deployable structure or even be manufacturable (due to very small dimensions) so it is important to define boundaries within which the Rhino results comply with its actual physical behaviour.

The approach used to arrive at the proposed guidelines is as follows.

- First, the radius is fixed at 5 cm as this is the design radius for the deployable structure demonstrator within the CubeSat (**ORI-CON-1**).
- For the fixed radius, the optimal number of sides and layers is identified.
- The Rhino model is used to identify the range within which the number of layers and number of sides work together. The unsuitable values are ones where the model does not generate or break upon folding due to incompatibility of geometric parameters.
- Next, the physical boundaries of the number of sides are to be identified. This is done by laser cutting paper prototypes with varying numbers of sides and testing their ability to fold to form the closed structure as well as fold to compress to a smaller volume. Solutions are deemed unfeasible if they tear or break upon trying to close the structure or fold it vertically. This process does not need to be repeated for the number of layers as that parameter is related to the number of sides, as is revealed during this step.

For radius 5 cm, the number of sides is varied - 10, 12, 14, 15, 16, and 17. As seen below in Figure 9.1, for 10-15 sides, the prototypes remain intact with minimal tears. These tears are

attributed to minor missteps during the manual folding process but do not necessarily affect the performance of the structure.

Structures with 16 and 17 sides, however, are nearly impossible to fold manually.



Figure 9.1: Prototypes with radius 5 cm - increasing number of sides(left to right)

Using the aforementioned approach, the following guidelines are formed.

1. Number of layers should not exceed $(2 \times \text{number of sides}) + 1$. Layers increased beyond this limit do not generate in the Rhino model, and with a prototype, it is impossible to fold into a cylinder.
2. From a manufacturing perspective, the maximum feasible number of sides is 15 for the fixed radius of 5 cm. Beyond 15, it is extremely difficult to fold manually to close the structure, and even if done, it is difficult to compress without tearing it.
3. Layer height should be greater than ≈ 2.8 cm. It is found that all models that break upon folding have a layer height lesser than 2.8 cm.

While these guidelines apply to a fixed 5 cm radius, to generate more general guidelines, the whole process is repeated for a radius of 4 cm. This helps identify patterns and rule out coincidences that may arise from only testing with a single radius.



Figure 9.2: Prototypes with radius 4 cm - increasing number of sides(left to right)

The guidelines thus obtained are:

1. Number of layers should not exceed $(2 \times \text{number of sides}) + 1$.
2. Layer height should be greater than ≈ 2.8 cm. It is found that all models that break upon folding have a layer height lesser than 2.8 cm in the Rhino model and the paper prototype.
3. The maximum feasible number of sides is three times the radius of the base polygon.

4. Fewer the sides, the better the manufacturability. However, it is also found via simulations[65] that a larger number of sides improves the structural performance. Therefore, a balance must be struck between optimising for manufacturability and structural performance.

However, it must be noted that these guidelines have been verified only with paper prototypes and not other materials. Hence, they must be used with reasonable discretion. While the structural behaviour may vary for different materials, the general patterns are expected to be similar.

These guidelines provide a general framework within which an optimal configuration can be identified.

10

Requirements Verification

This chapter delves into the pivotal phase of requirements verification, wherein the requirements defined at the start of the project are revisited to check if the proposed design concept complies with them. Each requirement is evaluated based on the verification method defined in Chapter 3 to determine if the acceptance criteria are met. The satisfied requirements are highlighted in green, and requirements that are partially satisfied (or not fully tested) are highlighted in yellow. One requirement has not been verified yet.

Table 10.1: Requirements compliance check

ID	REQUIREMENT	ACCEPTANCE CRITERIA	VERIFICATION METHOD	COMPLIANCE CHECK
ORI-KIL-1	The origami structure must be able to withstand deployment(unfolding) loads	The structure does not break or deform during deployment	Deployment test and simulation	The structure does not break or significantly deform and largely does not exceed material limits, as shown in Chapter 8.
ORI-KIL-2	The origami structure must be able to withstand compression(folding) loads	The structure does not break or deform during folding	Compression test and simulation	The structure does not break or significantly deform, as shown in Chapter 8.
ORI-DRI-1	The origami structure shall be deployable multiple times	The structure does not break or deform during multiple folding and unfolding cycles	Deployment and compression tests	The structure has been manually folded and unfolded multiple times without significant damage.
ORI-CON-1	The origami structure in its stowed configuration shall have a volume no larger than 100 x 100 x 150 mm ³	The folded configuration has a volume of no larger than half a 12U CubeSat, in accordance with tolerances i.e., 100 x 100 x 15 mm ³	Measurement of model and prototype	As shown in Chapter 6, the optimal configuration has a radius of 50 mm a stowed height of ~40 mm, and an outer volume of 3141.5 mm ³ .
ORI-CON-2	The origami structure shall not weigh more than ~10 kg (~41% of 24 kg)	The prototype has a weight of <=10 kg	Weight measurement of the prototype	Not verified yet.
ORI-DRI-2	The origami structure shall exhibit a predictable deployment	The prototype deploys in the correct direction at a consistent rate and does not get stuck during deployment.	Observation	This requirement is satisfied with manual folding and unfolding but has not been verified with inflation.
ORI-DRI-3	The origami structure shall be rigid once deployed.	The prototype shall not revert to its folded configuration after deployment is complete.	Observation	Once unfolded, the structure remains in its deployed configuration, as observed with the 3D printed prototype.
ORI-DRI-4	The origami structure shall be deployable from a stowed to unfolded configuration of atleast twice the height.	The deployed height of the prototype is atleast twice the height of the folded structure	Height Measurement	The deployed height of the 3D printed prototype is 7.7 times that of its stowed height, as seen in Chapter 7.
ORI-DRI-5	The material of the origami structure shall be easily available	The material is affordable and easily accessible for purchase online or in store	Observation	The chosen thermoplastic filaments are readily available in the TU Delft DASML laboratory.
ORI-DRI-6	The chosen manufacturing technique must be accessible	The manufacturing technique should be an existing one, accessible by institutional staff, and inexpensive to use.	Observation	The dual extrusion 3D printer required for manufacturing is readily available in the TU Delft DASML laboratory and can be used with minimal training.

11

Conclusions and Recommendations

This chapter marks the culmination of the thesis, providing an overview of results as well as recommendations to guide future research. First, the research questions formulated in Chapter 2 are answered, following which recommendations for future work are made based on lessons learned during the course of the project.

11.1. Research Questions

This section serves to answer the sub-questions posed in Chapter 2 to help answer the main research question,

"How can an origami-based deployable structure be designed for integration with a 12U CubeSat while ensuring structural integrity during and after folding and deployment?"

Q1: What origami pattern and deployment mechanism combination is suitable for simple, predictable, and repeatable deployment?

The most feasible combination was found to be the deployment of a Kresling patterned cylinder via inflation. To answer this question, a systems engineering approach is followed, as described in Chapter 3. First, a handful of suitable origami patterns and deployment mechanisms are selected based on past research studied during the literature review. The individual properties of each pattern and deployment mechanism are explored to assess their compatibility with one another. Four promising combinations are picked, namely,

- Yoshimura pattern - Telescopic deployment
- Kresling pattern - Lanyard deployment
- Kresling pattern - Inflation
- Yoshimura pattern - Booms

From these combinations, the pool was narrowed down to two candidates after a brief analysis of their advantages and disadvantages—Yoshimura with telescopic deployment and Kresling with inflation. These options are then traded off graphically, resulting in the Kresling structure with inflation deployment proving to be the most suitable for the mission requirements.

Q2: What pattern configuration is ideal for maximising inner volume and packaging ratio?

The optimal Kresling pattern configuration for maximum volume and packaging ratio was found to be:

Number of sides for the base polygon: 14

Number of cylindrical layers: 11

Deployed height: 39 cm

Chapter 6 delves into finding an optimal configuration for the chosen Kresling pattern. To do so, the Grasshopper model is used. An optimisation module based on evolutionary algorithms, Galapagos, is added to the model. With the number of sides, number of layers, and deployed height as inputs, Galapagos optimises for maximum available inner volume. With the optimal configuration found, the stowed height obtained is 4 cm and therefore, the packaging ratio is 9.72. The actual packaging ratio is expected to be a little lower to account for added thickness at the seams of the cylindrical structure. The available inner volume is found to be 2265 cm³.

However, as mentioned previously, evolutionary algorithms pick random pools from the population to optimise from, so it may be that there is a slightly better configuration that was left out of the initial population. To avoid neglecting a drastically better configuration, the optimisation procedure was run several times and was found to output similar results.

Q3: How can the proposed structure be manufactured?

The manufacturing aspect of the system design is explored in Chapter 7. First, a tradeoff was conducted between various manufacturing techniques explored during the literature study, following which it was decided to use additive manufacturing to create the origami prototype. With 3D printing, thermoplastic polymers are most commonly used; Polylactic acid (PLA) was chosen for the rigid sections of the origami and thermoplastic polyurethane (TPU) for the flexible sections i.e., the creases.

The pattern is printed flat and folded into a cylinder. The hot-end dual extrusion method was used to print both materials simultaneously such that each layer of the flat pattern has both rigid PLA panels and flexible TPU creases. The print parameters are varied systematically until high print quality is achieved.

While this method is suitable for building an origami prototype that folds as it should, it does have some shortcomings. With the facilities available, the printing time for one prototype is several days as it has to be printed in multiple parts.

Moreover, the bistability of the structure is not exhibited, so force will be required to hold it in its stowed configuration.

For future research, it is recommended to use a printer with a larger bed as well as specifically tune geometric parameters to exhibit bistability, as currently, the design does not explicitly account for it.

Q4: How do the folding and deployment loads affect the structural integrity of the proposed structure?

Chapter 8 delves into the computational analysis of the origami structure's behavior in response to folding and deployment loads.

The stresses experienced by the structure are found to be mostly lower than the yield strengths of PLA and TPU, except at the location of maximum stress, where it exceeds the yield strength of PLA. Other results are also studied, such as the evolution of strain energy, which indicates multiple stable states. The displacement-time plot indicates the height to which the structure bounces back after the compressive force is released. At this height, the structure is assumed to be in a stable state.

11.2. Recommendations

Based on lessons learned during the course of the project, some recommendations are made for future work in designing an origami-inspired deployable structure. With these action points, the design can be further developed to reach a TRL level of 4 ("technology validated in the lab"), following which it can be integrated with a 12U CubeSat for further validation and technology demonstration.

Recommendation 1

The current parametric 3D model developed in Rhino generates the origami structure, optimal configurations, and geometric parameters. However, it does not predict if the output origami structure is bistable in nature, thus making it impossible to determine if the manufactured prototype will be bi/multistable or monostable. It is important to know how many stable states the structure has as for the applications it is being designed for, a bistable structure that can maintain its fully folded configuration without considerable external forces is desired. This is a feature that future researchers could look into incorporating within the model so that only bistable structures are output and used in the prototyping stage.

Recommendation 2

With the present proposed manufacturing technique—dual extrusion 3D printing—the expected bistability is not exhibited in the prototype as it does in the laser-cut paper prototype. For future work, it is advised to consider how bistability can be brought about in the prototype with the 3D printing method. Alternatively, the other material and manufacturing option presented during the tradeoff, hand fabrication of dual matrix composites, can be explored.

Recommendation 3

In the present work, at the prototyping stage, only a simple structure with few polygon sides and layers is manufactured. This was done in an attempt to first determine ideal manufacturing conditions that enabled the structure to exhibit all expected behaviour. Since, at this stage, it was noted that exhibiting its bistable nature was still an issue, further prototyping efforts went into rectifying this and, therefore, could not proceed with manufacturing the optimal configuration found in Chapter 6. So, as the next step, it is advised to manufacture this optimal configuration once Recommendations 1 and 2 are sufficiently acted upon.

Recommendation 4

Lastly, the current work only studies the structural performance computationally, with an ABAQUS model. However, these results also need to be validated with experimentation. The recommended experiments are a compression test and an inflation test to extract the same results as in Chapter 8 to validate them.

Bibliography

- [1] S. Tkatchova and M. van Pelt, “Commercialisation Of Space Technology For Tomorrow’s Space Missions,” *Commerce in Space*, Jan. 2011. DOI: 10.4018/9781599046242.CH012.
- [2] *Bigelow Expandable Activity Module (BEAM) | NASA*. [Online]. Available: https://www.nasa.gov/mission_pages/station/structure/elements/bigelow-expandable-activity-module.html (visited on 02/05/2023).
- [3] *Axiom Commercial Space Station Axiom Space*. [Online]. Available: <https://www.axiomspace.com/axiom-station> (visited on 02/05/2023).
- [4] G. Valle, D. Litteken, and T. C. Jones, “Review of habitable softgoods inflatable design, analysis, testing, and potential space applications,” *AIAA Scitech 2019 Forum*, no. January, pp. 1–15, 2019. DOI: 10.2514/6.2019-1018.
- [5] M. Meloni, J. Cai, Q. Zhang, *et al.*, “Engineering Origami: A Comprehensive Review of Recent Applications, Design Methods, and Tools,” *Advanced Science*, vol. 8, no. 13, 2021. DOI: 10.1002/advs.202000636.
- [6] S. Li, H. Fang, S. Sadeghi, P. Bhovad, and K. W. Wang, “Architected Origami Materials: How Folding Creates Sophisticated Mechanical Properties,” *Advanced Materials*, vol. 31, no. 5, pp. 1–18, 2019, ISSN: 15214095. DOI: 10.1002/adma.201805282.
- [7] B. Sargent, J. Butler, K. Seymour, *et al.*, “An Origami-Based Medical Support System to Mitigate Flexible Shaft Buckling,” *Journal of Mechanisms and Robotics*, vol. 12, no. 4, Aug. 2020. DOI: 10.1115/1.4045846.
- [8] M. Pesenti, G. Masera, and F. Fiorito, “Exploration of Adaptive Origami Shading Concepts through Integrated Dynamic Simulations,” *Journal of Architectural Engineering*, vol. 24, no. 4, Dec. 2018, ISSN: 1076-0431. DOI: 10.1061/(ASCE)AE.1943-5568.0000323.
- [9] S. Li, J. J. Stampfli, H. J. Xu, *et al.*, “A vacuum-driven origami ‘magic-ball’ soft gripper,” *Proceedings - IEEE International Conference on Robotics and Automation*, vol. 2019-May, pp. 7401–7408, May 2019, ISSN: 10504729. DOI: 10.1109/ICRA.2019.8794068.
- [10] M. Schenk, A. D. Viquerat, K. A. Seffen, and S. D. Guest, *Review of inflatable booms for deployable space structures: Packing and rigidization*, 2014. DOI: 10.2514/1.A32598.
- [11] M. Schenk, S. G. Kerr, A. M. Smyth, and S. D. Guest, “Inflatable Cylinders for Deployable Space Structures,” *First Conference Transformables 2013*, no. September, pp. 1–6, 2013. [Online]. Available: <http://www.markschenk.com/research/files/schenk2013-Transformables.pdf>.
- [12] L. Wilson, S. Pellegrino, and R. Danner, “Origami sunshield concepts for space telescopes,” *54th AIAA/ASME/ASCE/AHS/ASC Structures, Structural Dynamics, and Materials Conference*, 2013. DOI: 10.2514/6.2013-1594. [Online]. Available: <https://arc.aiaa.org/doi/10.2514/6.2013-1594>.

- [13] W. Chen, G. Fang, and Y. Hu, "An experimental and numerical study of flattening and wrapping process of deployable composite thin-walled lenticular tubes," *Thin-Walled Structures*, vol. C, no. 111, pp. 38–47, Feb. 2017, ISSN: 0263-8231. DOI: 10.1016/J.TWS.2016.11.009. [Online]. Available: <https://www.infona.pl/resource/bwmeta1.element.elsevier-13ba56b2-2d4e-3c9f-8067-45b7074b6cf5>.
- [14] R. S. Pappa, J. O. Lassiter, and B. P. Ross, "Structural dynamics experimental activities in ultralightweight and inflatable space structures," *Journal of Spacecraft and Rockets*, vol. 40, no. 1, pp. 15–23, 2003, ISSN: 15336794. DOI: 10.2514/2.3934.
- [15] H. Heidt, J. Puig-Suari, A. Moore, S. Nakasuka, and R. Twiggs, "CubeSat: A New Generation of Picosatellite for Education and Industry Low-Cost Space Experimentation," 2000.
- [16] E. Peraza Hernandez, D. Hartl, R. Malak, and D. Lagoudas, "Origami-inspired active structures: A synthesis and review," *Smart Materials and Structures*, vol. 23, p. 094001, Aug. 2014. DOI: 10.1088/0964-1726/23/9/094001.
- [17] L. Puig, A. Barton, and N. Rando, "A review on large deployable structures for astrophysics missions," *Acta Astronautica*, vol. 67, no. 1, pp. 12–26, 2010, ISSN: 0094-5765. DOI: <https://doi.org/10.1016/j.actaastro.2010.02.021>. [Online]. Available: <https://www.sciencedirect.com/science/article/pii/S0094576510000743>.
- [18] M. Lee, "Tunable bistability of origami-based mechanical metamaterials," in *AIAA SciTech Forum - 55th AIAA Aerospace Sciences Meeting*, American Institute of Aeronautics and Astronautics Inc., 2017, ISBN: 9781624104473. DOI: 10.2514/6.2017-2007.
- [19] B. S. Yeow, C. J. Cai, M. S. Kalairaj, *et al.*, "Origami-Inspired Snap-Through Bistability in Parallel and Curved Mechanisms Through the Inflection of Degree Four Vertices," in *Proceedings - IEEE International Conference on Robotics and Automation*, vol. 2021-May, Institute of Electrical and Electronics Engineers Inc., 2021, pp. 10 863–10 869, ISBN: 9781728190778. DOI: 10.1109/ICRA48506.2021.9562094.
- [20] T. Hull, "On the mathematics of flat origamis," *Congressus Numerantium*, vol. 100, Nov. 1995.
- [21] Q. Lin, W. Jia, H. Wu, *et al.*, "Wrapping deployment simulation analysis of leaf-inspired membrane structures," *Aerospace*, vol. 8, no. 8, 2021. DOI: 10.3390/aerospace8080218.
- [22] D. N. Badodkar and T. A. Dwarakanath, *Machines, Mechanism and Robotics*. 2019, vol. li, p. 841, ISBN: 978-981-10-8596-3. [Online]. Available: <http://link.springer.com/10.1007/978-981-10-8597-0>.
- [23] K. Senda, T. Oda, S. Ohta, *et al.*, "Deploy experiment of inflatable tube using work hardening," *Collection of Technical Papers - AIAA/ASME/ASCE/AHS/ASC Structures, Structural Dynamics and Materials Conference*, vol. 4, no. May, pp. 2595–2612, 2006, ISSN: 02734508. DOI: 10.2514/6.2006-1808.
- [24] J. E. Suh, T. H. Kim, and J. H. Han, "New approach to folding a thin-walled yoshimura patterned cylinder," *Journal of Spacecraft and Rockets*, vol. 58, no. 2, pp. 516–530, 2021, ISSN: 15336794. DOI: 10.2514/1.A34784. [Online]. Available: <https://doi.org/10.2514/1.A34784>.

- [25] Q. Zhang and J. Cai, “Bistable behaviour of a deployable cylinder with Kresling pattern,” *7th International Meeting on Origami in Science, Mathematics and Education (7OSME)*, no. September, 2018.
- [26] Z. Zhai, Y. Wang, and H. Jiang, “Origami-inspired, on-demand deployable and collapsible mechanical metamaterials with tunable stiffness,” *Proceedings of the National Academy of Sciences of the United States of America*, vol. 115, no. 9, pp. 2032–2037, Feb. 2018, ISSN: 10916490. DOI: 10.1073/PNAS.1720171115.
- [27] N. Kidambi and K. W. Wang, “Dynamics of kresling origami deployment,” *Phys. Rev. E*, vol. 101, p. 063003, 6 Jun. 2020. DOI: 10.1103/PhysRevE.101.063003. [Online]. Available: <https://link.aps.org/doi/10.1103/PhysRevE.101.063003>.
- [28] H. Wu, H. Fang, L. Chen, and J. Xu, “Transient dynamics of a miura-origami tube during free deployment,” *Phys. Rev. Appl.*, vol. 14, p. 034068, 3 Sep. 2020. DOI: 10.1103/PhysRevApplied.14.034068. [Online]. Available: <https://link.aps.org/doi/10.1103/PhysRevApplied.14.034068>.
- [29] H. Yasuda, T. Yein, T. Tachi, K. Miura, and M. Taya, “Folding behaviour of Tachi-Miura polyhedron bellows,” *Proceedings of the Royal Society A: Mathematical, Physical and Engineering Sciences*, vol. 469, no. 2159, 2013, ISSN: 14712946. DOI: 10.1098/rspa.2013.0351.
- [30] H. Yasuda and J. Yang, “Reentrant origami-based metamaterials with negative Poisson’s ratio and bistability,” *Physical Review Letters*, vol. 114, no. 18, pp. 1–5, 2015, ISSN: 10797114. DOI: 10.1103/PhysRevLett.114.185502.
- [31] K. Miura and S. Pellegrino, “Forms and Concepts for Lightweight Structures,” *Forms and Concepts for Lightweight Structures*, Mar. 2020. DOI: 10.1017/9781139048569. [Online]. Available: <https://www.cambridge.org/core/books/forms-and-concepts-for-lightweight-structures/04D410C3465B75C54040E2788AEFB762>.
- [32] A. E. del Grosso and P. Basso, “Deployable Structures,” *Embodying Intelligence in Structures and Integrated Systems*, vol. 83, pp. 122–131, 2012. DOI: 10.4028/www.scientific.net/ast.83.122.
- [33] J. B. Samuel and D. Pines, “Design and Testing of a Pneumatic Telescopic Wing for Unmanned Aerial Vehicles,” 2007. DOI: 10.2514/1.22205. [Online]. Available: <http://www.geversaircraft.com>.
- [34] Haariet Martique, “ECHO-I Inflation System,” *Oxford University*, vol. XXX, p. 60, 1994.
- [35] R. E. Freeland, G. D. Bilyeu, G. R. Veal, M. D. Steiner, and D. E. Carson, “Large inflatable deployable antenna flight experiment results,” *Acta Astronautica*, vol. 41, no. 4-10, pp. 267–277, Aug. 1997, ISSN: 0094-5765. DOI: 10.1016/S0094-5765(98)00057-5.
- [36] Deploytech, “InflateSail Publishable Summary,” pp. 1–15, 2016. [Online]. Available: <https://cordis.europa.eu/docs/results/284/284474/final1-part1-deploytech-final-publishable-summary-%20v05-rt-clean.pdf>.
- [37] N. Grumman, “AstroMast Programs,” [Online]. Available: http://www.northropgrumman.com/BusinessVentures/AstroAerospace/Products/Documents/pageDocs/astromast_programs.pdf.

- [38] *BoPET* - Wikipedia. [Online]. Available: <https://en.wikipedia.org/wiki/BoPET> (visited on 02/05/2023).
- [39] *Apollo lunar module descent engine ablative chamber-injector compatibility improvement study. Torch test materials evaluation*, 1969.
- [40] J. Butler, J. Morgan, N. Pehrson, *et al.*, “Highly compressible origami bellows for harsh environments,” *Proceedings of the ASME Design Engineering Technical Conference*, vol. 5B-2016, 2016. DOI: 10.1115/DETC2016-59060.
- [41] M. Hildebrandt, “Conceptual design of deployable space structures,” Ph.D. dissertation, 2020. DOI: 10.1177/0266351193008001-203.
- [42] M. Peters, J. Kumpfert, C. Ward, and C. Leyens, “Titanium alloys for aerospace applications,” *Advanced Engineering Materials*, vol. 5, no. 6, pp. 419–427, 2003. DOI: <https://doi.org/10.1002/adem.200310095>. eprint: <https://onlinelibrary.wiley.com/doi/pdf/10.1002/adem.200310095>. [Online]. Available: <https://onlinelibrary.wiley.com/doi/abs/10.1002/adem.200310095>.
- [43] H. Zhang, S. Gu, J. Zhang, *et al.*, “Development of titanium diaphragms for space propellant tank,” *Journal of Physics: Conference Series*, vol. 2336, no. 1, p. 012002, Aug. 2022. DOI: 10.1088/1742-6596/2336/1/012002. [Online]. Available: <https://dx.doi.org/10.1088/1742-6596/2336/1/012002>.
- [44] T. W. Murphey, W. H. Francis, B. L. Davis, *et al.*, “High strain composites,” *2nd AIAA Spacecraft Structures Conference*, no. January, pp. 1–53, 2015. DOI: 10.2514/6.2015-0942.
- [45] M. Sakovsky, I. Maqueda, C. Karl, S. Pellegrino, and J. Costantine, “Dual-matrix composite wideband antenna structures for CubeSats,” *2nd AIAA Spacecraft Structures Conference*, no. January, pp. 1–26, 2015. DOI: 10.2514/6.2015-0944.
- [46] A. M. Gay, “Fabrication and Classification of Dual-Matrix Composites for Deployable Space Applications,” 2017. [Online]. Available: <https://repository.lib.ncsu.edu/bitstream/handle/1840.20/34542/etd.pdf?sequence=1&isAllowed=y>.
- [47] J. Rossiter, F. Scarpa, K. Takashima, and P. Walters, “Design of a deployable structure with shape memory polymers,” *Behavior and Mechanics of Multifunctional Materials and Composites 2012*, vol. 8342, no. June 2017, 83420Y, 2012, ISSN: 0277786X. DOI: 10.1117/12.915476.
- [48] H. Wang and M. Wang, “Structure Based on Miura-Origami,” pp. 1–6, 2016.
- [49] J.-M. Raquez, Y. Habibi, M. Murariu, and P. Dubois, “Polylactide (pla)-based nanocomposites,” *Progress in Polymer Science*, vol. 38, no. 10, pp. 1504–1542, 2013, Progress in Bionanocomposites: from green plastics to biomedical applications, ISSN: 0079-6700. DOI: <https://doi.org/10.1016/j.progpolymsci.2013.05.014>. [Online]. Available: <https://www.sciencedirect.com/science/article/pii/S007967001300066X>.
- [50] C. H. Zhou, B. Wang, H. Z. Luo, Y. W. Chen, Q. H. Zeng, and S. Y. Zhu, “Quasi-static axial compression of origami crash boxes,” *International Journal of Applied Mechanics*, vol. 09, no. 05, p. 1750066, 2017. DOI: 10.1142/S1758825117500661. eprint: <https://doi.org/10.1142/S1758825117500661>. [Online]. Available: <https://doi.org/10.1142/S1758825117500661>.

- [51] J. Harris and G. McShane, “Metallic stacked origami cellular materials: Additive manufacturing, properties, and modelling,” *International Journal of Solids and Structures*, vol. 185-186, pp. 448–466, 2020, ISSN: 0020-7683. DOI: <https://doi.org/10.1016/j.ijsolstr.2019.09.007>. [Online]. Available: <https://www.sciencedirect.com/science/article/pii/S0020768319304196>.
- [52] D. Notta-Cuvier, J. Odent, R. Delille, *et al.*, “Tailoring polylactide (pla) properties for automotive applications: Effect of addition of designed additives on main mechanical properties,” *Polymer Testing*, vol. 36, pp. 1–9, 2014, ISSN: 0142-9418. DOI: <https://doi.org/10.1016/j.polymertesting.2014.03.007>. [Online]. Available: <https://www.sciencedirect.com/science/article/pii/S0142941814000658>.
- [53] T. Langford, A. Mohammed, K. Essa, A. Elshaer, and H. Hassanin, “4d printing of origami structures for minimally invasive surgeries using functional scaffold,” *Applied Sciences*, vol. 11, no. 1, 2021, ISSN: 2076-3417. DOI: 10.3390/app11010332. [Online]. Available: <https://www.mdpi.com/2076-3417/11/1/332>.
- [54] W. Chen, C. Guo, X. Zuo, J. Zhao, Y. Peng, and Y. Wang, “Experimental and numerical investigation of 3d printing pla origami tubes under quasi-static uniaxial compression,” *Polymers*, vol. 14, no. 19, 2022, ISSN: 2073-4360. DOI: 10.3390/polym14194135. [Online]. Available: <https://www.mdpi.com/2073-4360/14/19/4135>.
- [55] N. Zosimovych and Z. Chen, “3d printing cubesat: A low-cost mode of space exploration,” *Aeronautics and Aerospace Open Access Journal*, vol. 2, Oct. 2018. DOI: 10.15406/aaobj.2018.02.00066.
- [56] M. Çarkac and M. Secmen, “The prototype of a wideband ku-band conical corrugated horn antenna with 3-d printing technology,” *Advanced Electromagnetics*, vol. 8, pp. 39–47, Mar. 2019. DOI: 10.7716/aem.v8i2.977.
- [57] J. A. Faber, A. F. Arrieta, and A. R. Studart, “Bioinspired spring origami,” *Science*, vol. 359, no. 6382, pp. 1386–1391, 2018. DOI: 10.1126/science.aap7753. eprint: <https://www.science.org/doi/pdf/10.1126/science.aap7753>. [Online]. Available: <https://www.science.org/doi/abs/10.1126/science.aap7753>.
- [58] H. Ye, Q. Liu, C. Jianxiang, *et al.*, “Multimaterial 3d printed self-locking thick-panel origami metamaterials,” *Nature Communications*, vol. 14, Mar. 2023. DOI: 10.1038/s41467-023-37343-w.
- [59] *Original prusa i3 mk3s+ 3d printer | original prusa 3d printers directly from josef prusa*. [Online]. Available: <https://www.prusa3d.com/product/original-prusa-i3-mk3s-3d-printer-3/>.
- [60] *The ultimaker 2+ specifications*. [Online]. Available: <https://support.makerbot.com/s/article/1667337915868>.
- [61] I. Uriol Balbin and P. Solano López, “Preliminary study of an origami-inspired deployable structure for a small-scale demonstrator,” Sep. 2022.
- [62] D. Piker, “Kangaroo: Form finding with computational physics,” *Architectural Design*, vol. 83, Mar. 2013. DOI: 10.1002/ad.1569.

-
- [63] E. T. Filipov, T. Tachi, G. H. Paulino, and D. A. Weitz, “Origami tubes assembled into stiff, yet reconfigurable structures and metamaterials,” *Proceedings of the National Academy of Sciences of the United States of America*, vol. 112, no. 40, pp. 12 321–12 326, 2015. DOI: 10 . 1073 / PNAS . 1509465112 / SUPPL _ FILE / PNAS . 1509465112 . SM05 . MP4. [Online]. Available: <http://www.pnas.org/cgi/doi/10.1073/pnas.1509465112>.
- [64] *3d printing materials | more than 35 plastics and metals | xometry europe*. [Online]. Available: <https://xometry.eu/en/ms/3d-printing/>.
- [65] E. V. Navarro, “Analysis and optimization of origami inspired deployable space structures,” 2023.